ISTANBUL TECHNICAL UNIVERSITY ★ GRADUATE SCHOOL OF SCIENCE ENGINEERING AND TECHNOLOGY

PRODUCTION OF TiO_2-POLY (ALKYLENEDIOXYTHIOPHENE) NANOSTRUCTURES FOR DSSC APPLICATION

Ph.D. THESIS

Timuçin BALKAN

Department of Polymer Science and Technology

Polymer Science and Technology Programme

OCTOBER 2016

ISTANBUL TECHNICAL UNIVERSITY ★ GRADUATE SCHOOL OF SCIENCE ENGINEERING AND TECHNOLOGY

PRODUCTION OF TiO_2-POLY (ALKYLENEDIOXYTHIOPHENE) NANOSTRUCTURES FOR DSSC APPLICATION

Ph.D. THESIS

Timuçin BALKAN
(515102003)

Department of Polymer Science and Technology

Polymer Science and Technology Programme

Thesis Advisor: Prof. Dr. A. Sezai SARAC

OCTOBER 2016

İSTANBUL TEKNİK ÜNİVERSİTESİ ★ FEN BİLİMLERİ ENSTİTÜSÜ

BOYA UYARIMLI GÜNEŞ PİLİ UYGULAMARI İÇİN TiO_2-POLİ(ALKİLENDİOKSİTİYOFEN) NANO YAPILARININ ÜRETİMİ

DOKTORA TEZİ

Timuçin BALKAN
(515102003)

Polimer Bilim ve Teknolojisi Anabilim Dalı

Polimer Bilim ve Teknolojisi Programı

Tez Danışmanı: Prof. Dr. A. Sezai SARAÇ

EKİM 2016

Timuçin BALKAN, a Ph.D. student of İTU Graduate School of Science Engineering and Technology student ID 515102003, successfully defended the thesis/dissertation entitled “PRODUCTION OF TiO_2-POLY (ALKYLENEDIOXYTHIOPHENE) NANOSTRUCTURES FOR DSSC APPLICATION”, which he prepared after fulfilling the requirements specified in the associated legislations, before the jury whose signatures are below.

Thesis Advisor :	**Prof. Dr. A Sezai SARAC** İstanbul Technical University	....
Jury Members :	**Prof. Dr. Ahmet AKAR** İstanbul Technical University	....
	Prof. Dr. Cemal OZEROGLU Istanbul University	....
	Prof. Dr. Aysen ONEN İstanbul Technical University	....
	Prof. Dr. Ayfer SARAC Yıldız Technical University	....

Date of Submission : 30 August 2016
Date of Defense : 12 October 2016

“Herşeyin üstüne gelip, seni dayanamayacak bir noktaya getirdiğinde sakın vazgeçme; işte orası kaderinin değişeceği noktadır...” (Mevlana Celaleddin Rumi)

Annem’e ve Babam’a,

FOREWORD

I would like to thank my advisor, Professor Dr. A. Sezai SARAC, for his guidance, continuous encouragement throughout this work, and discussions during my Ph.D. studies.

I also thank my thesis committee members Prof. Dr. Ahmet AKAR and Prof. Dr. Cemal OZEROGLU for their support.

I am really grateful to Zeliha GULER for her invaluable help, good suggestions, and supports. Her valuable comments helped me for improving the quality of my work. She still gives me inspiration.

I would like to thank Dr. Olga SOLCOVA, Dr. Magdalena MOROZOVA and Dr. Pavel DYTRYCH for their valuable supports.

My special thanks go to my lovely friends Aslı GENCTURK and Ilknur GERGIN. I really appreciate their encouragement and friendship during my Ph.D. education.

I would like to special thank my best friend Ugur KAYA for his friendship during all period of my life.

I like to thank to all electropol lab friends specially Selin GUMRUKCU for their support and friendship.

I would like to give my special thanks to my wife Husniye CAKMAK BALKAN for her support, patience, encouragement and love. You are my reward.

I would like to thank my sister and brother Esra BALKAN and Veysel BALKAN for their special helps during preparation of my thesis. Finally, I would like to offer the most gratitude to my parents for their patience, understanding, moral support and encouragement during all stages in the preparation of this PhD study.

August 2016

Timuçin BALKAN
(Polymer Chemist)

TABLE OF CONTENTS

ABBREVIATIONS

PEDOT:PSS : Poly(3,4-Ethylenedioxythiophene):Poly(Styrenesulfonate)
CP : Conductive Polymer
DSSC : Dye Sensitized Solar Cell
NR : Nano Rods
NP : Nano Particles
EIS : Electrochemical Impedance Spectroscopy
APTES : Amino Propyl Triethoxy Silane
PProdot : Poly(3,4-Propylenedioxythiophene)
CV : Cyclic Voltammetry
PVP : Poly(vinylpyrrolidone)
Ti(Iso) : Titanium Isopropoxide
FTO : Fluorine Doped Tin Oxide
CE : Counter Electrode

SYMBOLS

R_{ct} : Charge transfer resistance
R_s : Solution resistance
CPE : Constant phase element
Ip : Current density
C : Concentration
D : Diffusion coefficient
n : Number of electrons
υ : Scan rate
K : Shape factor (scherrer equation)
λ : X-ray wavelength (scherrer equation)
cos θ : Bragg angle

LIST OF TABLES

LIST OF FIGURES

Page

PRODUCTION OF TiO_2-POLY (ALKYLENEDIOXYTHIOPHENE) NANOSTRUCTURES FOR DSSC APPLICATION

SUMMARY

Annually sun sends 120.000 TW energy to the earth and only 0.02% of this energy is sufficient by itself to replace energy resources like fossil fuels and nuclear energy. Therefore, research on photovoltaic (PV) technologies has gained much importance because by this technology, solar light is directly converted to electricity. Nevertheless, currently this technology has two main disadvantages: First, silicon-based PV technologies (crystalline silicon, amorphous/crystalline heterojunction silicon solar cells, etc), have relatively high efficiencies between 20-25% but the cost of energy obtained by these technologies is too high to compete with energy resources. Second, the low cost third generation photovoltaic technologies which are based on organic materials have much lower conversion efficiencies than silicon-based photovoltaic technologies. The high production cost is an important drawback for more wide-spread use of PV technologies. Instead of high purity silicon materials and conventional PV manufacturing techniques, use of organic solar cells (OSC) and dye-sensitized solar cells (DSSC) as third generation PV technologies is seen as solution to this problem because organic materilas are employed with low cost manufacturing techniques for their fabrication. Among third generation technologies, DSSC has recently drawn great attention on account of their low cost, long-term stability and relatively high light-to-electricity conversion efficiencies. In addition, their photovoltaic properties through changing chemical and physical properties of materials by synthesis, which is undoubtedly of great advantage for DSSC. A typical DSSC is comprised of a nanocrystalline semiconductor (TiO_2), an electrolyte with redox couple (I_3^-/I^-), and a counter electrode (CE) to collect the electrons and catalyze the redox couple regeneration.

Counter electrode is a critical component of DSSC, which serves as a mediator for collecting electrons from external circuit and reducing I_3^- ions to I^- ions so as to regenerate the redox couple. Platinum (Pt) film has been widely used in DSSC so far, due to its high conductivity and catalytic activity for reduction of I_3^- ions. However, its practical application will be limited by its high cost and rare source. Therefore, it is necessary to develop efficient Pt free counter electrodes for DSSC. For this purpose, different types of counter electrodes composed of TiO_2 nano structure and conductive polymer were fabricated and characterized. All prepared electrodes showed comparable catalytic performance with conventional Pt electrode for the reduction of triiodide.

This thesis contains four main parts in order to follow step by step how to produce composite electrodes. In the first part, a cost-effective and scalable method to prepare high quality TiO_2 is developed nanofibers based on electrospinning technique using poly(vinylpyrrolidone) (PVP) as matrix polymer. After calcination at 450 ^{o}C, PVP was removed completely which allows TiO_2 nanofibers to be maintained in pure anatase phase with high crystallinity. Moreover, we found that diameter of TiO_2

nanofibers can be controlled by changing ratio between PVP and titanium isopropoxide (Ti(Iso)) of precursor solution.

The integration of TiO_2 layers onto a substrate is challenging and limits the application potential of TiO_2 and it is very crucial for not only DSSC application but also another application. Even though, several studies have been reported to solve this problem by applying various deposition methods, there is still lack of information about how these methods affect the electrochemical and photo-electrochemical properties of resulting electrodes. Therefore, in the second part, the TiO_2 layers possessing different morphologies, deposited on the conductive FTO glass by means of various different deposition techniques (dip-coating, electrospinning and electrospraying). The effects of surface morphology and crystal size of nanostructured layers on electrochemical impedance (EIS) and photo-electrochemical properties were investigated. An inverse ratio between charge transfer resistance (obtained from equivalent circuit model) and photo-current density was found.

In the third part, TiO_2 nanorods were obtained from TiO_2 nanofibers with using mechanical grinding (ball milling) method. Afterwards, TiO_2 nanorods and nanoparticles were mixed with certain amount of poly(3,4-ethylenedioxythiophene):poly(styrenesulfonate) (PEDOT:PSS). This solution was coated on a conductive glass substrate (thickness of prepared electrodes ≈ 20 μm) and used as counter electrodes for DSSC (figure 1). The catalytic activity of PEDOT:PSS for triiodide reduction was significantly improved after addition of TiO_2. This activity was followed by using cyclic voltammetry (CV) and electrochemical impedance spectroscopy (EIS). We found that, catalytic activity of electrodes depends on ratio of TiO_2 nanorod and TiO_2 nanoparticles. Charge transfer resistance which was obtained from EIS measurement decreased by increasing TiO_2 nanorod ratio.

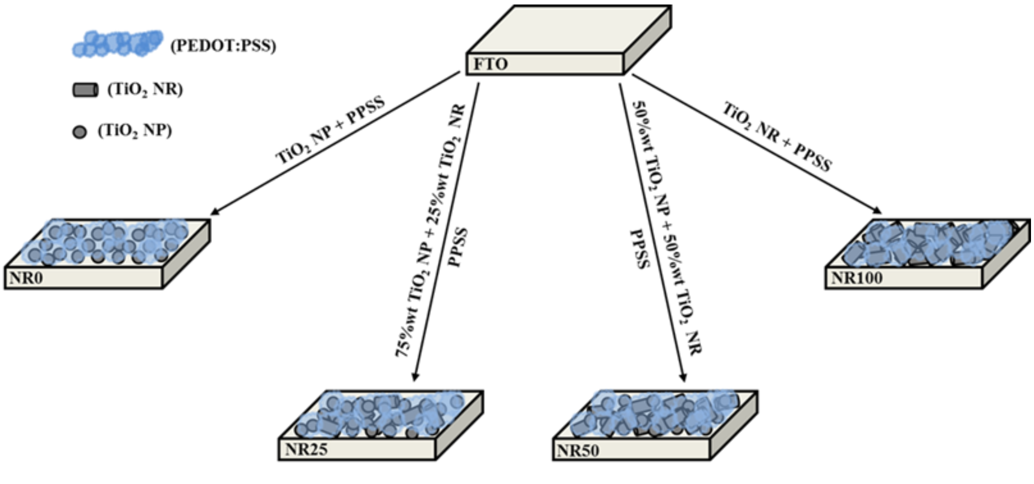

Figure 1: Schematic view of fabricated TiO_2 nanorod and nanoparticle/PEDOT:PSS electrodes.

In the last part, poly(3,4-alkylenedioxythiophene)/FTO (fluoride tin oxide) and poly(3,4-propylenedioxythiophene)/TiO_2 nanorod modified with 3-aminopropyltriethoxysilane/FTO electrodes were produced by using an electrochemical deposition method (figure 2). The surface roughness and I_3^-/I^- redox reaction behaviour of electrodes were characterized and their performances were compared. Cyclic voltammetry and EIS results of electrodes indicated that the poly(3,4-propylenedioxythiophene)/modified TiO_2 nanorod/FTO electrode shows better catalytic activity towards I_3^-/I^- redox reaction than poly(3,4-alkylenedioxythiophene)/FTO electrodes. We found that catalytic activity become better with increasing roughness of the electrode surfaces. Moreover, this values were superior to that of Pt counter electrode.

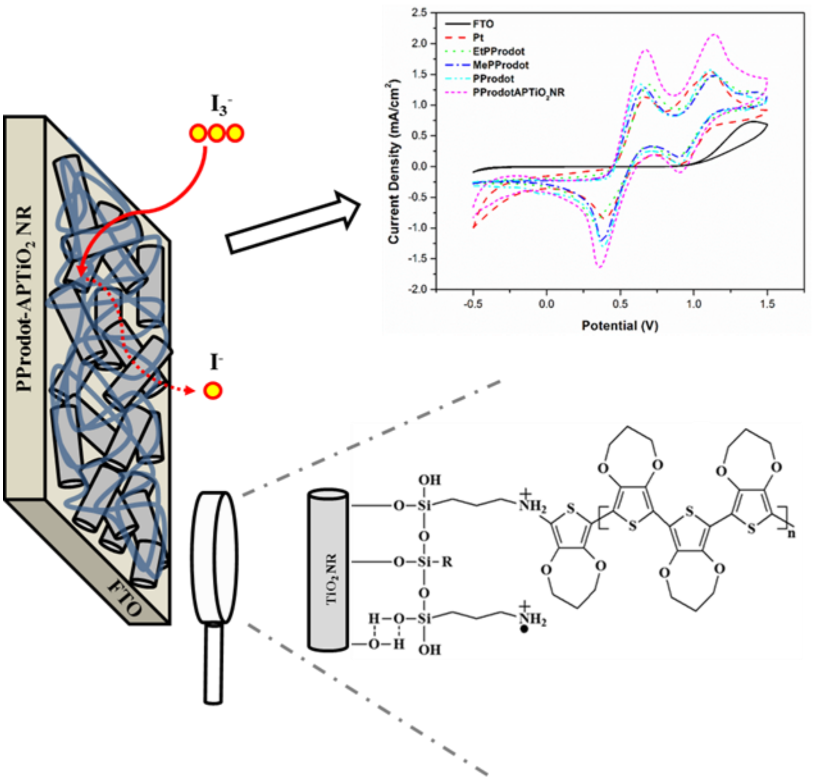

Figure 2 : CV graph and chemical structure of electrochemically fabricated PProdot-$APTiO_2$ electrodes.

BOYA UYARIMLI GÜNEŞ PİLİ UYGULAMARI İÇİN TiO_2-POLİ (ALKİLENDİOKSİTİYOFEN) NANO YAPILARININ ÜRETİMİ

ÖZET

Güneşin bir yılda dünyaya gönderdiği enerji 120.000 TW'dır. Bu enerjinin yalnızca %0.02'si tek başına fosil yakıtlarının ve nükleer enerji gibi enerji kaynaklarının yerini almaya yetecek miktardadır. Son yıllarda yapılan çalışmalarla büyük hız kazanan fotovoltaik (FV) teknolojisi ile güneş ışığının fotoelektrik etki ile doğrudan elektrik enerjisine dönüştürülmesi sağlanmaktadır. Ne var ki bu alanda uygulanan mevcut teknolojinin başlıca iki temel dezavantajı vardır. Bunlardan birincisi, verimleri % 20-25 arasında olan silisyum tabanlı (kristal silisyum, amorf/kristal heteroeklem FV hücreler, vb…) FV teknolojileri ile elde edilen enerji üretimlerinin mevcut enerji kaynaklarına göre pahalı olması; ikincisi ise üretim maliyeti silisyum FV hücrelere göre düşük olan üçüncü nesil FV hücrelerin veriminin düşük olmasıdır. Fotovoltaik teknolojisinin kullanımının yaygınlaştırılmasındaki üretim maliyeti sorunu, yüksek saflıkta silisyum tabanlı malzemelerin ve geleneksel FV aygıt fabrikasyonu yöntemlerinin yerine, organik malzemelerin kullanıldığı üçüncü nesil FV teknolojiler olan organik güneş pilleri ve boya ile duyarlaştırılmış güneş pillerinin (DSSC) kullanılması ile çözümlenmeye çalışılmaktadır. Üçüncü nesil güneş pilleri arasında, DSSC'ler düşük maliyetleri, uzun vadeli kararlılıkları ve nispeten ışığın elektriğe dönüşüm verimliliğinin yüksek olması sebebiyle son yıllarda çok dikkat çekmektedr. Bunun yanı sıra, fiziksel ve kimyasal özelliklerinin sentezleri sırasında kontrol edilebilmesi DSSC'lerin en büyük avantajlarındandır. Tipik bir DSSC hücresi üzerine ışığa duyarlı boya adsorbe edilmiş nanokristal yarı iletken bir TiO_2 tabaka (foto-anot), I_3^-/I^- redoks çiftini içeren bir elektrolit ve redoks çiftinin yenilenmesi için katalizör görevi yapan yardımcı elektrottan oluşmaktadır.

DSSC'yi oluşturan önemli bileşenlerden biri olan yardımcı elektrot, dış devreden geçen elektronların toplanmasına ve bu sayede I_3^- iyonunun indirgenerek I^- iyonuna dönüşmesine aracılık eder ve redoks çiftinin yenilenmesine neden olur. FTO üzerine kaplanan platin (Pt) film elektrotların I_3^- iyonunun indirgenmesi için katalitik aktivitelerinin yüksek olması ve yüksek iletkenliğe sahip olmalarından dolayı DSSC'lerde kullanılan en yaygın yardımcı elektrotlardır. Ancak, platinin hem pahalı bir malzeme olması hem de nadir bir element olması DSSC'lerin pratik uygulamalarını sınırlandırmaktadır. DSSC'ler için platinin yerine geçebilecek yüksek verimlilik sağlayacak yardımcı elektrotların geliştirilmesi partik uygulamalar açısından önem arz etmektedir. Bu amaçla tez kapsamında, TiO_2 nano (çubuk, partikül vb.) yapılardan ve iletken polimerlerden oluşan çeşitli yardımcı elektrotlar üretilmiş ve karakterize edilmiştir. Hazırlanan tüm elektrotların I_3^- iyonunun indirgenmesi için platin elektrot ile karşılaştırılabilir katalitik performans gösterdiği bulunmuştur.

Kompozit yardımcı elektrotların üretim aşamasının daha kolay anlaşılabilmesi için tez dört ana başlığa bölünmüştür. Tezin ilk kısmında, TiO_2 nanoliflerinin hazırlanması için basit ve ucuz bir yöntem olan elektro çekim yöntemi kullanılmıştır.

Elektro çekim sırasında taşıyıcı polimer olarak PVP seçilmiştir. Elde edilen kompozit nanoliflerin 450 ^{o}C'de kalsine edilmesinden sonra PVP yapıdan tamamen uzaklaştırılmış ve yüksek kristal yapısına sahip anataz fazda TiO_2 nanoliflerinin eldesi sağlanmıştır. Ayrıca, elde edilen TiO_2 nanoliflerinin çaplarının, öncü elektro-çekim çözeltisindeki PVP ve Ti(Iso) oranlarının değişimi ile kontrol edilebileceği bulunmuştur.

Bir substrat üzerine TiO_2 tabakaların özellikle TiO_2 nanoliflerin entegrasyonunun zor olması TiO_2'nin uygulama alanlarını sınırlandırmaktadır. Bu entegrasyonun arttırılması TiO_2'nin sadece DSSC uygulamalarında değil TiO_2'nin diğer uygulama alanları içinde önem teşkil etmektedir. Her ne kadar bu sorunun çözümü için çeşitli kaplama yöntemlerinin kullanılması rapor edilse de bu yöntemlerin elde edilen elektrotların elektrokimyasal ve foto-elektrokimyasal özelliklerine etkisi hakkında bilgi eksikliği mevcuttur. Bu nedenle, ikinci kısımda, farklı kaplama yöntemleri kullanılarak (daldırma, elektro çekim, elektro spray) farklı morfolojilere sahip TiO_2/FTO elektrotları üretilmiştir. FTO üzeine kaplanan nano yapılı tabakanın yüzey morfolojisinin ve kristal büyüklüklerinin elektrokimyasal impedans ve foto elektrokimyasal özelliklere etkisi araştırılmıştır. Eş değer devre modellemesinden elde edilen yük transfer değerleri ile ışık altında üretilen akım değerleri arasında ters bir orantı olduğu bulunmuştur.

Tezin üçüncü kısmında, mekanik kırma (ball milling) yöntemi kullanılarak ilk aşamada elde edilen TiO_2 nanolifleri öğütülerek TiO_2 nanoçubukları elde edilmiştir. Daha sonra elde TiO_2 nanoçubuklar ve TiO_2 nano partiküller belirli bir miktar PEDOT:PSS ile karıştırılmıştır. Hazırlanan karışım baget ile FTO üzerine sürülerek (kalınlıklar $\approx$ 20 µm) yardımcı elektrotlar hazırlanmıştır (Şekil 1). Yapıya TiO_2'nin katılmasından sonra PEDOT:PSS'in redoks çiftine (I_3^-/I^-) karşı olan katalitik aktivitesinin önemli ölçüde arttığı görülmüştür. Bu durum, döngülü voltametri ve elektrokimyasal impedans ölçümleriyle takip edilmiştir. Elektrotların katalitik aktivitelerinin TiO_2 nano çubuk-TiO_2 nano partikül oranına bağlı olduğu bulunmuştur. Elektrokimyasal ölçümlerden elde edilen elektrotlara ait yük taşıma dirençleri kompozit malzemedeki TiO_2 nano çubuk miktarının artması ile azalmıştır.

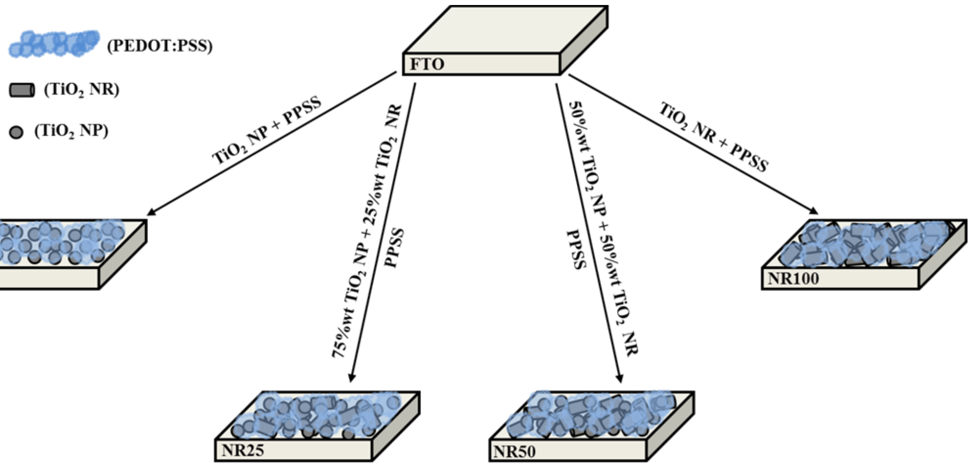

Şekil 1 : Hazırlanan TiO_2 (nanoçubuk ve nanotanecik)/PEDOT:PSS elektrotlara ait şematik gösterim.

Tezin son kısmında, elektrokimyasal kaplama yöntemi kullanılarak poli (3,4-alkilendioksitiyofen)/FTO ve poli (3,4-alkilendioksitiyofen)/3-aminopropiltrietoksi silan ile modifiye edilmiş TiO_2 nano çubuk/FTO elektrotları üretilmiştir (Şekil 2). Elektrotların yüzey pürüzlülükleri ve redoks çiftine (I_3^-/I^-) karşı katalitik aktiviteleri karakterize edilmiş ve performansları karşılaştırılmıştır. Döngülü voltametri ve impedans sonuçları yapıda modifiye edilmiş TiO_2 nano çubuk içeren elektrodun elektrokatalitik aktivitesinin sadece poli (3,4-alkilendioksitiyofen) türevlerinden üretilen elektrotlardan daha iyi olduğunu göstermiştir. Elektrotların yüzey pürüzlülüklerinin artması ile katalitik aktivitelerinin arttığı bulunmuştur. Dahası bu elektrotlardan elde edilen katalitik aktivite değerlerinin en az platin elektrodun katalitik aktivitesi kadar iyi olduğu görülmüştür.

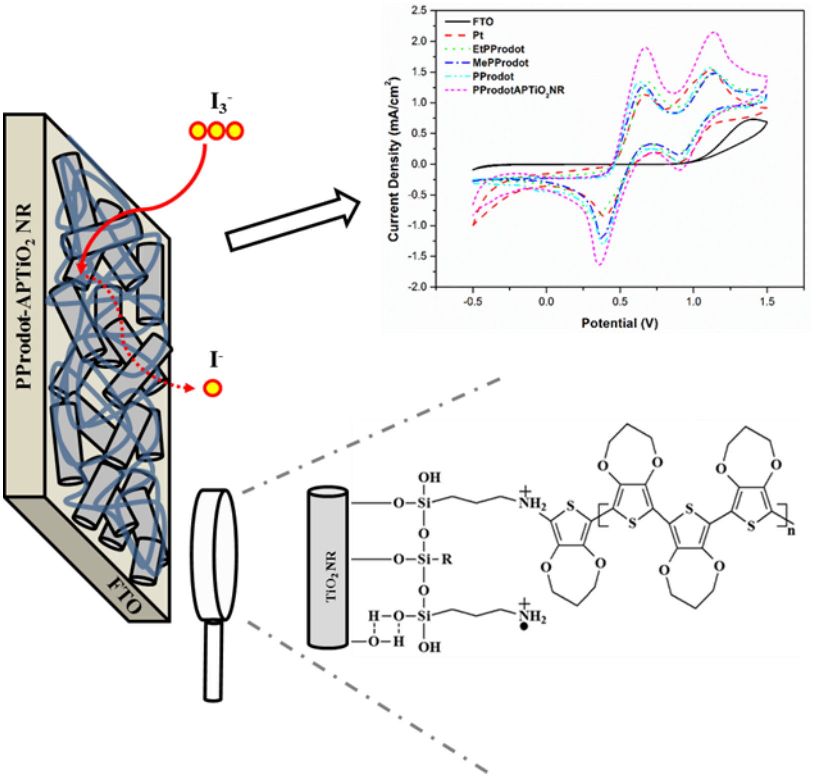

Şekil 2 : Elektrokimyasal yöntem ile hazırlanan PProdot-APTiO2 elektrotlarının kimyasal yapısı ve bu elektrotlara ait döngülü voltametre grafiği.

1. INTRODUCTION

One of the most important problems of mankind in the 21st century are environmental pollution and global warming caused by fossil fuels usage for energy production because of increasing population and rising energy demand for developing countries. In order to solve these problems, renewable energy resources should be used more efficiently. A very popular alternative energy resources called photovoltaic device (solar cell) which converts sunlight directly into energy. Up to now, commercially available photovoltaic technologies are based on inorganic materials, which require high costs and highly energy consuming preparation methods. In addition, several of those materials, like CdTe, are toxic and have low natural abundance. Organic photovoltaics are produced to overcome these problems. However, the efficiencies of organic-based photovoltaic cells are still lower than inorganic based photovoltaic technologies (Nazeeruddin, Baranoff, & Grätzel, 2011). Since significant breakthroughs in 1991, dye-sensitized solar cells (DSSCs) have entered public view and garnered more and more research attention. Among the various solar cells, dye-sensitized solar cells (DSSCs) have many advantages compare to other photovoltaic devices, such as high efficiency, low cost, simple fabrication procedures, environmental friendliness. Although a DSSC prototype has showed excellent device performance under laboratory conditions, several limitations hinder the large scale applications and commercialization of DSSCs in the future. Hence, the development of more advanced, cost-affective, new materials are necessary for the bring DSSCs available to even larger number of people (Toivola, 2010). We have tried to improve new counter electrodes to achive this goal in this thesis.

Typically, under illumination to DSSCs, charge separation occurs by electron emision from photo-excited dye to conduction band of photoanode (TiO_2). Electrons are transported to external load via nano-porous photoanode network and transparent conductive oxide (FTO): Electrons are injected into electrolyte by catalytic reactions of counter electrode (generally platinium) and oxidized dye molecules are finally reduced to the ground state by electrons supplied from electrolyte (figure 1.1) (Seo, Son, Itagaki, Koga, & Shiratani, 2016).

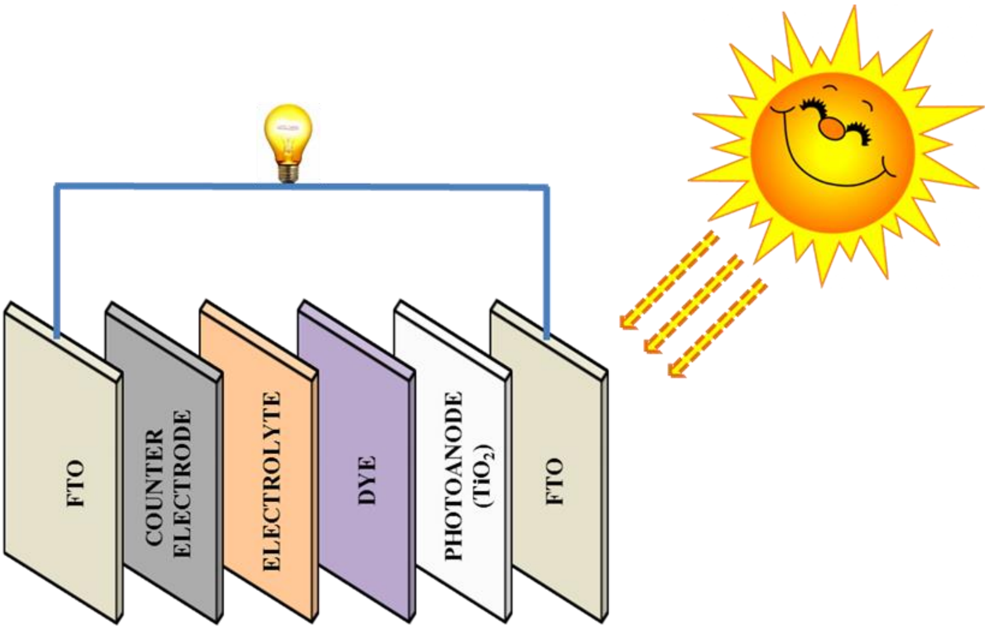

Figure 1.1 : Schematic representation of the dye sensitized solar cell (Theerthagiri, Senthil, Madhavan, & Maiyalagan, 2015).

In this cycle, each part of the device plays a significant role to determine cost and efficiency of DSSCs. Therefore, from its invention to present many researchers have focused on the modificaton of the each component for practical applications (Ye et al., 2015). As can be seen in Figure 1.2, areas of researchs have included the design of nanostructured semiconductor photoanodes with effective morphologies for high dye loading and fast electron transport, the synthesis of sensitizers with strong visible light harvesting ability, the utilization of redox electrolytes with useful compositions for efficient hole transport, the optimization of the Pt counter electrode as well as the development of other equivalent alternatives at lower costs (Ye et al., 2015).

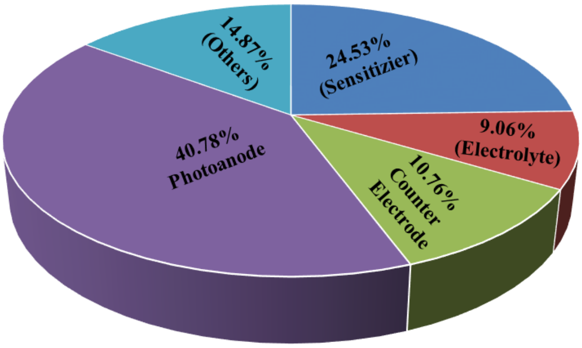

Figure 1.2 : Percentage of publications for each component of DSSCs in 2012 (Ye et al., 2015).

The counter electrode (CE) is one of the most important components in DSSCs. The main task of the counter electrode to collect electrons from external circuit and catalyze the reduction of redox electrolyte or transport holes in solid-state electrolyte. Therefore, high electrical conductivity for charge transport, good electrocatalytic activity for reducing the redox couple and stability are the primary requirements for CE materials (Hou et al., 2013). Noble metals, generally platinium (Pt), gold (Au) and silver (Ag) are the most popular CE materials because of their high electrocatalytic activity (e.g. Pt) for the reduction of redox couples in liquid electrolytes or effective hole transfer in solid-state electrolytes (e.g. Au and Ag). However, noble metals are very expensive and their corrosion in liquid electrolytes deteriorates their long term stability (Theerthagiri, Senthil, Madhavan, & Maiyalagan, 2015). In order to overcome this problem, several type of low-cost Pt free materials have been introduced to use as CE catalysts. As can be seen in figure 1.3, these catalysts contain carbon materials, conductive polymers, inorganic materials and composites (Wu & Ma, 2014).

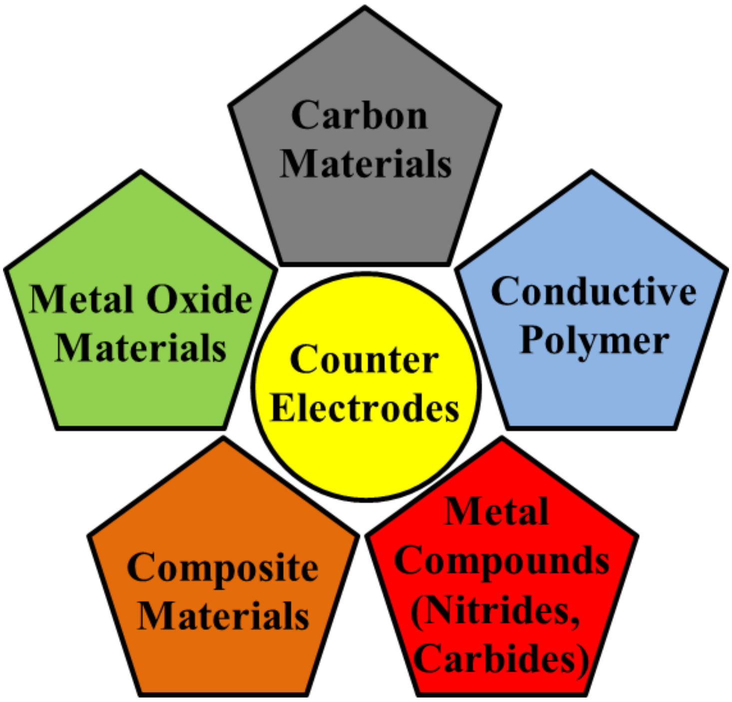

Figure 1.3 : Materials used for counter electrode fabrication.

Composite materials are made by combining two or more materials that can be used as efficient catalysts for DSSCs. In recent years, fabricated composite counter electrodes has become more and more popular because of high catalytic acivity for redox couple reaction. Normally, conductive polymers (CPs) which is considered for use as a DSSC counter electrode because of its unique properties: good catalytic activity, good conductivty and comparatively lower price than Pt. However, many researchers observed that pure CP counter electrodes generate lower cell efficiency than Pt-based DSSC. In order to enhance polymer based DSSC performance, other materials are incorporated with polymer to increase the film surface area, conductivity or catalytic activity. Metal oxides are one of the suitable materials which enhance electrocatalytic activity due to their high surface area and electronic properties. Thus, combination of CPs with metal oxides create a synergetic effect and enhance the counter electrode performance. Generally, TiO_2-CPs composite counter electrodes have showed better performance than the other metal oxides (Saranya, Rameez, & Subramania, 2015). Therefore, in this thesis, different types of TiO_2-CPs composite counter electrodes which have different morpholgy were produced by using chemical and electrochemical methods. Two main electrochemical methods were used in order to characterize fabricated counter electrodes as described below:

First method, cyclic voltammetry (CV) is a popular technique for its relative simplicity and it provides additional information about the working electrode. It is utilized mostly as an analytical method for revealing catalytic ability and electrochemical active surface area of the working electrode (labelled as counter electrode for this thesis) (Saranya, Rameez, & Subramania, 2015).

Another method electrochemical impedance spectroscopy (EIS) is a most suitable technique to describe the charge transfer kinetics of electrochemical systems. The electrocatalytic activity of counter electrodes toward reduction of redox couple can be obtained by EIS, using the symmetric cell system (which means there is no need whole DSSC cell). The Nyquist plot provides charge transfer resistance (R_{ct}) value by measuring the electron mobility between the CE and electrolyte. The magnitude of R_{ct} depends on the diameter of the semicircle and the corresponding chemical capacitance (CPE) of the electrode/electrolyte interface. As known, the lower R_{ct} indicates facile electron transfer for counter electrodes (Saranya, Rameez, & Subramania, 2015).

1.1 Purpose of Thesis

The aim of this thesis to develop new materials for dye sensitized solar cells which represent the so-called third generation of photovoltaics (crystalline silicon being the first, and thin film technologies such as cadmium telluride (CdTe), copper-indium-gallium selenide (CIGS), copper-indium sulphide (CIS) and amorphous silicon (a-Si) being examples of the second generation). DSSC is a potential candidate for the traditional solar cells (1st and 2nd generation) due to its simple and energy-efficient manufacturing, for the most part low cost, non-toxic and recyclable materials, and suitability for wide variety of end-user products, from small scale power production to consumer goods such as mobile phone chargers or “smart” clothing. Also, as the DSSC works better with low light intensities it is especially practical in indoor applications (Toivola, 2010). The main factors that hinder the development of DSSC technology can be listed as low power conversion efficieny, low long-term stability and high production cost due to the use of platinium as a counter electrode. And in order to realize long-term developments and practical application of the dye-sensitized solar cells (DSCs) requires a robust increase of the power conversion efficiency (PCE) and a significant decrease of the production cost (Wu & Ma, 2014). The best DSSC efficiency value of 12.3% was achived by using cobalt based redox couple combined with organic dye (Yella et al., 2011). This result is comparable to the values typical for thin film technologies (5 – 13 %) but still lack behind the crystalline silicon values which are already almost 20-25 %. Obviously, dye design and redox copule selection are the key path to improve the PCE, while developing low cost counter electrode (CE) catalysts is one of the promising paths to reduce the production cost of DSSC by replacing the expensive Pt counter electrode. Therefore, in this thesis, we mainly focused on to develop TiO_2-Poly (alkylenedioxythiophene) based counter electrode materials which have electrocatalytic ability for reduction of I_3^- (triiodide) (chapter 4 and chapter 5). Detailed characterization (such as impedance properties, morphological properties) of these electrodes were discussed. Apart from this, different TiO_2 nanofiber-nanoparticle-nanorod electrodes which have different surface morphology were fabricated and photoelectrochemical properties were compared in order to understand relation between morphology and photo current density (chapter 2 and 3). We believe that this information will be useful to design both counter electrode and photoanode for DSSC application.

2. NEW PREPARATION ROUTE OF TiO_2 NANOFIBERS BY ELECTROSPINNING: SPECTROSCOPIC AND THERMAL CHARACTERIZATIONS[1]

In the recent years, titanium dioxide (TiO_2) has been focused on by a series of studies since it has a huge application potential owing to its remarkable properties such as transparency to visible light, high refractive index and low absorption coefficient (Rao, 2002). Other than these properties, TiO_2, especially in the anatase form, is one of the most promising materials for a variety of applications such as sensors (Junshui Chen et al., 2005), air purification and water disinfection (Fujishima, Rao, & Tryk, 2000; Lazar, Varghese, & Nair, 2012), solar cell (Fujihara, Kumar, Jose, Ramakrishna, & Uchida, 2007; Viswanathamurthi, Bhattarai, Kim, Kim, & Lee, 2004) and catalytic devices (Kwon, Shin, Kim, Choi, & Yoon, 2004) due to its photocatalytic activity (T. Berger, Lana-Villarreal, Monllor-Satoca, & Gómez, 2006). Photocatalytic properties of TiO_2 arise from the semiconductor nature, especially from the ability of the light quantum absorption followed by the charge carrier generation (Gracia, Holgado, & González-Elipe, 2004; Hashimoto, Irie, & Fujishima, 2005). Nevertheless, TiO_2 photocatalytic activity significantly depends on the crystal structure, morphology and dimensions that must be optimized (Šolcová et al., 2008; Y. Zhang, Weidenkaff, & Reller, 2002). It is important to use such preparation method which enables size, texture and crystallinity to be tailored precisely. Simplicity, high yield, effectiveness and low costs of the method would be another advantage for the upcoming applications.

Electrospinning is a promising technique that meets the requirements. It is the most widely preferred method among several techniques for fabrication of TiO_2 nanofibers (Barakat, Hamza, Al-Deyab, Qurashi, & Kim, 2012). Electrospinning provides a great control over dimensions, surface area and morphology of nanofibers which possess high surface area to mass or volume ratio (D. Li & Xia, 2003).

---

[1] This chapter based on the paper "Solcova, O., Balkan, T., Guler, Z., Morozova, M., Dytrych, P. and Sarac, A.S. (2014). New Preparation Route of TiO_2 Nanofibers by Electrospinning: Spectroscopic and Thermal Characterization, *Science of Advanced Materials*, 6(12), 2618-2624.''

In this study we report the preparation of TiO_2 nanofibers by electrospinning through titanium isopropoxide Ti(Iso). For the tailored preparation of titania nanofibers in anatase form by electrospinning, nanofibers of Ti(Iso) in acetic acid- PVP solution were calcinated at various temperatures. Ti(Iso)/PVP and TiO_2 nanofibers were thoroughly characterized by FTIR-ATR, Raman Spectroscopy, Physical adsorption of inert gases, TGA and SEM. The photo-excitation properties of the TiO_2 nanofibers and the ability of photocurrent generation were investigated by the photo-induced electrochemical method – amperometry.

2.1 Experimental Part

2.1.1 Preparation of TiO_2 nanofibers by electrospinning

Polyvinylpyrrolidone (M_w ~1.300.00 g/mol, Acros Organics) stock solution (10 wt%) was obtained by dissolving PVP (2 g) in anhydrous ethanol (18 g) (Sigma-Aldrich, Analytical Grade). Various amounts (5, 10, 15 wt% according to PVP solution) of Titanium (IV) isopropoxide (98%, Sigma-Aldrich) and 0.5 mL acetic acid (Merck, Analytical Grade) were added to PVP stock solution and the solution rested for 1-2 hours before electrospinning. Acetic acid was used to stabilize the solution and to control the hydrolysis reaction. PVP/Ti(Iso) nanofibers were fabricated by an electrospinning method (Fujihara et al., 2007).

The electrospinning setup consisted of a syringe and a stainless steel gauge 20 G needle as a nozzle. A High Voltage DC power supply was used to generate the high electrical potential between the tip of the nozzle and the grounded target, a sheet of Al foil and Indium thin oxide (ITO-Sigma-Aldrich 8 Ώ/sq) glass for photoelectrochemical measurements. The electrical potential of 10 kV was applied over PVP and PVP/Ti(Iso) spinning solutions with a collection distance of 10 cm and 1 mL/h feeding rate at room temperature.

As-electrospun PVP/Ti(Iso) nanofibers were calcinated in a furnace (NEY 2-525 Series II, USA) at various temperatures 400°C, 450°C, 500°C at a rate of 2.5°C/min respectively for 1, 3, 4.5 and 6 hours.

2.1.2 Characterization of PVP/Ti(Iso) and TiO_2 nanofibers

To investigate the transformation of Ti(Iso) to TiO_2 depending on the applied temperature and the time, the as-electrospun PVP/Ti(Iso) nanofibers were subjected to a thermogravimetric analysis (TGA) (TA TGA Q50). 10 mg of nanofiber mat was heated to 800°C with the rate of 20°C/min under nitrogen purge.

Morphology of PVP/Ti(Iso) and TiO_2 nanofibers was monitored with a scanning electron microscope (SEM-FEI Quanta 450 FEG-EDS) with 10 kV, 15 kV and 20 kV operating voltages, respectively. The average diameters of nanofibers were determined by Image J to randomly measure the diameters of 20 individual fibers shown in SEM images. Structural analyses of nanofibers were performed by FTIR-ATR (Perkin Elmer FTIR-ATR Spectrophotometer Spectrum One with universal ATR attachment with a diamond and ZnSe crystal).

The Raman spectroscopy (Nicolet Almega XR; ThermoNicolet, USA) with wavelength 473 nm and the XRD spectroscopy (Shimadzu XRD-6000) were used to determine the structure and the crystallinity of the calcinated PVP/Ti(Iso) nanofibers.

Textural properties (S_{BET}, S_{meso}, V_{micro}, pore-size distribution) of samples were evaluated from nitrogen physical adsorption-desorption isotherms at 77 K obtained with the ASAP2020M instrument (Micromeritics, USA). Before the analysis, all samples were dried at 50 °C or 110 °C (calcinated samples) at least for 12h *in vacuo* (1 Pa). The mesopore surface area (S_{meso}) and the micropore volume (V_{μ}) were evaluated from the measured nitrogen physical adsorption-desorption isotherms by two independent methods; modified BET equation (Petr Schneider, 1995) and t-plot constructed with the use of Lecloux- Pirrard standard isotherm (P Schneider, Hudec, & Solcova, 2008). Results from both methods were identical. The pore-size (r_P) was determined by BJH method.

2.1.3 Photoelectrochemistry of TiO_2 nanofibers

Photoelectrochemical measurements were performed at room temperature in the three-electrodes Pyrex cell by means of electrochemical methods. All potentials were referred to Ag/AgCl/KCl(sat) electrode whereas the Pt sheet was used as a counter electrode. The exposed area of the working TiO_2 electrode (prepared nanofiber layer at ITO glass) for the UV illumination and photoelectrochemical reaction was 1 cm^2.

Measurements were performed with a computer-controlled Voltalab 10 PGZ-100 potentiostat. For all electrochemical experiments the 0.1 M solution of Na_2SO_4 in ultrapure water (0.06 $\mu S \cdot cm^{-1}$) was used as the working electrolyte. A 500 W polychromatic lamp (Hg, LOT-Oriel) with a water filter was used for UV-Vis irradiation and the incident light beam was modified by the interference filter (Melles Griot) producing spectrally narrow flux of photons (365 ± 10 nm). The applied irradiance was measured by means of a UV sensor (UVA Light Meter) having the intensity of 10 $mW \cdot cm^2$ in most of the experiments. The generated photocurrent as a function of time at constant inserting potential (600 mV) was measured by amperometry. The detailed description of this method had been reported previously (Morozova, Kluson, Krysa, Gwenin, & Solcova, 2011).

2.2 Results and Discussion

2.2.1 SEM analyses and fiber diameter distribution of PVP/Ti(Iso) nanofibers

The SEM images of PVP and PVP/Ti(Iso) nanofibers demonstrated that no bead formation was observed in resulting nanofibers (Figure 2.1). The average diameter of PVP nanofibers was in the range from 400 to 600 nm. PVP/Ti(Iso) nanofibers exhibited irregular shapes following the insertion of Ti(Iso) into the PVP solution (Figure 2.1 (b)-(d)) and the fibers diameters ranged between 100 and 700 nm related to Ti(Iso) concentration.

The fabrication of PVP/Ti(Iso) nanofibers with electrospinning became challenging at higher Ti(Iso) concentrations since the viscosity of the spinning solution was increased and conductivity of the solution was decreased (Barakat et al., 2012; J. Y. Park & Kim, 2009). The viscosity and the electrical conductivity of the electrospinning solution play a role on fiber formation as they are strongly dependent on the ratio between Ti(Iso) and PVP. At 5 wt% of Ti(Iso) [1:2 Ti(Iso)/PVP(w/w) ratio], the condensation of Ti(Iso) starts and by the increase of this ratio (~1:1 and 2:1 -10wt % and 15 wt % respectively) leads to a more viscous and low conductive solution, resulting in an increase of the fiber diameters and broader size distribution (Figure 2.2). 1:2 Ti(Iso)/PVP(w/w) ratio [5 wt% of Ti(Iso)] seems to be the best ratio for exchange (or complexation) ligands of titanium isopropoxide coordination sites with carbonyl group of PVP during condensation.

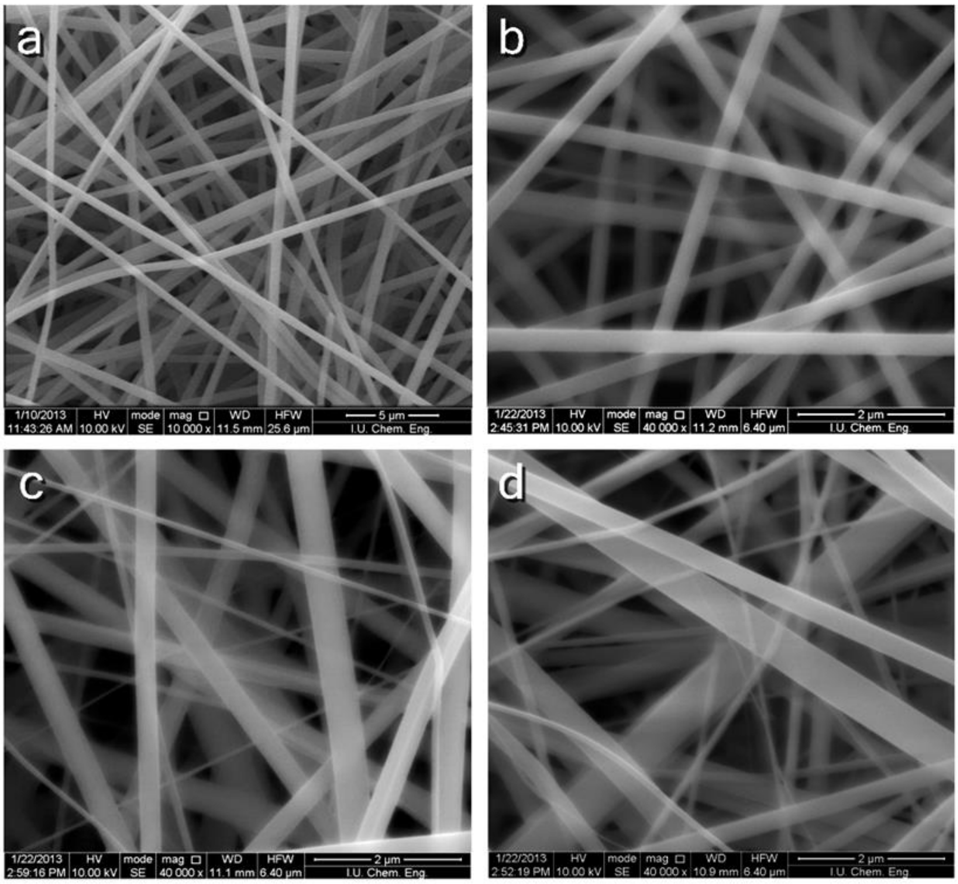

Figure 2.1 : SEM images of PVP (a) and 5 wt% (b), 10 wt% (c), 15 wt% (d) Ti(Iso) containing PVP/Ti(Iso) nanofibers.

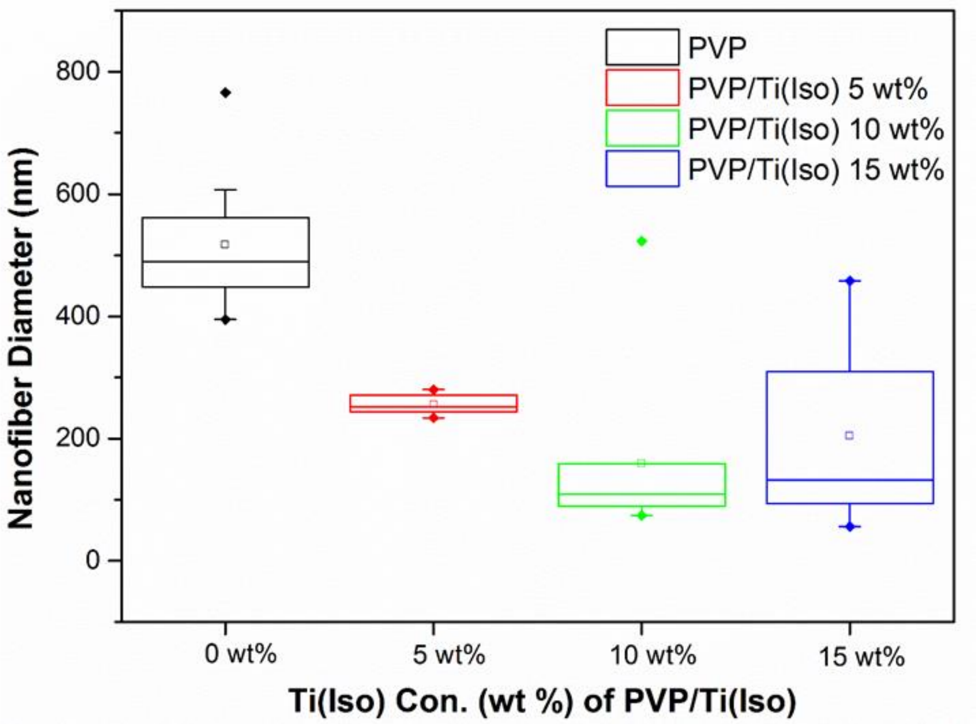

Figure 2.2 : Nanofiber diameter distribution of PVP and 5 wt%, 10 wt%, 15 wt% Ti(Iso) containing PVP/Ti(Iso) nanofibers.

2.2.2 TGA analyses of PVP/Ti(Iso) nanofibers

According to TGA results of PVP/Ti(Iso), a minor weight loss of 10 wt% at the temperature below 380 °C was attributed to the desorption of water and some organic residuals (Figure 2.3). The remaining organic residuals and PVP were completely decomposed between 400 °C and 480 °C which was supported by FTIR-ATR spectrum (section 2.2.3). Since all the organic component was thoroughly decomposed at this temperature, 450 °C was chosen as the appropriate calcination temperature for the preparation of TiO_2 nanofibers (Juengsuwattananon, Rujitanaroj, Supaphol, Pimpha, & Matsuzawa, 2008). When TGA profiles of PVP/Ti(Iso) were analyzed at 750 °C, the remaining amount of material left as 20, 25, 30 wt%; regarding 5, 10, 15 wt% Ti(Iso) containing PVP/Ti(Iso) nanofibers respectively, was attributed to the newly formed TiO_2 (Figure 2.3 inlet graph).

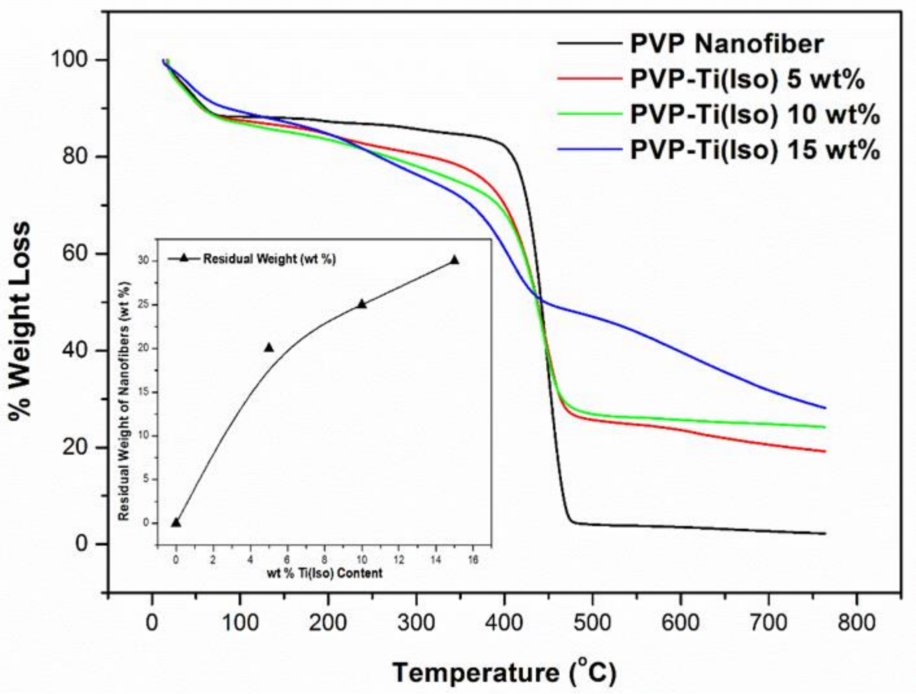

Figure 2.3 : A TGA profiles of PVP and 5 wt%, 10 wt%, 15 wt% Ti(Iso) containing PVP/Ti(Iso) nanofibers and the inlet graph represents the residual weight of PVP/Ti(Iso) nanofibers after TGA analysis.

2.2.3 FTIR-ATR characterization of nanofibers

FTIR-ATR spectra of commercial anatase TiO_2 nanoparticles as reference, nanofibers of PVP and PVP/Ti(Iso) and obtained TiO_2 nanofibers following to calcination at 450 °C are shown in Figure 2.4 (a). Since PVP completely degraded and removed from the nanofibers during the calcination process, no peaks related to PVP can be seen in the TiO_2 nanofiber sample after calcination (Figure 2.4 (a)).

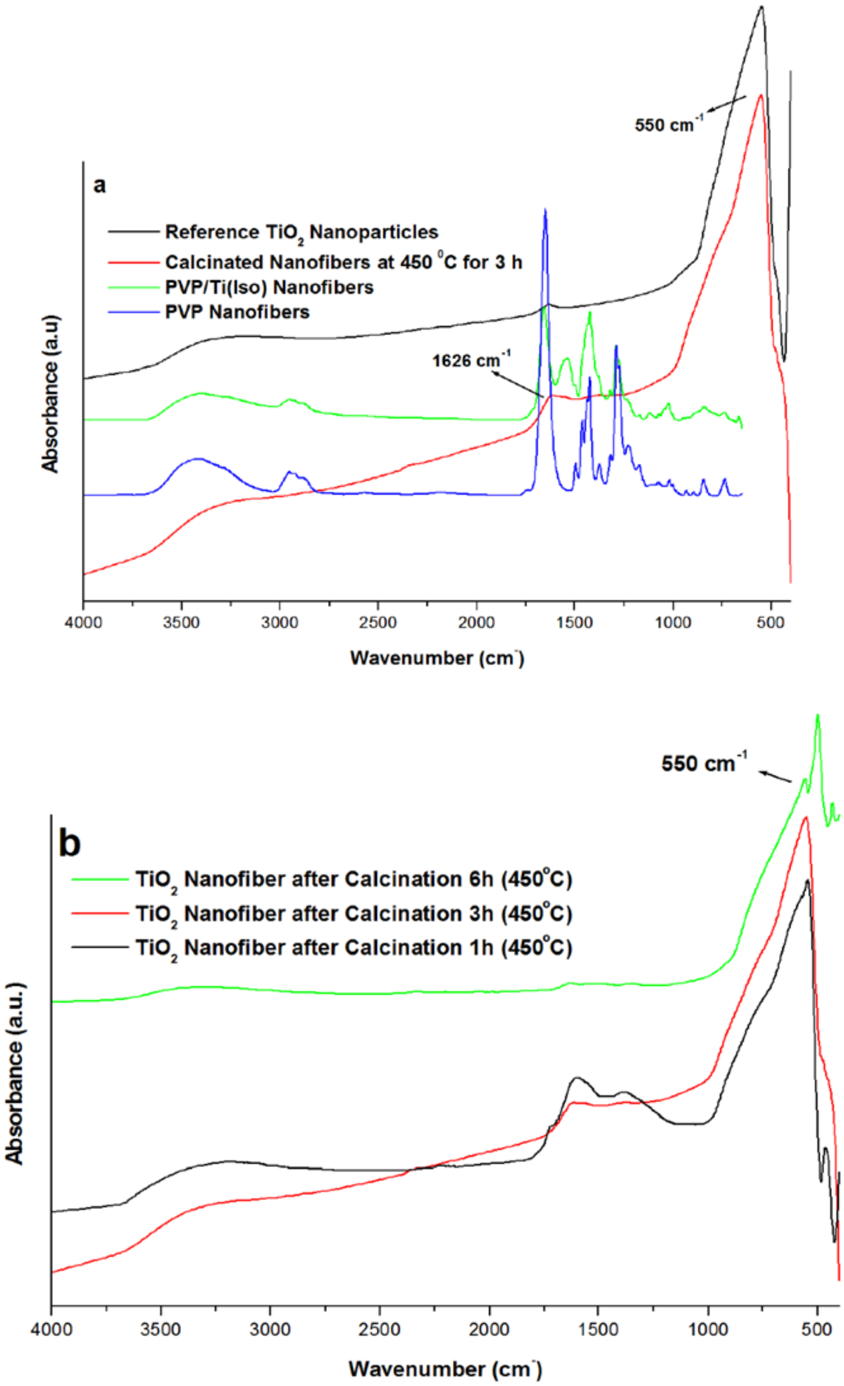

Figure 2.4 : FTIR-ATR spectra of PVP, PVP/Ti(Iso) and calcinated nanofibers and commercial TiO_2 nanoparticles (a). Spectra of TiO_2 nanofibers dependence on calcination temperature (b).

Additionally, all the samples exhibit very strong peaks between 3400-3500 cm^{-1} corresponding to the O–H stretching vibration of hydroxyl groups while the band at 1626 cm^{-1} was likely due to O–H bending of water molecules absorbed. The peak dominated by crystalline TiO_2 at 550 cm^{-1} Ti–O-Ti stretching mode declines in the samples of calcinated nanofibers and TiO_2 nanoparticles (Chun & Jo, 2014; Vasudevan, Thomas, Biju, Sudarsanakumar, & Unnikrishnan, 2012; Watthanaarun, Pavarajarn, & Supaphol, 2005; L. Zhang, Li, Zhang, & Wang, 2013). Figure 2.4 (b) shows the effect of calcination time on the removal of organic residuals through TiO_2 nanofibers formation from PVP/Ti(Iso) nanofibers by calcination. After 1 h calcination at 450 ^oC there were organic residuals; however, these residuals were completely degraded by increasing the duration of calcination.

2.2.4 Determination of crystallinity of TiO_2 nanofibers

The crystallinity of TiO_2 nanofibers which contain various amounts of Ti(Iso) (5 wt, 10 wt and 15wt%) before calcination at 450 °C for 6h was measured by Raman spectroscopy. The Raman spectra for all samples are shown in figure 2.5. All samples possess TiO_2 only in the anatase form with a small portion of the amorphous titania that decreases with the increasing amount of Ti(Iso). No rutile was detected at samples calcinated at 450°C. The size of anatase crystals was found to be very small at first. Nevertheless, after longer illumination by a laser, the thermal processes involved in the Raman spectroscopy generated bigger crystals.

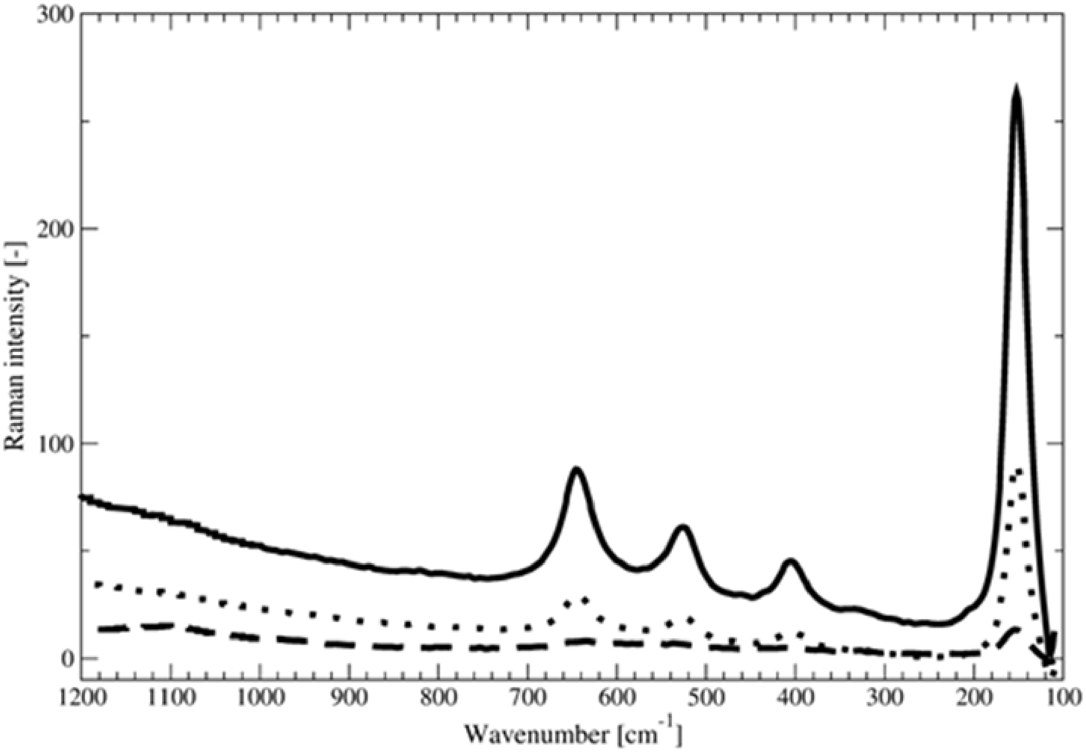

Figure 2.5 : Raman Spectra of PVP/TiO_2 with 5% TiO_2 (dashed line), 10 % TiO_2 (dotted line) and 15 % TiO_2 (full line).

X-ray diffraction patterns of were taken from the nanofibers, which were calcinated at 475 °C for 3 h at higher angles to evaluate the wall crystallinity (Figure 2.6 (a)).

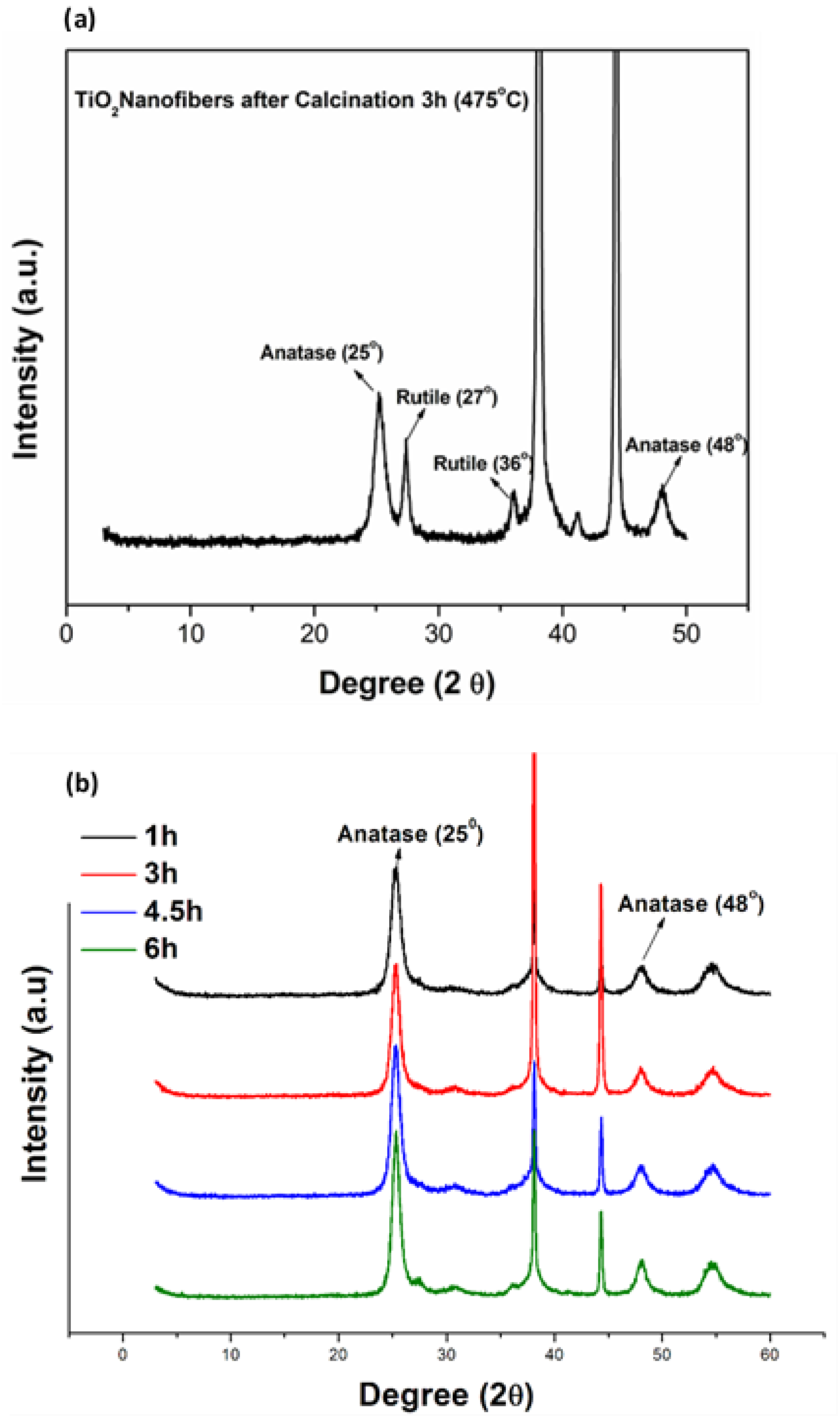

Figure 2.6 : XRD spectra of TiO_2 nanofibers after calcination at 475 °C for 3 hours (a) and at 450 °C for 1h, 3h, 4,5h and 6h (b).

XRD pattern of the sample shows that when calcination temperature increases at 475 °C, 20 wt% of the anatase TiO_2 in the nanofibers transforms to a rutile form (27° and 36°) while remaining 80 wt% of TiO_2 conserved in the anatase form (25° and 48°)

(Watthanaarun et al., 2005). The peaks at 35° and 45° correspond to the aluminum foil support. The data obtained from Raman spectrum and XRD prove that the ideal calcination temperature to obtain TiO_2 nanofibers in almost all anatase form is 450 °C. The crystallinity of TiO_2 nanofibers, which were calcinated at 450 °C for 1h, 3h, 4.5h and 6h, were analyzed by XRD, as well (Figure 2.6 (b)) and the crystal size of nanofibers were calculated in terms of Scherrer equation ($K=0.94$, $\lambda=1.542$ A°, $2\theta=25°$). The crystal sizes were calculated as 7.42 nm, 8.57 nm, 8.00 nm and 9.48 nm with respect to increasing calcinations time at 450 °C.

2.2.5 SEM analyses of calcinated TiO_2 nanofibers

The SEM images of TiO_2 electrospun nanofibers indicated that the fiber shape was still conserved after calcination at 450 °C for 6h (Figure 2.7 and 2.8).

Table 2.1 : Diameter distribution of TiO_2 nanofibers after calcination.

Temperature (°C)	**Calcination Time (h)**	**Ti(Iso) wt%**	**Diameter (nm)**
450	1	5	84±11
450	3	5	78±8
450	4,5	5	83±6
450	6	5	86±6
450	6	15	147±20

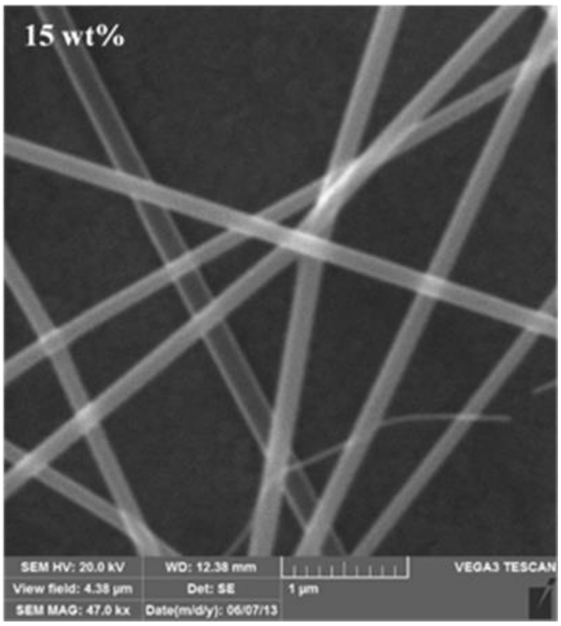

Figure 2.7 : SEM images of TiO_2 nanofibers containing 15 wt% Ti(Iso) after calcination at 450 °C for 6 h.

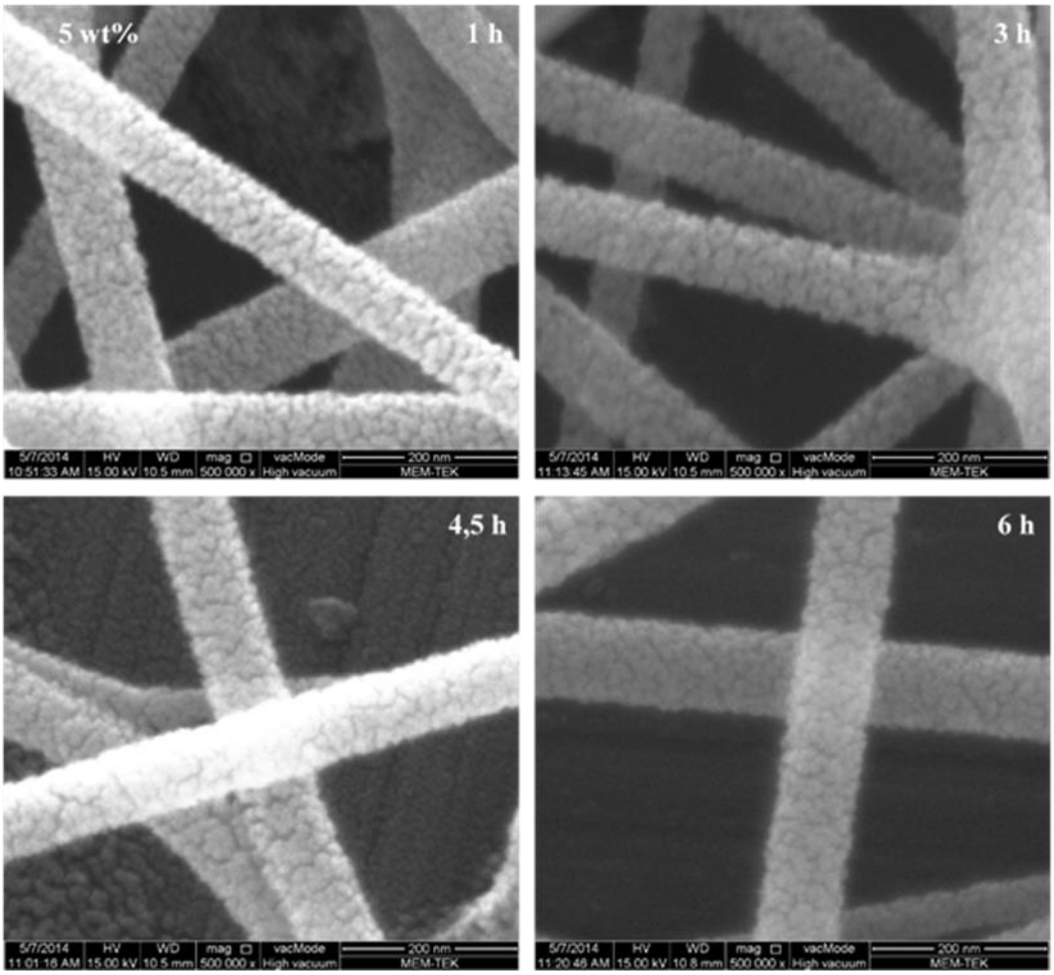

Figure 2.8 : SEM images of 5 wt% Ti(Iso) containing PVP/Ti(Iso) nanofibers with different calcination times.

The fiber diameters were significantly decreased and the average diameter was 147±20 nm after calcination of 15 wt% Ti(Iso) containing PVP/Ti(Iso) nanofibers compare to initial state. After calcination of nanofibers, TiO_2 nanofibers with narrow size distribution with porous surface were obtained. By the calcination of 5 wt% Ti(Iso) containing PVP/Ti(Iso) nanofibers the average diameter of 70-95 nm were obtained.(Figure 2.8). And also, it was found that calcination time did-not effect on diameters of TiO_2 nanofibers. These results were summarized in Table 2.1 (above).

2.2.6 Textural properties of PVP/Ti(Iso) and TiO_2 nanofibers

PVP with 5wt % of Ti(Iso) was chosen for evaluation of the influence of calcination temperature and time on texture properties. The obtained data of the individual samples were summarized in Table 2.2. It was obvious that even the untreated sample (PVP/Ti(Iso)) possesses a relatively high surface area (20 m^2/g) with poly-dispersed pore-size distribution. With the increasing calcination temperature, the original poly-disperse structure of the pore-size distribution has become mono-disperse, even after the one-hour long calcination. The mono-disperse structure with the significant peak at 2–4 nm occurred with the sample calcinated at 450 °C. Similarly, the increase of BET surface area can be easily detected with the maximum 100 m^2/g again for the sample calcinated at 450 °C for 1 hour. Another increase of the calcination temperature up to 500 °C caused a sharp reduction of the surface area at the value of the untreated sample. It is probably caused by the sintration of TiO_2 nanofibers, which is also assisted by the gradual transformation of the crystallographic form to brookite and rutile which corresponds with literature data provided in literature, e.g. (Enriquez & Pichat, 2006; Matějová, Matěj, & Šolcová, 2012; Schattauer et al., 2012). Thus, the textural analysis confirmed 450°C as the optimal calcination temperature for the preparation of TiO_2 nanofibers.

Table 2.2 : Effect of different calcination temperature and time on texture properties.

Sample	**S_{BET} (m^2/g)**	**S_{meso} (m^2/g)**	**V_{micro} (liq) (mm^3/g)**	**r_p (nm)**
PVP/Ti(Iso)	19.9	14.8	2.7	1;12;30
PVP/TiO_2 (400°C) 1h	30.3	26.6	2.9	1;2;12
PVP/TiO_2 (450°C) 1h	99.7	63.4	19.8	2;4
PVP/TiO_2 (500°C) 1h	20.7	15.1	2.8	4
PVP/TiO_2 (450°C) 3h	128.2	83.2	27.8	2;3
PVP/TiO_2 (450°C) 4,5h	93.5	69.8	16.8	2;3
PVP/TiO_2 (450°C) 6h	72.8	53.1	13.6	2;3

According to the TGA analysis, the remaining organic residuals in prepared nanofiber TiO_2 layers were completely decomposed between 400°C and 480°C. Nevertheless, in this process not only calcination temperature but also calcination time plays an important role. Therefore, the influence of calcination time on texture properties of prepared materials was studied. It is evident (Table 2.2) that the surface area of TiO_2 nanofiber layers goes through the maximum for three hours calcination at 450 °C.

The longer calcination time and the higher calcination temperature which caused the crystal enlargement and subsequently the decrease of surface area (Krysova et al., 2014; C.-H. Lin, Chao, Liu, Chang, & Wang, 2008; Yu, Yu, Cheng, & Trapalis, 2006). However, the extension of calcination time had no impact on pore-size distribution of the tested samples.

2.2.7 Photoelectrochemical measurements of TiO_2 nanofibers

Amperometry measurements (Figure 2.9) express the ability of the TiO_2 nanofiber layer on ITO electrode to produce measurable photocurrent values during the irradiation interval at constant potential 0.6 V. The obtained curves indicate the photocurrent-time behaviour of the TiO_2 nanofiber layers, where the photocurrent densities varied between 0.5 - 1 μA/cm^2. These results correspond with the works by Kerkez (Kerkez & Boz, 2014) and Lv (Lv, Zhang, & Chang, 2012), who obtained similar photocurrent densities (1-3.5 μA/cm^2) for pure TiO_2 nanorods under comparable conditions. All measured TiO_2 samples containing various amounts of Ti(Iso) (5 wt, 10 wt and 15 wt%) before calcination embodied a very fast reaching the maximal current density values, almost immediately at the first moment under the light.

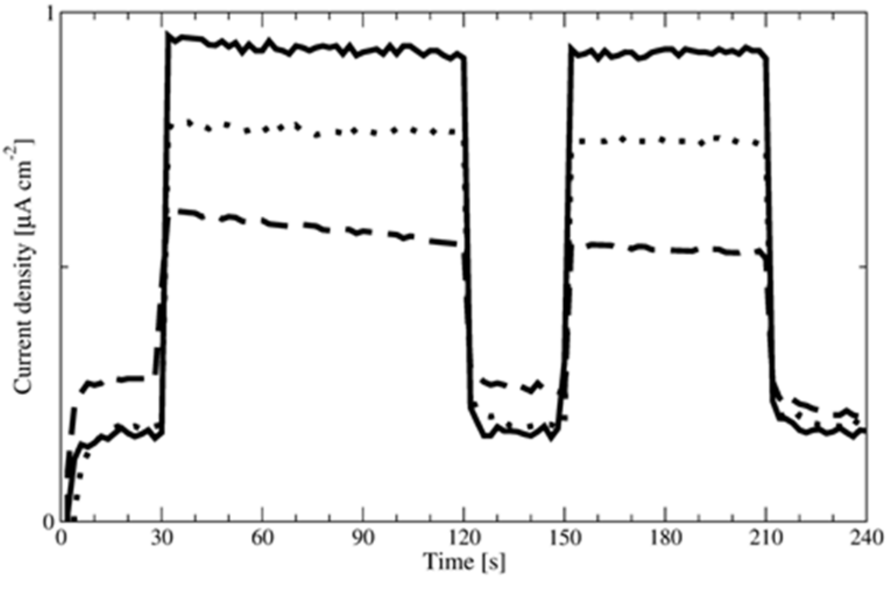

Figure 2.9 : Photocurrent-time behavior of the nanofiber layer of TiO_2 on ITO electrode, PVP/TiO_2 with 5wt% TiO_2 (dashed line), 10wt% TiO_2 (dotted line), 15wt% TiO_2 (full line).

Further, the curves stay at the reached steady state current densities during the irradiation time. The instantaneous increase of current density values means a rapid electron-hole pairs generation and separation at the space charge region. Almost no decrease that would correspond to their recombination was detected. The influence of the amount of titania is evident; the current density values increase proportionally to the increasing amount of initial Ti(Iso) precursor in prepared nanofiber layers.

2.3 Conclusion

PVP/Ti(Iso) nanofibers with Ti(Iso) concentrations up to 15 wt% were successfully fabricated without any beads. The average diameter of pure PVP nanofibers was in the range from 400 to 600 nm. PVP/Ti(Iso) nanofibers exhibited irregular shapes with fiber diameters between 100 and 700 nm depending on the Ti(Iso) concentration. FTIR-ATR Spectra confirmed the incorporation of Ti(Iso) into PVP/Ti(Iso) nanofibers. According to TGA analysis and the physical adsorption of nitrogen the calcination temperature at 450 °C, which guarantees no organic residual and really good texture properties (surface area about 100 m^2/g), was chosen as the optimal calcination temperature for the preparation of TiO_2 nanofibers. All prepared samples possess TiO_2 in the anatase form with a small portion of amorphous titania that rapidly decreases with the increasing amount of titania.

The photoelectrochemical efficiency of the nanofiber TiO_2 layers was determined by the amperometry measurements. It was proved that TiO_2 nanofiber layers/ITO electrodes prepared by electrospinning (TiO_2 thin nanofiber layers on ITO glass used as photoanode) are highly stable and possess really good photoinduced properties. The obtained electrochemical curves of nanofiber layers reflect the ability to react to a UV light signal by generating charge carriers. The electrochemical measurements confirmed a high potential of the TiO_2 nanofiber layers prepared by electrospinning for a variety of photoelectrochemical applications where the precisely tailored structure, morphology and texture of TiO_2 based layers are required.

3. THE EFFECT OF DEPOSITION ON ELECTROCHEMICAL IMPEDANCE PROPERTIES OF TiO_2/FTO PHOTOANODES[2]

Dye-sensitized solar cells (DSSCs) are great candidates as next generation photovoltaic devices to substitute for Si-based solar cells since they have higher theoretical energy conversion efficiency and low fabrication cost. A typical DSSC consists of three main components: dye-sensitized photoanode, Pt-coated counter electrode, and electrolyte containing redox active species. The nanostructured photoanode of a DSSC plays a critical role in dye absorption and charge transport (Saji & Pyo, 2010). Therefore it is the key component which affects the whole efficiency of a DSSC system. Since an optimal DSSC substrate should have high transparency, low sheet resistance, and good stability (Miettunen et al., 2009), titanium dioxide (TiO_2), especially in the anatase form, is one of the most promising materials for solar cells with respect to its unique properties, such as high refractive index, low absorption coefficient and photocatalytic activity (T. Berger et al., 2006; Fujihara et al., 2007; Gao et al., 2008; Viswanathamurthi et al., 2004). Conventionally, TiO_2 nanoparticles are used for photoanode, however TiO_2 in a one-dimensional (1-D) nanostructured forms such as nanofibers, nanowires, nanotubes and nanoribbons, enhance the performance and efficiency of the device (Tammawat & Meethong, 2013). These 1-D TiO_2 structures with ultrahigh specific surface area guarantees a good dye-loading and a light-harvesting due to their higher electrode/electrolyte contact area and shorter transport path lengths for electrons (Saji & Pyo, 2010).

Electrospinning is one of the easiest and the cost effective way to fabricate nanofibers (NFs) of TiO_2 (Barakat et al., 2012). It provides a great control over dimensions, surface area and morphology of nanofibers which possess high surface area to mass or volume ratio (Formo, Lee, Campbell, & Xia, 2008). However,

---

[2] This chapter based on the paper “Balkan, T., Guler, Z., Morozova, M., Dytrych, P., Solcova, O. and Sarac, A.S. (2016). The Effect of Deposition on Electrochemical Impedance Properties of TiO_2/FTO Photoanodes, *Journal of Electroceramics*, 36(1), 102-111’’.

fabrication of TiO_2 nanofibers is not the challenging part; it is the integration of these nanofibers onto a suitable substrate. For the electronic devices it is necessary to deposit the metal oxide nanofibers onto the conductive substrate. An optimal electrode substrate should form a low resistance ohmic contact with the TiO_2 layer while it effectively blocks an electron transfer to the oxidized species in the electrolyte. Fluorine-doped tin oxide-coated glass (FTO-glass) serves these properties therefore; FTO-glass is the most commonly used substrate for DSSC photoanode (Miettunen et al., 2009). The composite fibers could easily crack and peel off the substrate after calcination due to the shrinking effect and the poor adhesion (Du, Song, Xiong, & Cui, 2013; Zhu et al., 2008). In our previous study, TiO_2 nanofibers were fabricated by an electrospinning of a sol-gel solution (PVP/Ti(Iso)). The detailed description of the electrospinning set-up and properties of the TiO_2 nanofibers had been reported previously (Solcova et al., 2014). A very thin film of TiO_2 nanofiber layer was deposited onto ITO-glass since we also observed partial cracks on nanofiber layer. Although, this integration problem limits the application potential of TiO_2 nanofibers on DSSC systems, several studies have been aimed to solve this problem, and various pre-treatment methods have been developed. The composite fibers were treated with THF solvent vapour and adhesion of the calcinated nanofiber films were enhanced by Kim et.al. (Song, Kim, Ihn, Jo, & Kim, 2004). Onozuka et al. (Onozuka et al., 2006) employed a similar treatment by using DMF. They also applied a hot press treatment for the composite fibers to enhance their adhesion (Kokubo, Ding, Naka, Tsuchihira, & Shiratori, 2007). Ramakrishna et al. obtained short nanorods from long nanofibers by mechanical grinding (Fujihara et al., 2007). In addition, Ramakrishna’s group developed an improved method by depositing an ultrathin layer between nanofiber film and glass substrate to enhance the interfacial adhesion (Zhu et al., 2008). These methods have made a substantive progress in solving the adhesion problem. However, these studies are focused only on adhesion problem and the comparison of photo-electrochemical and electrochemical properties of these types of the electrodes were limitedly investigated.

In this study, we focused on the investigation of deposition method effect on electrochemical impedance and photo-electrochemical properties of TiO_2/FTO photoanode prepared by three different deposition techniques. The TiO_2 nanofibers were in all cases fabricated by electrospinning of a sol-gel solution (PVP/Ti(Iso)). Three electrodes were fabricated on FTO substrate by calcination of PVP/Ti(Iso) layer following to dip-coating of sol-gel solution, electrospinning on the dip-coating solution and electrospraying of calcinated and breaked TiO_2 nanofibers. This study represents a comparison of effects of various deposition techniques on the structural, photo-electrochemical and electrochemical impedance properties of electrodes.

3.1 Experimental Part

3.1.1 Preparation of TiO_2 electrodes

In order to prepare stable electrodes for photo-electrochemical measurements, three methods were performed (Figure 3.1). In the first method, sol-gel solution of polyvinyl pyrrolidone/titanium(IV) isopropoxide (PVP/Ti(Iso)) was deposited onto fluorine-doped tin oxide (FTO, Solaronix, 7 Ω/sq) by dip-coating (Dip-coating/FTO electrodes), in second the sol was electrospun onto previous electrodes and they called as Dip-coating-Nanofiber/FTO electrodes. In the third method, the annealed TiO_2 fibers ultrasonically dispersed in ethanol to get nanorods and then coated directly onto FTO glass substrate were used for preparation of Nanorod/FTO electrodes.

The sol-gel solution for electrospinning was prepared from polyvinyl pyrrolidone (PVP, Mw=1.300.000 g/mol, Acros Organics), ethanol (EtOH, Merck, Analytical Grade), titanium (IV) isopropoxide (Ti(Iso), 98%, Sigma-Aldrich) and acetic acid (Analytical Grade, Merck). The polymeric solution was prepared by dissolving PVP in EtOH (10 wt %). Ti(Iso) (0.45 g) was added to the PVP solution (2.55 g) together with acetic acid (0.5 mL). The resulting solution was stirred for 1 h at 25 °C before electrospinning and dip-coating processes.

In order to prepare dip-coating/FTO electrodes, FTO-glasses (0.5x2.5cm) were dipped into the electrospinning solution and withdrawn slowly to obtain thin films at room temperature. The dipping time was 15 s.

The TiO_2 nanofibers were prepared as follows: Electrospinning was carried out at a 10 kV accelerating voltage (Gamma High Voltage) and at a 1 mL/h flow rate (New-Era Syringe Pump). The polymeric nanofibers containing Ti(Iso) were collected on Dip-coating/FTO electrode placed 10 cm away from spinneret. To obtain the Dip-coating-Nanofiber/FTO electrodes, Ti(Iso)/PVP nanofibers were deposited on the Dip-coating/FTO electrodes for 3 min. The samples were sintered air at 450 °C to remove PVP and allow nucleation and growth of TiO_2 particles in the fiber structure.

In the third method; typically 1 g of nanofibers was ultrasonically dispersed in 100 mL of EtOH for durations of 5 min to 20 min to obtained TiO_2 nanorods. Dispersed TiO_2 nanorods were coated directly on FTO glass substrates by electrospraying for 3 min with the feed ratio of 5 mL/h without using any addition of adhesive. Then, these electrodes (Nanorod/FTO) were dried at 80 °C to remove EtOH.

All three types of electrodes were calcinated at 450 °C at a rate of 2.5 ^{o}C/min for 3 h in a furnace (NEY 2-525 Series II, USA).

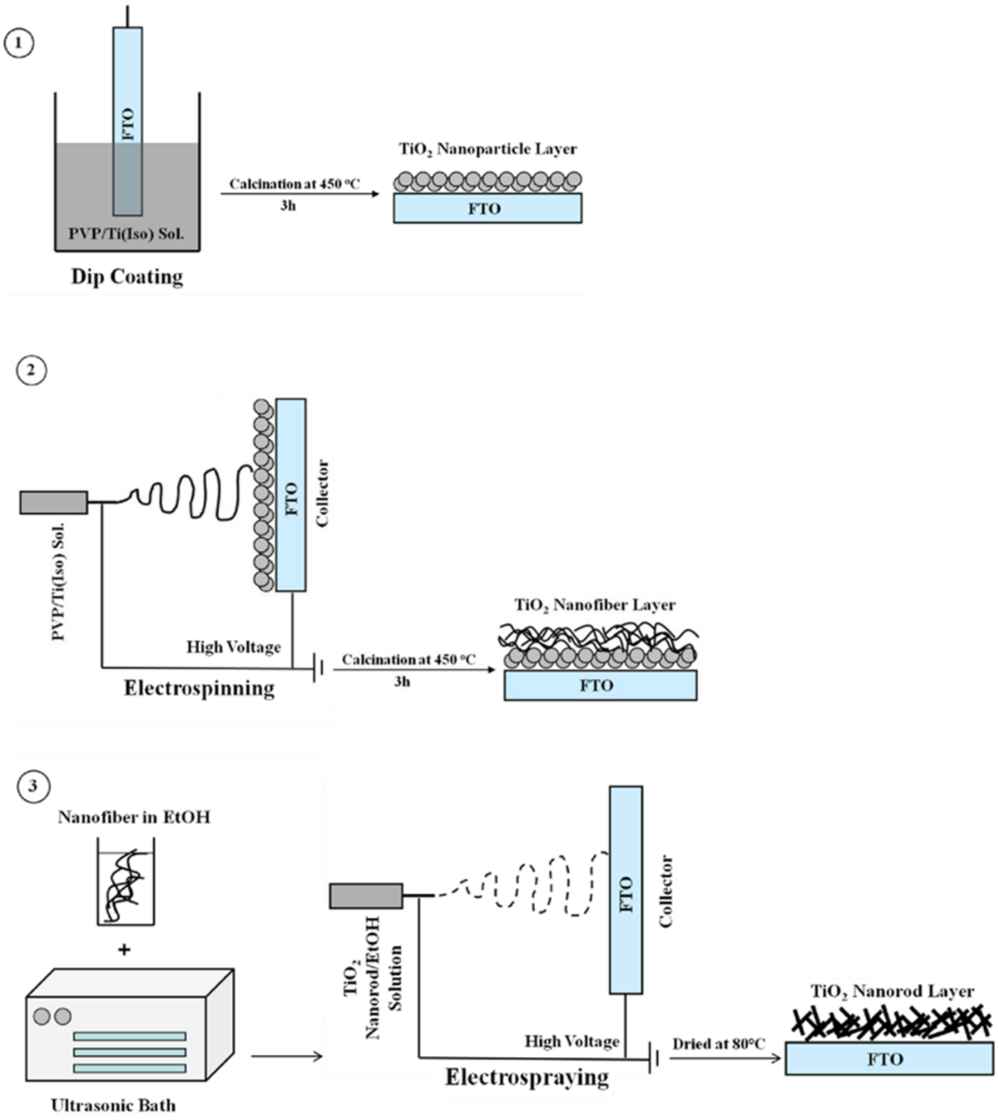

Figure 3.1 : Schematic view of production process of the electrodes.

3.1.2 Characterization of TiO_2 electrodes

Structural analyses of nanofibers were performed by FTIR-ATR (Perkin Elmer FTIR-ATR Spectrophotometer Spectrum One with universal ATR attachment with a diamond and ZnSe crystals before and after calcination process. The structure of the electrodes was analysed by XRD (Shimadzu XRD-6000) and the Raman spectroscopy (Nicolet Almega XR; ThermoNicolet, USA) with wavelength 473 nm. Surface morphologies were determined by SEM (SEM-FEI Quanta 450 FEG-EDS) and thicknesses of the electrodes were measured with Image J program.

Electrochemical impedance spectroscopy (EIS) was employed to study electron transport and the quality of the prepared TiO_2/FTO electrodes, by using Parstat 2263 potentiostat (Princeton Applied Research, USA). EIS measurements were performed in a three electrode configuration. TiO_2/FTO electrodes as working, a platinum wire as counter and a silver wire as a pseudo reference electrode were used. The pseudo reference was calibrated externally using a 5 mM solution of ferrocene in the electrolyte ($E_{1/2}$ (Fc/Fc^+)) = +0.51 V vs. silver wire in of 0.1 M $NaClO_4$/ACN). All measurements were performed in the frequency range of 0.01 Hz – 100 kHz and AC voltage of 10 mV at an applied bias of open-circuit voltage. The responds of working TiO_2/FTO electrodes were measured from the surface area of 1 cm^2 which were dipped into the electrolyte solution of 0.1 M $NaClO_4$/ACN. All measurements were repeated three times for confirmation. Equivalent circuit modelling for the simulation of the EIS spectra of the TiO_2/FTO electrodes was performed with ZSimp Win programme (v3.10).

Photo-induced electrochemical properties were measured by electrochemical methods (cyclic voltammetry, linear voltammetry, amperometry) combined by the UV light irradiation in the three-compartment electrochemical cell. As an electrolyte water solution of 0.1 M Na_2SO_4 or non-aqueous solution of 0.1 M $NaClO_4$/ACN (acetonitrile) were used. The TiO_2/FTO electrode served as a working electrode with exposed area of 1 cm^2. A saturated Ag/AgCl electrode and a platinum plate were used as the reference and the auxiliary electrodes, respectively. The polychromatic mercury lamp was employed as the UV source. The incident light (365 ± 5nm) was used for the irradiation of samples, with the light intensity of 1 mW/cm^2 in the most experiments. The photoelectrochemical reaction was monitored by the computer-controlled Voltalab 10 PGZ-100 potentiostat. The detailed description of the electrochemical set-up and the used electrochemical methods had been reported previously (Morozova et al., 2011).

3.2 Results and Discussion

3.2.1 Morphologies of TiO_2 nanoparticles, nanofibers and nanorods

Morphologies of three types of electrodes were characterized by scanning electron microscopy (SEM). SEM images and cross section views of the electrodes are shown in Figure 3.2. From the cross section views, multilayer structure of electrodes can be seen clearly. Figure 3.2 (a) represents TiO_2 nanoparticle layer onto the FTO glass substrate. According to Figure 3.2 (a) deposition of the TiO_2 NPs layer were achieved homogeneously. For dip-coating-nanofiber/FTO electrodes, a nanoparticle layer is sandwiched between the FTO glass substrate and the TiO_2 nanofiber layer. The total thickness of the electrode film is nearly 6 µm (Figure 3.2 (b)). The average diameter of the nanofibers is about 120-180 nm. Figure 3.2 (c) shows TiO_2 nanorod/FTO electrodes. The cross section view (Figure 3.2 (c)) of TiO_2 nanorod/FTO electrodes looks like more dense compare to surface view because convenient covered region was chosen to measure thickness of TiO_2 nanorods film.

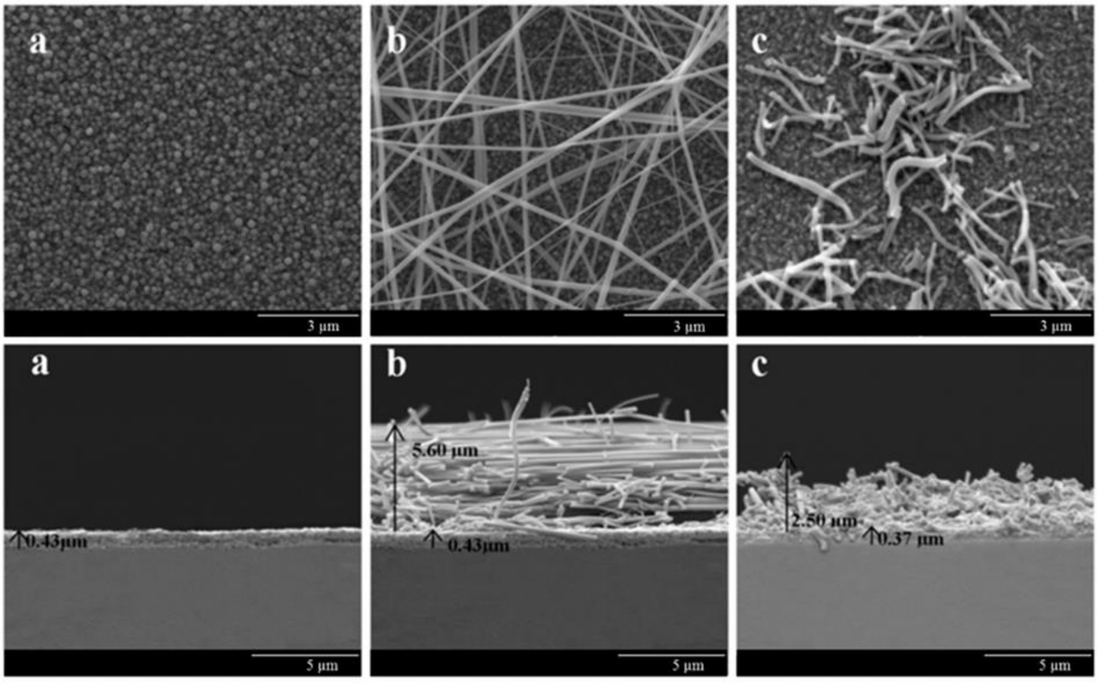

Figure 3.2 : Top and cross-section SEM images of Dip-coating/FTO (a), Dip-coating-Nanofiber/FTO (b) and Nanorod/FTO electrodes (c).

3.2.2 Crystallographic and spectrophotometric characterization

Crystallinity of the TiO_2 based electrodes were analysed by XRD analysis and Raman spectroscopy. Figure 3.3 shows an XRD pattern of the calcined samples. The diffraction peaks can be indexed to the (101), (200) and (211) crystallographic planes of (tetragonal) anatase-phase TiO_2 according to JCPDS No. 21- 1272 after calcination at 450 °C in air for 3 h. Two peaks with the biggest intensity belong to the aluminium foil support. The crystal sizes of TiO_2 nanoparticles, nanofibers and nanorods were calculated as 17.73 nm, 7.15 nm and 7.88 nm, respectively, in terms of Scherrer equation ($K=0.94$, $\lambda=1.542$ A°, $2\theta=25°$).

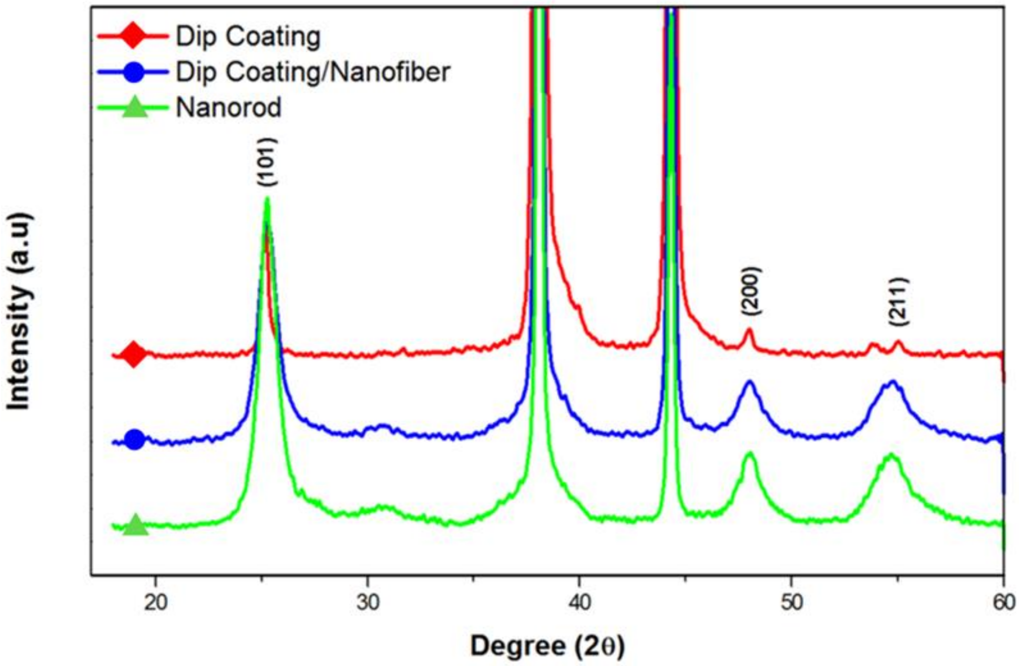

Figure 3.3 : XRD patterns of calcinated electrodes.

Obtained results were corroborated by Raman spectra which are depicted in Figure 3.4. It can be seen that all samples possess the crystal structure of anatase. For all types of samples the characteristic phonon modes were observed app. at 650, 525, 400 and 150 cm^{-1} (H. Berger, Tang, & Levy, 1993; Lagarec & Desgreniers, 1995). Dip-coating/FTO electrodes reveal the most crystalline structure with rather small crystals with size below 20 nm. The lowest crystallinity was observed for Nanorod/FTO electrodes.

FTIR-ATR results also supported absence of PVP and formation of TiO_2 in the nanofibers. After calcination of nanofibers all specific peaks of PVP (especially C=O vibration at 1650 cm^{-1}) units disappeared and vibration of Ti-O-Ti bond was observed at 550 cm^{-1} in Figure 3.5 (Solcova et al., 2014).

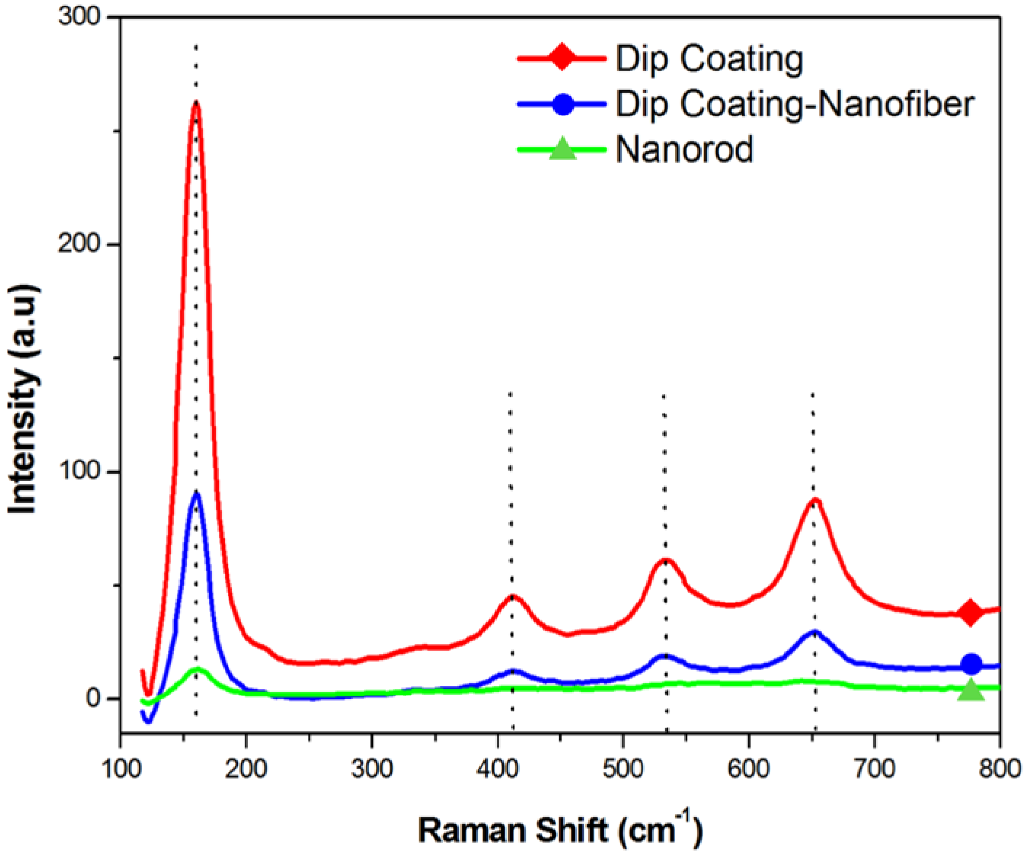

Figure 3.4 : Raman spectra of calcinated three types of electrodes.

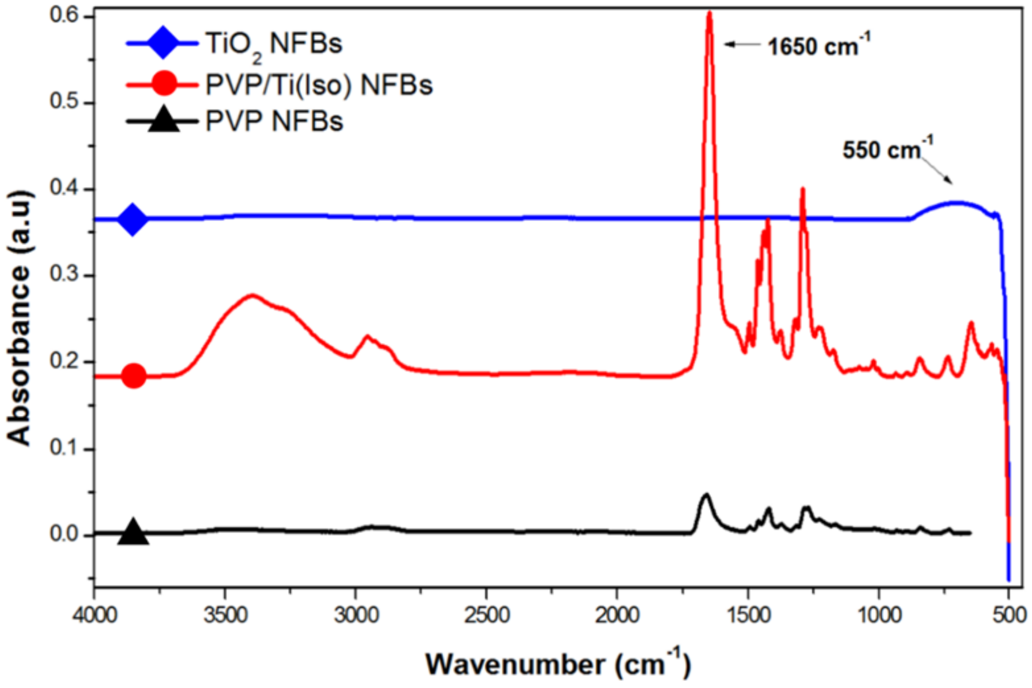

Figure 3.5 : FTIR-ATR spectrum of TiO_2 nanofibers before and after calcination.

3.2.3 Impedance spectroscopy and equivalent circuit modelling

Physicochemical and interfacial properties of TiO_2/FTO electrodes prepared by three different techniques were determined by electrochemical impedance spectroscopy (EIS). The EIS data provide information about the nature of electrochemical process occurring at the electrode/electrolyte interface (Gu, Su, & Loh, 2005). During EIS measurements, electrodes exhibited electroactivity and stability, without any deformation or decomposition.

Nyquist plots of Dip-coating/FTO electrode and Dip-coating-Nanofiber/FTO electrode exhibited a semi-circle (Figure 3.6 (a)) (Sarac, Gencturk, Schulz, Gilsing, & Serantoni, 2007). Dip-coating/FTO electrode with 30 degrees of phase angle showed nearly resistive behaviour. Dip-coating/FTO electrode with the TiO_2 nanofiber layer on top, exhibited 40 degrees phase angle (Figure 3.6 (b)) which indicates nanofiber layer enhance the electrical properties of Dip-coating/FTO electrodes. The maximum phase angle values of three types of electrodes changed at higher frequency domain of Bode phase plots. This change in phase angle represents the additional capacitive elements arising from deposited layers on the electrode surface and electronic behaviour of electrodes (De Crombrugghe, Yunus, & Bertrand, 2008; Gu et al., 2005; Sarac, Gencturk, et al., 2007). The medium frequency response can be related with the porosity of the TiO_2 electrodes. This response in medium frequency is determined by the electronic and ionic conduction through the porous TiO_2 (Rammelt, Hebestreit, Fikus, & Plieth, 2001).

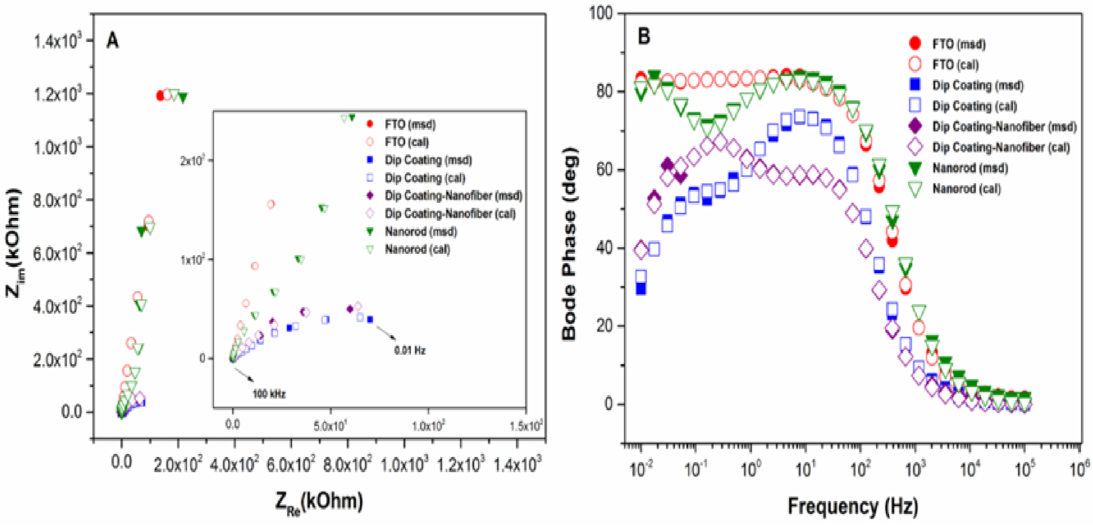

Figure 3.6 : Nyquist (A), and Bode Phase (B) plots of three types electrodes indicating that measured and calculated data.

The EIS spectra were modelled to evaluate kinetics of the systems by using ZSimpWin software and calculated data and measured data which were well fitted with the chosen equivalent circuit (Figure 3.7). The circuits which describe the physical properties of the system and provide a good fit to the measured data with a reasonable number of circuit elements and low fitting Chi-squared errors were chosen. The errors values were in the range of 10^{-4} which is regarded as low and represented precise measurement (Dagli, Guler, & Sarac, 2015; Guler & Sarac, 2016). The electrodes have layers consisting of a porous layer formed with TiO_2 in different forms and of a more compact layer (FTO). The interfacial properties of a layered electrode give rise to different equivalent circuit models. Therefore equivalent circuits consisting of capacitances and resistances were chosen in order to describe the electronic and ionic conduction through the porous layer and a high frequency time constant for the compact layer at the interface between TiO_2 and FTO (Rammelt et al., 2001). The chosen model accounts for the interfacial charge transfer at the TiO_2/electrolyte boundary as well as for reactions in the pores and solid layer (Kityakarn et al., 2012). At higher frequencies, resistance of the solution is predominant while the capacitance and resistance phenomena occurring at the TiO_2/FTO interface predominate (Acevedo-Peña et al., 2009). Besides capacitors and resistors or their combinations, it is necessary to employ constant phase elements (CPE) to take disorders into account in the electrode structure (Kityakarn et al., 2012). The impedance spectra for Dip-coating-Nanofiber/FTO, Dip-coating/FTO and Nanorod/FTO electrodes and FTO described by the equivalent circuits of R(QCR)(CR)(CR), R(QCR)(CR), R(QCR)(CR) and R(QCR) respectively (Figure 3.7). The resistances and capacitors in circuit represent various complex interfacial processes between TiO_2 layers, FTO and electrolyte (Archana, Jose, Yusoff, & Ramakrishna, 2011; Mukherjee, Teng, Jose, & Ramakrishna, 2009). The first component of the circuits was the solution resistance of the electrolyte, (R_s) (R. Li et al., 2010). The solution resistance (R_s) is defined as the sum of resistances due to the presence of the electrolyte on the surface of electrode. R_s value for Dip-coating/FTO electrode and Dip-coating-Nanofiber/FTO electrode was 64.91 Ω and 80.76 Ω, respectively. The Rs values correspond to the behaviour of the electrolyte, filling pores of the TiO_2 layers (Radecka, Wierzbicka, & Rekas, 2004). Since the nanofiber layer has a more porous structure than dip-coating layer, the electrodes with nanofibers have higher solution resistance. It was reported that electrodes with higher photoactivity (Dip-coating/FTO electrodes, in our case) have smaller electrolyte resistance (Kityakarn et al., 2012). Q corresponds to constant phase element (CPE). CPE was applied in the equivalent circuit for the simulation of the impedance data. The presence of the CPE can be attributed to the nanofiber composition, and to the inhomogeneity in conductance (Giray, Balkan, Dietzel, & Sarac, 2013). CPE is defined by the formula of ($Z_{CPE} = T_{CPE}(jw)^{-n}$) where TCPE and n are frequency-independent constants; w is the angular frequency (Gu et al., 2005). The exponent n of CPE which, arises from the slope of the log Z versus log f plot, is a manifestation of the electrode nature and it is a correction factor related the inhomogeneity and roughness of electrode surface. The values for n are ranging between 0 and 1. n = 1 denotes the CPE element is an ideal capacitor, while n=0 and 0.5, denotes a resistance and Warburg behaviour, respectively (H. Li et al., 2009). Table 3.1 represents the fitting parameters for the equivalent circuit elements by modelling of the impedance spectra in Figure 3.6. The n values for Dip-coating/FTO and Dip-coating-Nanofiber/FTO electrodes were 0.70 and 0.50 respectively; which indicates that the TiO_2 nanofiber layer reduce the capacitive behaviour of electrodes. The film of TiO_2 nanofibers has higher surface area and porous structure than TiO_2 dip-coating layer; therefore the addition of nanofiber layer onto Dip-coating/FTO electrodes increased the porosity of the electrodes and enhanced the diffusion process. First C of the circuits for three types of electrodes was attributed to double layer capacitance (C_{dl}) between electrolyte and TiO_2 layer onto electrode surface. C_{dl} arises from alignment of solvated counter ions along electrode surface. The electron transfer through electrode occurs by overcoming activation barrier, charge transfer resistance and solution resistance. Once the electron transfer begins, the electrode kinetics determined by Warburg impedance (W) due to the mass transport (J.-Y. Park & Park, 2009). C1 for Dip-coating/FTO electrodes was ($1.19x10^{-5}$ F) and it was slightly increased with addition of TiO_2 nanofiber layer ($1.36x10^{-5}$ F). C2 represents the capacitance between TiO_2 layers (dip-coating or nanorod) and FTO. For Dip-coating-Nanofiber/FTO electrodes, another capacitance (C3) is added to circuit to explain the capacitance ($19.35x10^{-5}$ F) between TiO_2 nanofibers and TiO_2 particle thin film. The difference between these capacitance values can be explained by the different interfacial structures, assuming different particle sizes and particle surfaces for TiO_2 nanoparticles and FTO or by the different structures of TiO_2 such as nanofiber, nanorod or particle (Kityakarn et al., 2012). Other two R, correspond to the charge transfer resistance (R_{ct}) between the electrolyte and electrode surface (R1) or the different layers of electrodes (R2) (R. Li et al., 2010). R1 represents the charge transfer resistance between electrolyte and TiO_2 layers. The R1 of 1.27×10^5 Ω for Dip-coating/FTO electrodes was decreased to 310.40 Ω for Dip-coating-Nanofiber/FTO electrodes. R2 is attributed to R_{ct} between TiO_2 layers and FTO. R2 values for Dip-coating/FTO and Dip-coating-Nanofiber/FTO and Nanorod/FTO electrodes were 2823 Ω, 1.03×10^5 Ω and 1.13×10^8 Ω, respectively. Dip-coating-Nanofiber/FTO electrodes also have another R_{ct} (R3) at the interphase between TiO_2 nanofibers and particles. The conductivity of the porous TiO_2 layer depends on the geometry of the contact zone and structure of TiO_2 layers (Kityakarn et al., 2012). Densely packed nanocrystalline TiO_2 layer allows the formation of an energy barrier at the electrode/electrolyte interface and enhances the percolation of electrons by acting as an effective hole-blocking layer and decrease the charge transfer resistance (Mane, Lee, Pathan, & Han, 2005).

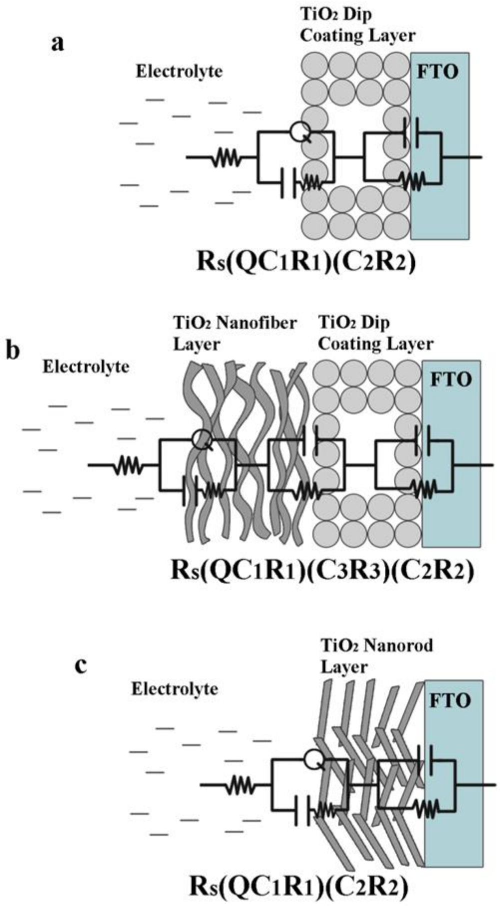

Figure 3.7 : Equivalent circuit for the simulation of the EIS spectra of Dip-coating/FTO (a), Dip-coating-Nanofiber/FTO (b) and Nanorod/FTO (c) electrodes.

TiO_2 nanorod/FTO electrode showed a vertical line in Nyquist plot (Figure 3.6 (a)) and exhibited high capacitance of approximately 80 degrees phase angle (Figure 3.6 (b)). The 1-D nanorods act as a single crystal and provide rapid electron transport. The TiO_2 layer with random packing of 1-D nanorods helps the electrolyte to penetrate into the electrode because of the porosity. 1-D structure of TiO_2 nanorods induce fast electron transport and enhance the photoactivity (Jung, Park, Oh, Kim, & Hong, 2013). However, the photocurrent density of the Nanorod/FTO electrode was the lowest compared to other two types of electrodes. Moreover, the electrochemical impedance spectra of TiO_2 Nanorod/FTO electrodes are quite similar to those of FTO-glasses. This result was expected because the stability and adhesion of TiO_2 nanorod layer on FTO-glass were weak and the nanorod layer was peeling of the FTO-glass surface as shown in SEM images (Figure 3.2 (c)). Therefore, their response during EIS measurements interfered with the response of the FTO-glass. For Nanorod/FTO electrodes, the n value was 0.90 while n value of FTO was 0.88 (data not shown), which indicates almost an ideal capacitor with a porous structure (Rodríguez-Sevilla, Ramírez-Silva, Romero-Romo, Ibarra-Escutia, & Palomar-Pardavé, 2014). Charge transfer resistance (R2) between TiO_2 nanorod and FTO was found 1.13×10^8 Ω and it may be related with the discontinuities at electrode surface.

Table 3.1 : Fitting values for the equivalent circuit elements by the simulation of the impedance spectra in Figure 3.6.

CIRCUIT NOTATION	**Dip-coating/FTO R(QCR)(CR)**	**Dip-coating-Nanofiber/FTO**	**Nanorod/FTO R(QCR)(CR)**
R_s(Ω)	64.91	80.76	69.28
Q (10^{-5})	5.29	15.38	1.38
C1(F) (10^{-5})	1.19	1.36	1.00E-15
R1(Ω)	1.27 E5	310.40	5.88 E4
C2(F) (10^{-5})	6.12	15.24	1.31
R2(Ω)	2823	1.03 E5	1.13 E8
C3(F) (10^{-5})	-	19.35	-
R3(Ω)	-	8964	-
n	0.70	0.50	0.90
Chi-squared error (10^{-4})	7.71	8.64	1.41

Electrolyte, solvent and counter ions can penetrate the porous TiO_2 layer and form a three-dimensional interface (Rammelt et al., 2001). This penetration explains the increase in double layer capacitance (C1) and capacitance (C2) when porous TiO_2 nanofiber layer was introduced into the electrodes.

3.2.4 Photo-electrochemical measurements of electrodes

Amperometry measurements were applied to obtain the ability of the prepared TiO_2/FTO electrodes to produce the measurable photocurrent values during the irradiation interval at constant potential 0.6 V. Two supporting electrolytes aqueous (0.1M Na_2SO_4) and non-aqueous solution of 0.1M $NaClO_4$/ACN were used. The obtained curves (see Figure 3.8) indicate the photocurrent-time behaviour of the three various TiO_2/FTO electrodes.

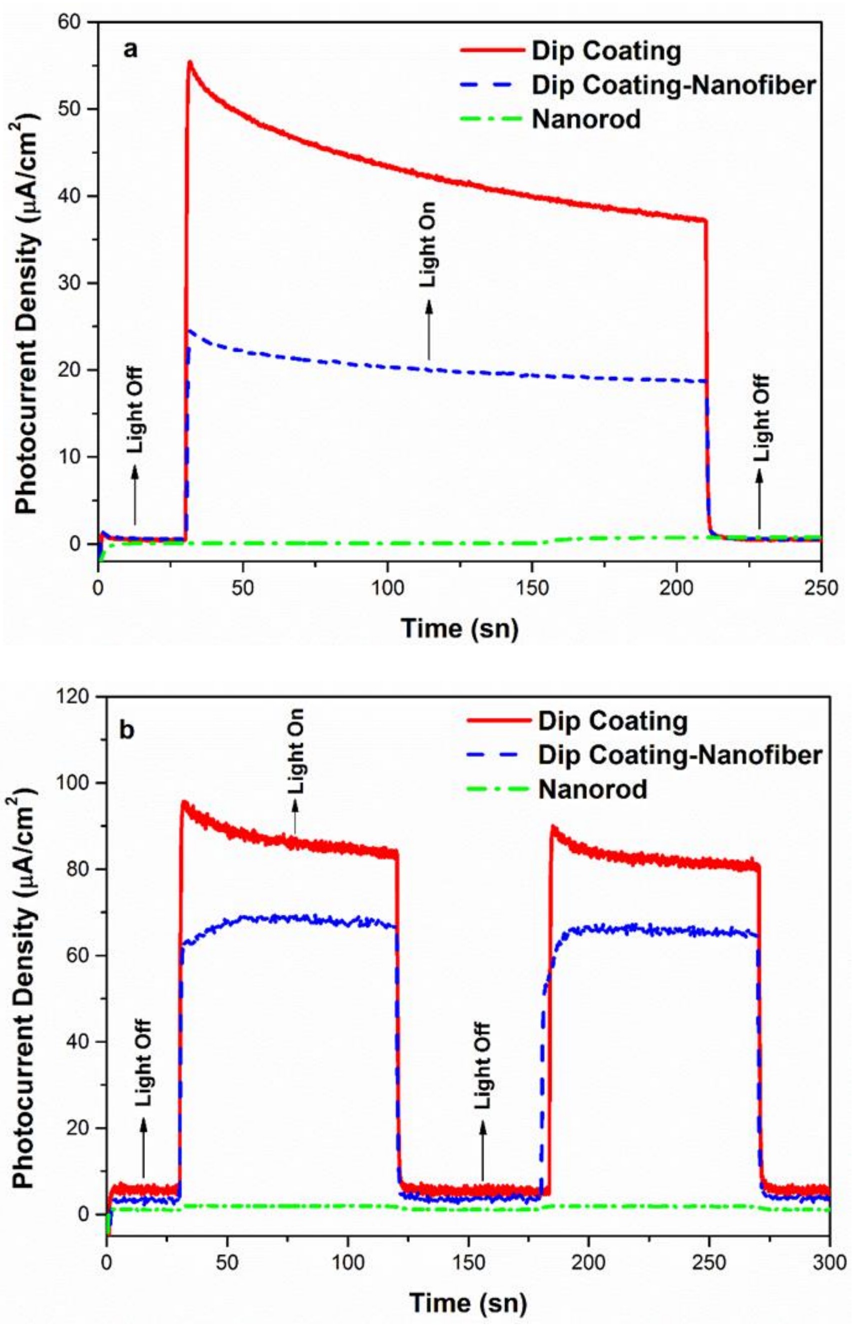

Figure 3.8 : Photocurrent-time behaviour of the three various TiO_2/FTO electrodes in aqueous (a) and non-aqueous electrolyte (b).

It can be seen that the choice of electrolytes significantly influences the photocurrent densities generation for the individual electrodes. The generated photocurrent density in aqueous solution was approximately two times lower than in acetonitrile electrolyte despite the fact that increasing solvent polarity increases the electron transfer rate (Thompson et al., 1993; Eberspacher et al., 2006). Significant role plays also the fact that in aqueous solution the TiO_2/FTO electrodes are not mechanically stable and also the adhesion to substrate is not good. Moreover, layers are probably soluble in water and during the electrochemical measurements they can be partially dissolved. Therefore, the amount of photo-generated electrons is lower and also their transport to the conductive FTO support is difficult. The acetonitrile in the non-aqueous electrolyte has also lower oxidation potential leading to higher photogenerated current densities. Moreover, the increase in photocurrent in acetonitrile solution may be related with the photooxidation intermediates or partial blocking effect of acetonitrile on TiO_2 surface (Morand et al., 2002).

Nevertheless, the best photo-electrochemical properties were obtained for the pure dip-coated electrode in both types of electrolytes, aqueous and non-aqueous. The TiO_2/FTO electrode prepared by dip-coating possesses the higher photocurrent densities in comparison with electrode containing additional layer of nanofibers. It is probably caused by the worst electrolyte penetration through nanofibers layer together with the higher amount of the recombination processes. Therefore, the irradiated area of electrode with nanofibers is smaller than the pure dip-coated electrode and the electron transport in the nanofibers area is difficult. On the other hand, the photocurrent density of the electrode with nanofibers is comparable with published results (Xie et al., 2010). Very low response on the UV light signal showed the electrode with nanorods. In this case the contact between TiO_2 nanorods with conductive FTO support is very low and the amount of recombination centres in the area of crossing nanorods is very high. The reached photocurrent density values by the nanorod layer varied between 0.5–1 $\mu A/cm^2$ and correspond with literature (Kerkez et al., 2014; Lv et al., 2012).

The higher photocurrent density of Dip-coating/FTO electrodes can be explained with the information obtained by electrochemical impedance measurements. Charge transfer resistance between FTO and TiO_2 layers (R2) was increased when the porosity and homogeneity of the electrode was increased. When R_{ct} increases, capacitance constant decreases which results in higher value of the impedance. As a result, it becomes more difficult for the chemical reaction to take place on the electrode due to the higher energy barrier. This phenomenon explains why Dip-coating/FTO electrodes have higher photocurrent density than the other two types of electrodes (Tang et al., 2008). The decrease in the photocurrent density of Dip-coating-Nanofiber/FTO electrodes compared to Dip-coating/FTO electrodes can also be explained by the increase in TiO_2 layer thickness. The thickness of TiO_2 nanofiber layer was 5.6 μm while thickness of TiO_2 nanoparticle layer was 0.43 μm. The decrease of the photocurrent for thicker layers may be explained with a higher loss of promoted electrons by recombination and by the charge transfer processes into the solution during diffusion across the TiO_2 layers (Kityakarn et al., 2012).

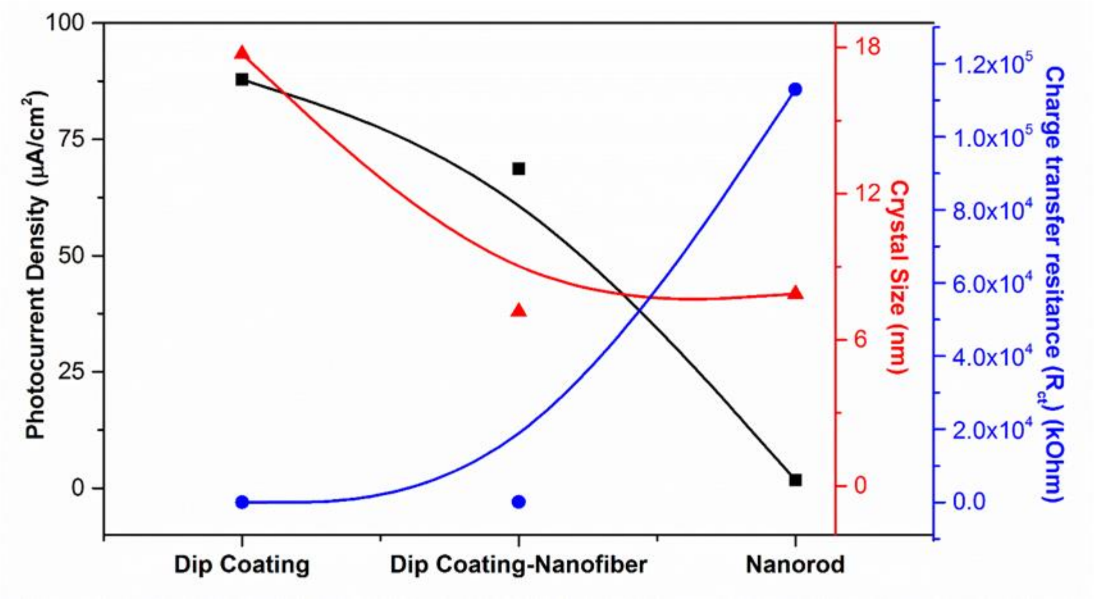

Figure 3.9 : The relationships among photocurrent density, charge transfer resistance and crystal size.

When the crystal size of TiO_2 is increased the grain boundary between crystals decreases. Therefore, the electron transport becomes fast thus the charge transfer resistance is decreased which resulted an increase in the photocurrent density (Jung et al., 2013). Figure 3.9 shows the relationships among photocurrent density, charge transfer resistance and crystal size of three types of electrodes. In accordance with the data provided in the literature, Dip-coating TiO_2 layer have the biggest crystal size and lowest charge transfer resistance which result the highest photocurrent density.

3.3 Conclusion

The TiO_2 nanofibers were successfully prepared by electrospinning of a sol-gel solution (PVP/Ti(Iso)). Three types of TiO_2 electrodes were fabricated on FTO substrate by different deposition techniques. Dip-coating/FTO, Dip-coating-Nanofiber/FTO and Nanorod/FTO electrodes were developed by calcination of PVP/Ti(Iso) layer following to dip-coating of the sol-gel solution, electrospinning on the dip-coating solution and electrospraying of calcinated and breaked TiO_2 nanofibers, respectively. All samples possess the crystal structure of anatase with the size of 17.7 nm for the nanoparticle layer, while crystal sizes for nanofibers and nanorods were significantly lower, 7.2 nm and 7.9 nm. Nanoparticle TiO_2 layer revealed smooth compact surface, the average diameter of the prepared TiO_2 nanofibers put onto TiO_2 layer was about 120-180 nm with a big pores between nanofibers. TiO_2 nanorods deposited directly onto FTO glass covered its surface only partially owing to their low adhesion. It was found that these properties significantly affected electrochemical impedance and photo-electrochemical properties of samples. The Dip-coating/FTO electrode possessed the highest photocurrent densities among the three types of electrodes, resulted the best photo-electrochemical properties. The photocurrent density for Dip-coating-Nanofiber/FTO electrodes was comparable with results in literature. Compared to Dip-coating/FTO electrodes, the decrease in photocurrent density for Dip-coating-Nanofiber/FTO electrodes was attributed to the significant increase in TiO_2 layer thickness (10 x) and big pores between nanofibers. Especially, Nanorod/FTO electrodes showed very low response to the UV light signal. In accordance with the photo-electochemical data, the electrochemical impedance results showed that the Dip-coating/FTO electrodes have the lowest charge transfer resistance and the higher electroactivity. The electrochemical impedance spectra of TiO_2 Nanorod/FTO electrodes were quite similar to those of FTO substrate. These results on photo-electrochemistry and EIS were caused by the weak stability and adhesion of TiO_2 nanorod layer on FTO-glass which resulted to the worst electrolyte penetration through nanorod layer. As a conclusion; dip-coating technique has been proved to be the most suitable method to fabricate the stable TiO_2 electrodes. Dip-coating/FTO electrodes possessed the biggest crystal size, lowest charge transfer resistance and highest photocurrent among the other electrodes prepared in this study.

4. MORPHOLOGICAL EFFECT OF COMPOSITE TiO_2 NANOROD-TiO_2 NANOPARTICLE/PEDOT:PSS ELECTRODES ON TRIIODIDE REDUCTION[3]

Amoung various solar cells, dye sensitized solar cells have attracted considerable attention because of their simple fabrication, low fabrication costs and high conversion efficiency (Grätzel, 2001; O'regan & Grfitzeli, 1991). A typical DSSC comprises the dye sensitized nano crystalline TiO_2 photo anode, redox electrolyte and a counter electrode with a catalytic layer deposited on conductive glass substrate such as fluorine tin oxide (FTO) (Balkan et al., 2016). The main tasks of counter electrode in DSSC are to collect electrons from the external circuit, transfer them back to the redox electrolyte, and catalyze the reduction of triiodide ions into iodide ions (Xu et al., 2012). Therefore, counter-electrode materials should possess high electrical conductivity and a superior electrocatalytic activity (Xin, He, Han, Jung, & Lin, 2011). Platinum (Pt) film has been widely used in DSSC so far as a counter electrode, due to its high conductivity and catalytic activity for reduction of triiodide (I_3^-) ions. However, its practical application will be limited by its high cost, rare source and corrosion of Pt in the presence of I_3^-/I^- redox couple (Bu, Tai, Liu, Guo, & Zhao, 2013). Therefore, it is necessary to develop efficient platinum-free counter electrodes for DSSC.

In order to reduce the production cost of DSSC, alternative counter electrodes are produced by using such as carbon materials (Jikun Chen et al., 2009; Veerappan, Bojan, & Rhee, 2012; Wu, Lin, Wang, Qiu, & Ma, 2011), metal compounds (Jang, Ham, Ramasamy, Lee, & Lee, 2010; Jiang, Li, & Gao, 2009; Mulmudi et al., 2011; M. Wang et al., 2009) and conductive polymers (Q. Li et al., 2008; Maiaugree et al., 2012; Yuan et al., 2013; Z. Zhang et al., 2012). One of the most known conductive polymers, PEDOT:PSS has been developed as low cost alternative counter electrode

---

[3] This chapter based on the paper "Balkan, T. and Sarac, A.S. (2016). Morphological Effect of Composite TiO_2 Nanorod-TiO_2 Nanoparticle/PEDOT:PSS Electrodes on Triiodide Reduction, *Express Polymer Letters*, (in press).''

which has many unique properties such as high conductivity, high stability and good catalytic activity for I_3^- reduction (Sakurai, Jiang, Takahashi, & Kobayashi, 2009). However, PEDOT:PSS electrodes exhibit a poor fill factor and generate lower cell efficiency than pristine Pt electrodes. One way to solve this problem, other materials are combined with PEDOT:PSS in order to increase the surface area of the film and also the catalytic activity. For example, Maiaugree et. al. (Maiaugree et al., 2012) incorporated TiO_2 nanoparticles which have different diameters into the PEDOT:PSS. They investigated diameter effect of TiO_2 nanoparticles on DSSC efficiency. They obtained highest efficiency by using mixture of large TiO_2 nanoparticles (30% wt) and small TiO_2 nanoparticles (70% wt). Sudhagar et. al. (Sudhagar et al., 2011) enhanced PEDOT:PSS based on DSSC efficiency by adding cobalt sulfide (CoS) to polymer. The efficiency was improved from 3.8% to 5.4% after incorporation of CoS nanoparticles. Zhao et. al. (Zhao et al., 2014) fabricated TiO2-PEDOT:PSS/PEDOT:PSS/glass electrodes which allow Pt and FTO free counter electrodes. According to these articles, ıt is obvious that by mixing nanoparticles into PEDOT:PSS, surface area of the polymer can be enlarged. And it is known that small particles provide high electrocatalytic activity owing to the large surface area, but they also provide lower electron transport efficiency owing to the abundant grain boundaries and defects (G. r. Li, Wang, Jiang, Gao, & Shen, 2010). In particular, nanorods (NRs) are believed to have exceptional electron transport properties and have been considered as an alternative to nanoparticles (NPs) (Kang et al., 2008).

Therefore, in the present work, we report a newly designed counter electrode comprised of TiO_2 nanomaterials (nanoparticles, nanorods and their mixture) incorporated into PEDOT:PSS in order to understand the influence the morphologies of TiO_2. Hence, single ratio between TiO_2 and PEDOT:PSS was chosen to figure out how the performance of electrodes change depends on only morphologies of TiO_2 instead of TiO_2-PEDOT:PSS ratio. TiO_2 was selected because it is non-toxic and inexpensive. The effect of incorporating TiO_2 nanorod and TiO_2 nanoparticles at several ratios upon film structure was investigated. The electrocatalytic activities and impedance properties of electrodes were analyzed by using cyclic voltammetry (CV) and electrochemical impedance spectroscopy (EIS) measurements. Results showed that electrochemical properties of the electrodes can be manipulated by governing morphologies of TiO_2 nanomaterials.

4.1 Experimental Part

4.1.1 Preparation of TiO_2 nanorods

First TiO_2 nanofibers were produced by using electrospinning technique according to our previous study (Solcova et al., 2014). Afterwards, these nanofibers were broken mechanically by ball milling method in order to obtain TiO_2 nanorods (diameter: 153±37 nm, length: 390±160 nm).

4.1.2 Preparation of TiO_2-PEDOT:PSS and Pt electrodes

Two different TiO_2 forms (nanorod and nanoparticle) were used for preparing four TiO_2 compositions on the basis of weight percentage: 1-) 100% TiO_2 NPs (< 25 nm, Sigma-Aldrich) - 0% TiO_2 NRs, 2-) 75% TiO_2 NPs – 25% TiO_2 NRs, 3-) 50% TiO_2 NPs – 50% TiO_2 NRs, 4-) 0% TiO_2 NPs – 100% TiO_2 NRs. These electrodes were labelled as NR0, NR25, NR50 and NR100, respectively. In a typical procedure, a paste of PEDOT:PSS (PEDOT:PSS) (Sigma-Aldrich, 1.3 wt%) and TiO_2 was prepared by mixing 0.16 g TiO_2 in 0.4 mL PEDOT:PSS. Then, TiO_2 was dispersed ultrasonically for 20 minutes. Further, the solution was kept under stirring for 1-2 hour to get homogenous composite solution. Composite TiO_2-PEDOT:PSS pastes were coated onto a FTO (Teknoma, $R_s < 10\ \Omega/cm^2$) using a glass rod and dried at 85 ^oC. Thickness of films was measured ≈ 20 μm except NR100 (≈ 30 μm) by Mitutoyo Digimatic Outside Micrometer (MDC-25SB). For a comprasion, platinum electrode was prepared by spray coating from 0.01 M H_2PtCl_6 (Sigma-Aldrich) solution in isopropanol (Merck) and subsequently by sintering at 450 ^oC for 30 min. In addition, the drop casting technique has been used to deposit pristine the PEDOT:PSS film.

4.1.3 Characterization

The X-ray diffraction spectrometer (BrukerTM D8 X-Ray Diffractometer) was employed to characterize the crystalline structure of TiO_2/PEDOT:PSS composite electrodes. FTIR measurements of composite films were performed using Perkin-Elmer FTIR system. Raman measurements were carried out by using Thermo DXR Raman (Massachusetts, USA) with wavelength 780 nm and 532 nm. The morphologies of the counter electrodes were evaluated by field emission scanning electron microscopy (SEM, FEI-QUANTA FEG 450). The conductivity measurements were performed with the four-point probe technique at the room temperature. A Lucas Labs four-point probe resistivity stand (S-302-4) with a Signatone four-point probe head (SP4-40-085-TFS) was used to make electrical contact with the pellet. Constant current (microamperes) was applied between external probes using a Keithley 2400 (Ohio, USA) programmable current source, while the resulting voltage was measured between two central probes with a Keithley 2000 multimeter. The film catalytic activity towards to I_3^-/I^- redox couple was measured by cyclic voltammetry (CV) in a three compartment cell at a scan rate of 20 mV/s in 10 mM LiI, 1mM I_2 and 0.1 M $LiClO_4$ in ACN solution (Gamry REF 600, USA). TiO_2-PEDOT:PSS/FTO electrodes as working, a platinum wire as counter and a silver wire as a pseudo reference electrode were used. Surface area of composite films were measured by Costech Instruments Sorptometer 1042. The electro-active polymer area was investigated by CV in 5 mM Ferrocene and 0.1 M $NaClO_4$-ACN solution in a three compartment cell at a scan rate of 25, 50, 100, 150, 200 and 250 mV/s. The electrochemical impedance spectra (Gamry REF 600, USA) was measured by using the symmetric sandwich-type configuration to understand the charge transfer process at the interface between the electrolyte and the counter electrode, frequency varied from 0.01 Hz to 100 kHz with an AC amplitude 10 mV. For EIS measurement, a solution which contained 0.5 M LiI, 0.05 M I_2 and 0.5 M 4-tert-butylpyridine (TBP) in ACN was prepared. Spectra were analyzed by using ZSimp Win version 3.1 software.

4.2 Results and Discussion

4.2.1 Spectroscopic analysis of electrodes

FTIR spectra of both pristine PEDOT:PSS and TiO_2-PEDOT:PSS composite films were shown in figure 4.1. It can be seen that the FTIR spectrum of pristine PEDOT:PSS exhibits the characteristic peaks at around 1185 cm^{-1}, 1079 cm^{-1} which may be assigned to C-O-C bond. Peak at 1036 cm^{-1} belongs to O-S-O vibration of sulfonic acid group of PEDOT:PSS. For the composite films in which TiO_2 were dispersed in PEDOT:PSS, the characteristic peaks of PEDOT:PSS can be seen for all samples. Moreover, increasing in absorbance between 900 cm^{-1} - 500 cm^{-1} was obtained after the incorporation of TiO_2 which may belongs to Ti-O and O-Ti-O bonds vibration (Liu et al., 2015).

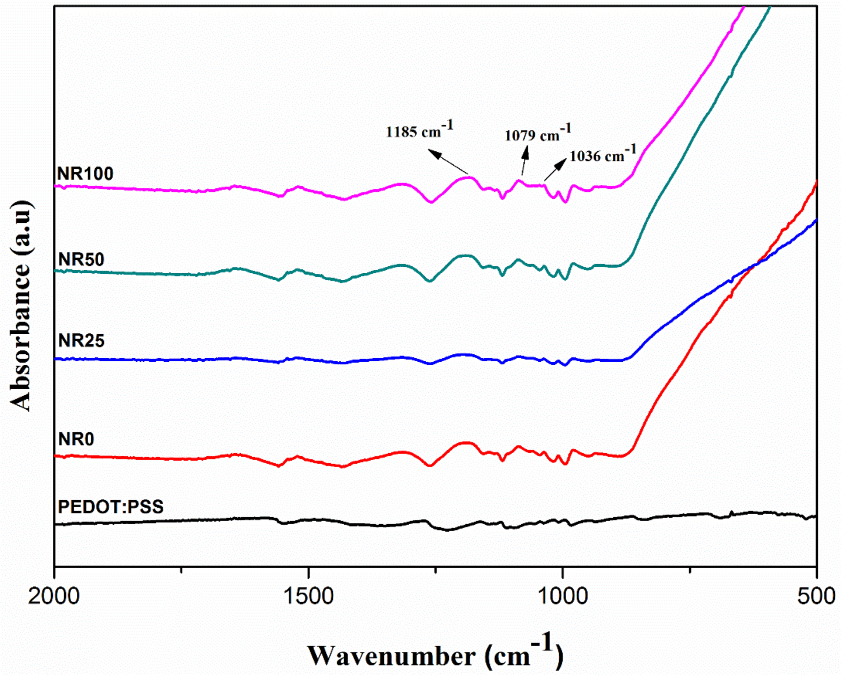

Figure 4.1 : FTIR spectrum of pristine PEDOT:PSS film and composite films.

Figure 4.2 shows Raman spectra of PEDOT:PSS and PEDOT:PSS-TiO_2 composite electrodes.

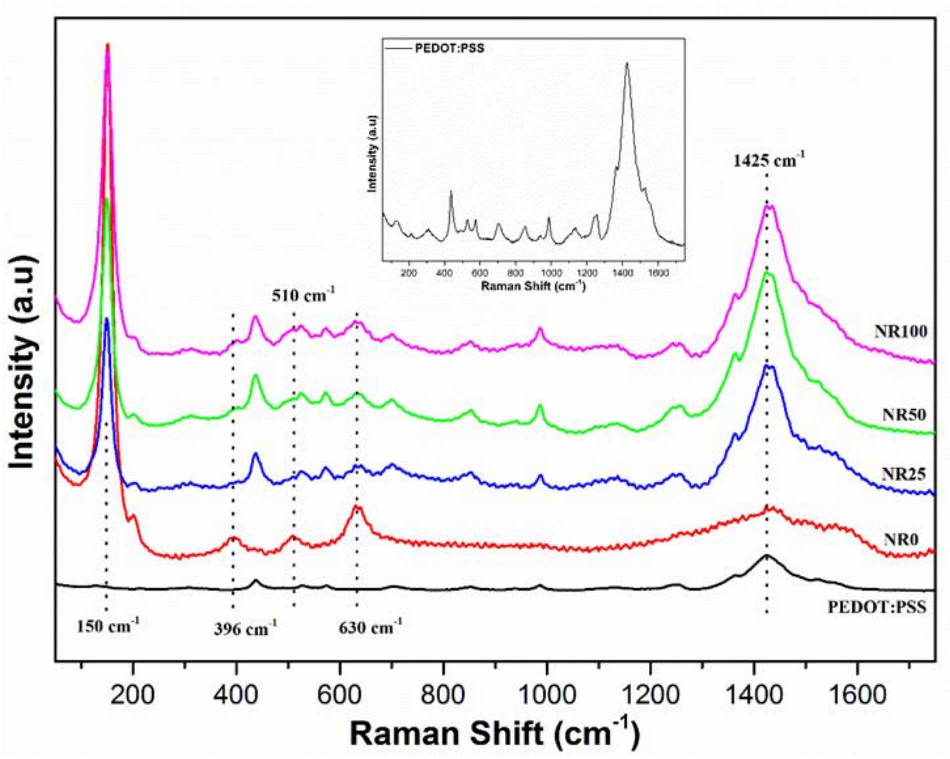

Figure 4.2 : Raman spectrum of pristine PEDOT:PSS (inset) and composites.

It can be seen that all composite samples possess crystal structue of anatase after TiO_2 incorporation. The characteristic peaks were observed at 150, 396, 510 and 630 cm^{-1} (Balkan et al., 2016). As expected, these peaks didn’t appear for pure PEDOT:PSS. In addition, the band at 1425 cm^{-1}, which belongs to the stretching vibration of $C_\alpha=C_\beta$ on the five member ring of PEDOT were obtained for all composite samples and PEDOT:PSS (Jhang et al., 2013). Crystal structural characterizations of PEDOT:PSS and TiO_2-PEDOT:PSS powders were shown in figure 4.3.

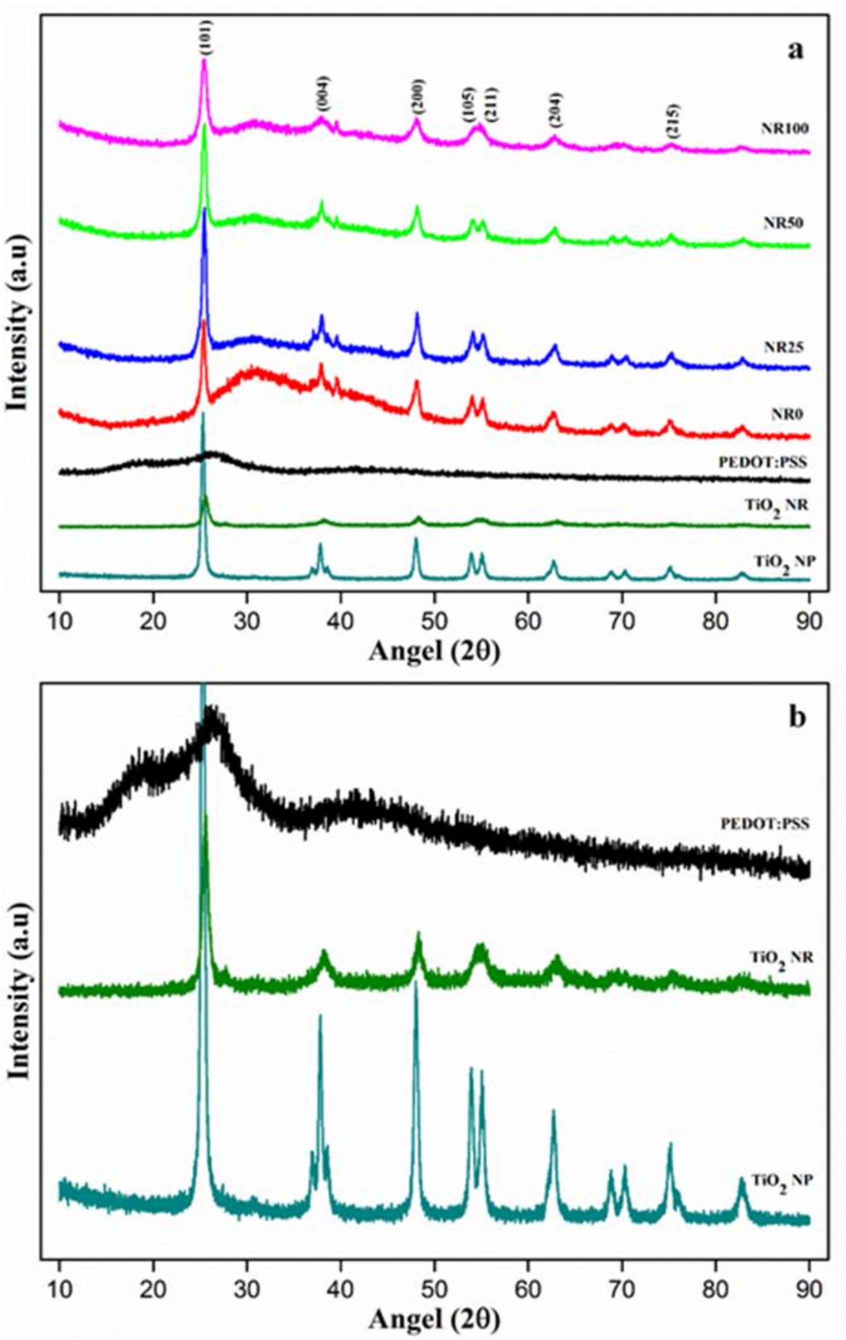

Figure 4.3 : XRD patterns of PEDOT:PSS and TiO_2-PEDOT:PSS powders.

Only one broad peak at around 26° was observed for the PEDOT:PSS powder which was related to its poor crystalline structure and this peak was shifted to 30° after combined with TiO_2 may be due to weak physical interaction between TiO_2 and PEDOT:PSS. In contrast, XRD patterns of TiO_2 NP, TiO_2 NR and all TiO_2-PEDOT:PSS composite powders exhibited same strong diffraction peaks. These peaks can be assigned to the (101), (004), (200), (105), (211), (204) and (215) crystallographic planes of tetragonal anatase phase TiO_2 (Thamaphat et al., 2008). Rutile phase wasn't observed in the composites. Moreover, there is no major effect of PEDOT:PSS on TiO_2 crystal structure was obtained. Interestingly, decreasing in peak intensity at 25° (101) was obtained with increasing amount of TiO_2 NR (NR100) in the composite powders. This is because during ball milling process nanofibers were distorted in order to produce nanorods. Hence peak intensity decreased depending on TiO_2 nanorods ratio. XRD and FTIR measurements verified presence of TiO_2 nanostructures in the composite films.

4.2.2 Morphological analysis of electrodes

Figure 4.4 shows the low and high magnifacition SEM images of TiO_2-PEDOT:PSS composite films on FTO substrates. It was seen that the surface of NR0 (a) is very rough and porous which is good for catalytic reduction of I_3^- in comparison to NR100 composite films. PEDOT:PSS film has very smooth surface. The surface roughness of composite films was also found to vary with TiO_2 NRs to TiO_2 NPs ratio. According to high magnification images, composite films with decreased TiO_2 nanoparticles loading showed less cracks in the films. As known, film thickness affects the film active area, film catalytic activity and film impedance. Therefore, the film thickness of composite electrodes were determined with using SEM cross-section images (Figure 4.5) and micrometer. Image J program was used to measure the film thickness. Measurements were done from 3-4 different region and average thickness were calculated and listed in table 4.1. As can be seen in table 4.1, the average film thichkness of NR0, NR25 and NR50 were found almost same and NR100 showed higher film thickness for both method. It was expected result because of dimension of TiO_2 NRs. In addition, it was noted that the film thickness were found to be higher by micrometer compare to cross-section methods. We believe that results obtained from micrometer measurements were more reliable than cross-section measurements because it was a direct method. Surface area measurements (BET) of composite films were compatible with SEM images.

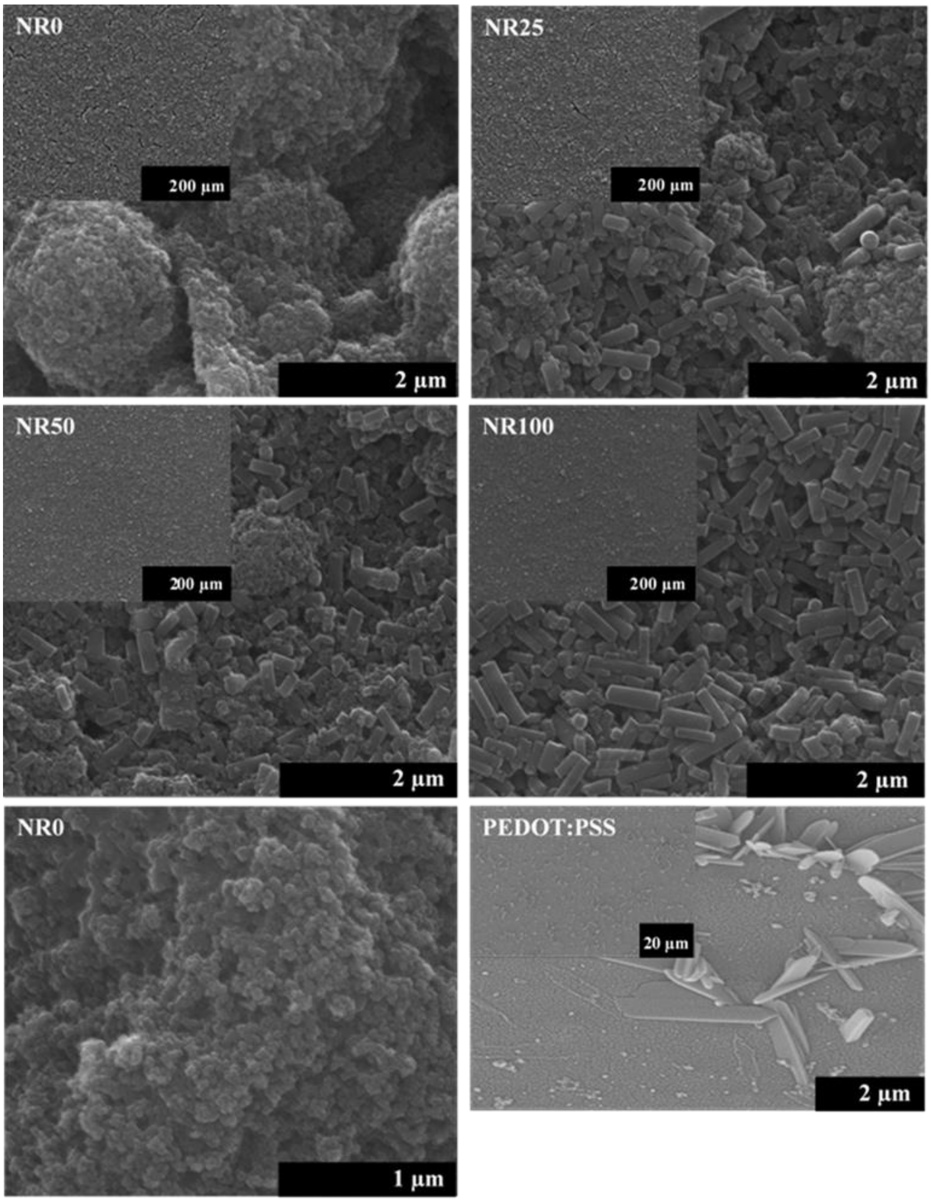

Figure 4.4 : SEM images of PEDOT:PSS, NR0, NR25 , NR50 and NR100.

Table 4.1 represents surface area results of pure TiO_2 NPs, pure TiO_2 NRs and composite films. The surface area decreases with increasing TiO2 NRs loading. The surface area of NR0 was almost the same as pure TiO_2 NPs sample. The same relation was found for NR100 and TiO_2 NRs samples which means that there is no contribution of PEDOT:PSS due to its low surface are (0.13 m^2/g) to the surface areas of composite films (Okuzaki et al., 2010). These results show that these TiO_2 nanorods or nanoparticles dispersed in PEDOT:PSS, forming a network structure, are beneficial for electron conduction (Zhao et al., 2014).

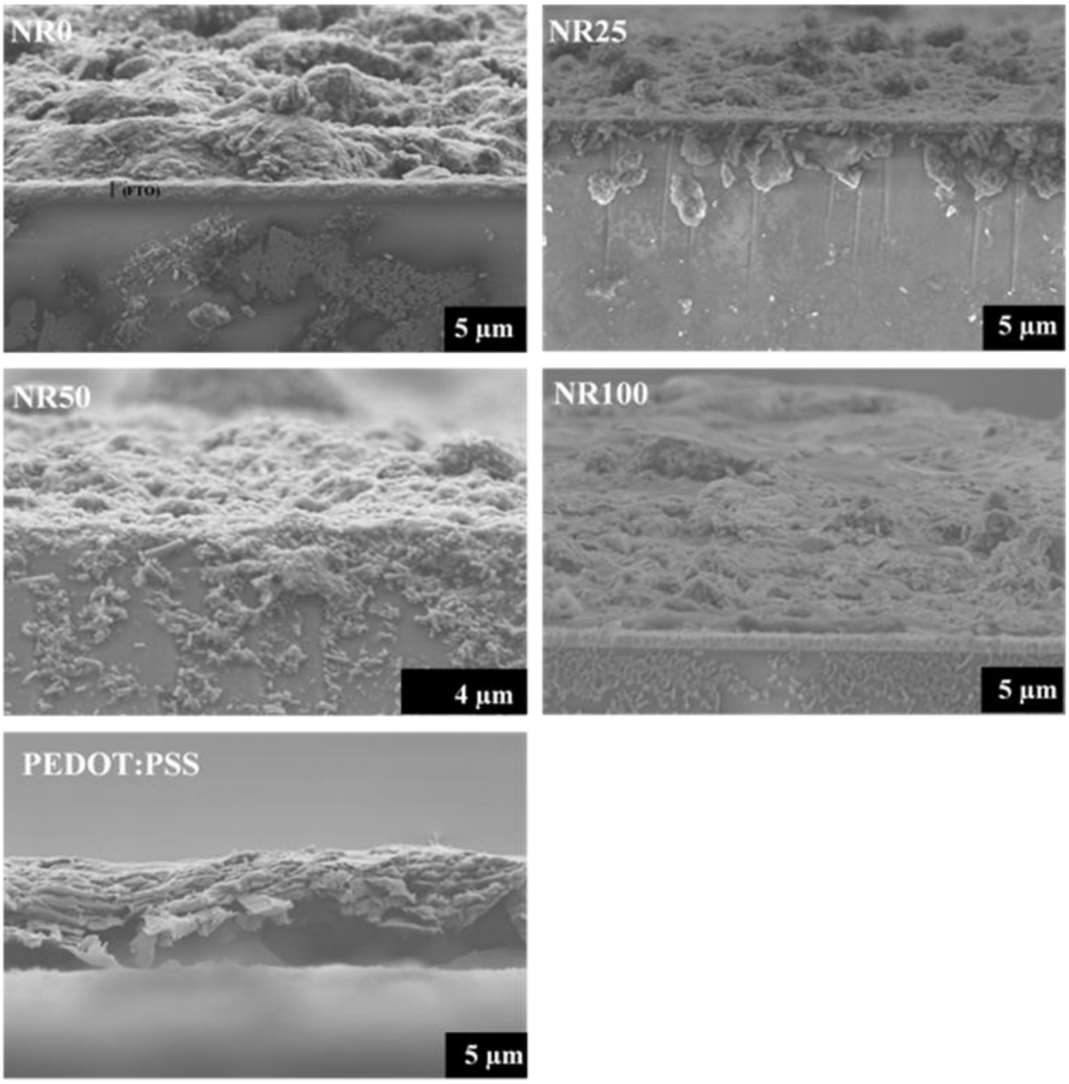

Figure 4.5 : Cross section view of PEDOT:PSS and composite electrodes.

Table 4.1 : Surface area and thickness of PEDOT:PSS, TiO_2 and composites.

Sample Name	**Surface Area (m^2/g)**	**Average Thickness by SEM (µm)**	**Average Thickness by Micrometer (µm)**
TiO_2 NP	50.95	-	-
TiO_2 NR	21.59	-	-
NR0	50.08	4	19
NR25	-	4.1	21
NR50	36.71	3.5	22
NR100	19.03	7	30
PEDOT:PSS	0.13	6.7	5

4.2.3 Electrochemical and electrical analysis of electrodes

Figure 4.6 (a-e) exhibits the current density versus applied voltage of the PEDOT:PSS and composite electrodes at different scan rates in the ferrocene solution.

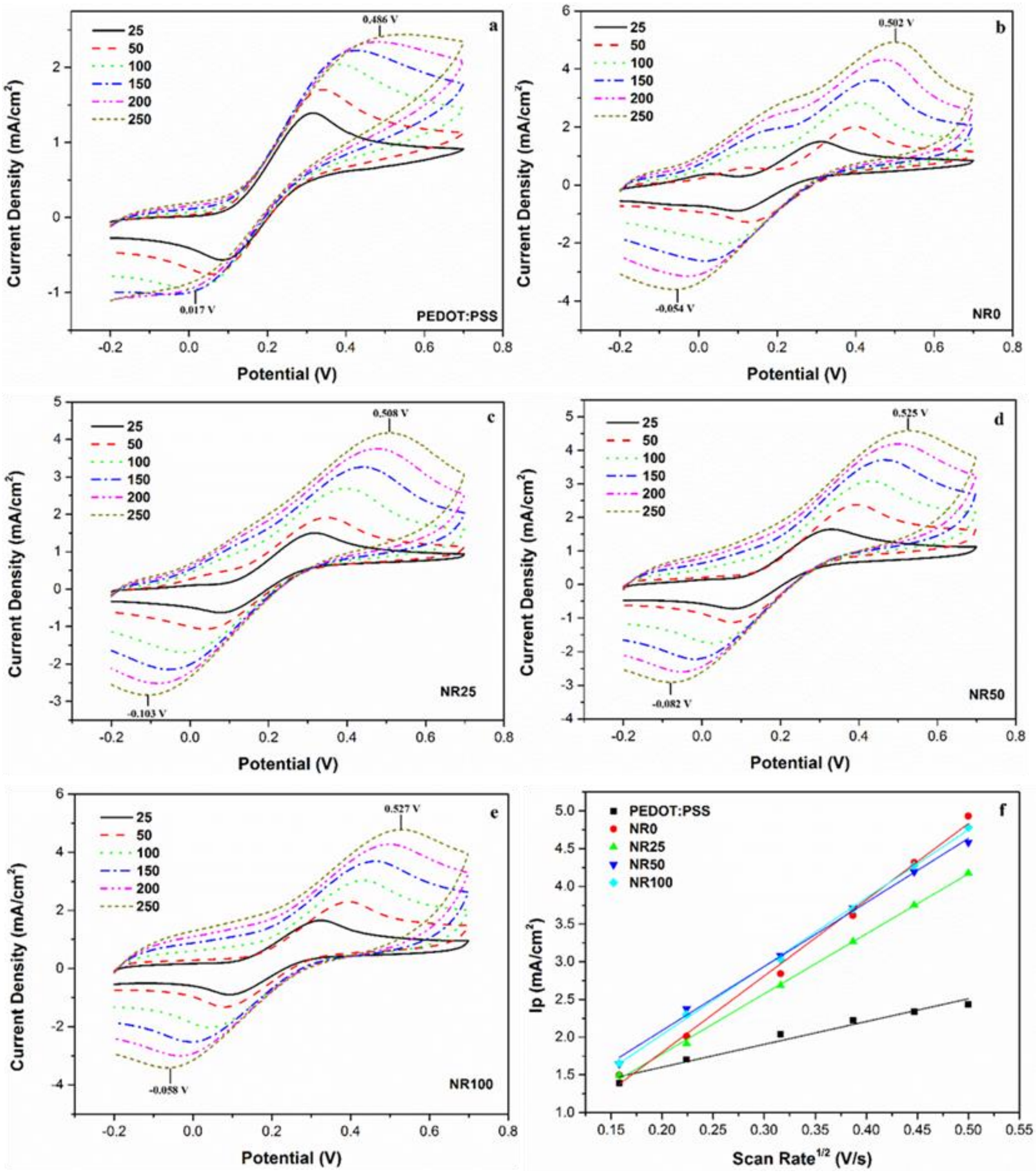

Figure 4.6 : CV curves of PEDOT:PSS (a) and composite films (b-e) at different scan rates in the ferrocene solution. Curves and fitting curves of current density of ferrocene versus the square root of scan rate for all samples (f).

It can be seen that current density increases with scanning rate. The current density (I_p) which is coming from these graphs versus the square root of the scanning rate ($v^{1/2}$) curves their fits of the PEDOT:PSS and composite films were shown in Figure 4.6 (f). All curves obeyed the Randles-Sevcik equation, $I_p = 2.69.10^5 n^{3/2} A D^{1/2} C\ v^{1/2}$

(equation (1)) whereas n electron number, A surface area (cm^2), D diffision coefficient (cm^2/s) and C concentration (mol/cm^3). The linearship between I_p and $v^{1/2}$ indicates the diffusion limitation of the redox reaction on the electrodes. This phenomenon shows the adsorption of ferrocene species is little affected the redox reaction at the PEDOT:PSS and PEDOT:PSS-TiO_2 electrodes surface under these conditions and this also suggest that no specific interaction between Fc/Fc^+ (ferrocene) redox couple and PEDOT:PSS, PEDOT:PSS-TiO_2 electrodes (Saito et al., 2004). During measurements, same polymer and same solution medium were used therefore n, C and D values in the Randles-Sevcik equation should be the same. This assumes that TiO_2 doesn't undergo oxidation and reduction with ferrocene. Thus, the slope of the curves relates only to the film electro-active area (Maiaugree et al., 2012). The slopes of the curves were found 3.02 (PEDOT:PSS), 10.1 (NR0), 7.96 (NR25), 8.48 (NR50), 9.05 (NR100), respectively. The slope values of composite films were found higher than that of the pure PEDOT:PSS film. The increase in the slope values of composite films supports the enlargement of their electro-active areas. Interestingly, according to BET measurements, the surface area of NR0 two times higher than NR100 but they have almost the same slope values which are related with the electro-active surface area. The reason for this distinction is that the BET measurement, performed in a gas phase, determines area based on specific chemically reactive surface states. The electrochemical method determines the area to which the ferrocene ions can reach and where the electron transfer is a facile process (Porter, DeArmitt, Robinson, Kirby, & Bott, 1989). It is also known that one dimensional nanostructures such as nanorods improve the electron transport process therefore electro-active area of NR100 may be almost the same as NR0 (B. Liu & Aydil, 2009). The electrical conductivity of composite electrodes can be used to understand this situation (Table 4.2). As can be shown in table two, the conductivity of PEDOT:PSS (10^{-3} S/cm) decreased 10 times after combination with TiO_2 nanostructures as expected. Although NR100 showed smallest values., similar conductivity (10^{-4} S/cm) values were obtained for all composite electrodes. These results can be another explaination why all composite electrodes have similar electro-active area. CV graphs of the PEDOT:PSS, TiO_2-PEDOT:PSS composite counter electrodes and the Pt electrode towards to I_3^-/I^- redox couple were presented in figure 4.7. Except PEDOT:PSS, the Pt and TiO_2-PEDOT:PSS composite electrodes showed two pairs of similar redox peaks.

Table 4.2 : Conductiviy values of PEDOT:PSS and composite electrodes.

	PEDOT:PSS	**NR0**	**NR25**	**NR50**	**NR100**
Conductivity (S/cm)	$1.09*10^{-3}$	$2.91*10^{-4}$	$3.63*10^{-4}$	$1.75*10^{-4}$	$1.01*10^{-4}$

The left reduction peaks labelled as ✙ are vital for its operation in DSSC and are associated with the reduction of triiodide ($I_3^- + 2e \longrightarrow 3I^-$). The right peaks labelled as ☆ correspond to $3I_2 + 2e \longrightarrow 2I_3^-$ and are unimportant for the performance of DSSC (Yue et al., 2013). The main mission of counter electrodes in DSSC to catalyse the reduction of I_3^- to I^- so the characteristic of the left pair are our focus (Bu et al., 2013; Q. Li et al., 2008). The TiO_2 based counter electrodes exhibited higher peak current density than Pt and PEDOT:PSS counter electrodes which suggests a faster reaction rate of I_3^- reduction on the TiO_2-PEDOT:PSS composite films, thus a higher electro-catalytic activity of TiO_2-PEDOT:PSS counter electrodes. In addition, comparing the reduction peak positions, the pure PEDOT:PSS counter electrode has higher reduction voltages (≈ 0.8 V) than the TiO_2-PEDOT:PSS and Pt counter electrodes (≈ 0.67 V). Decreasing in reduction peak potential after TiO_2 addition into the PEDOT:PSS depends on enlargement of the film active area or lower film resistance (Maiaugree et al., 2012). In order to optimize the electrocatalytic preformances of conductive polymers based counter electrodes, their specific areas and conductivity are maximized (Zhou et al., 2016). Adding TiO_2 into the PEDOT:PSS provides larger specific surface areas with more exposed active sites for enhancing catalytic activity of composite electrodes (Zhou et al., 2016). These results were supported with BET and electro-active measurements as expected. Compare to pure PEDOT:PSS, all composite electrodes showed higher surface area. The influence of the contents of TiO_2 NRs on the catalytic activity of TiO_2-PEDOT:PSS counter electrodes also were shown in figure 4.7. NR100 showed highest current density (not very much) compare to another counter electrodes but actually almost same current densities were obtained with increasing of TiO_2 NRs contents. The current densities of composite electrodes varied between 1.5-2 mA/cm^2. These results correspond with the works by Shi and Ho who obtained similar current densities (1-3 mA/cm^2) with using acid treated PEDOT:PSS-rGO (reduced graphene oxide) and PEDOT:PSS-TiS_2 electrodes under comparable conditions (Zhou & Chen et al., 2016; Li & Lee et al., 2013). As explained above, altough NR0 has highest surface area according to BET measurement, all composite counter electrodes have almost same electro-active surface area. It is obvious that electro-active area is more effective parameter than surface area, therefore no too much differences were obtained for reduction current density of I_3^-.

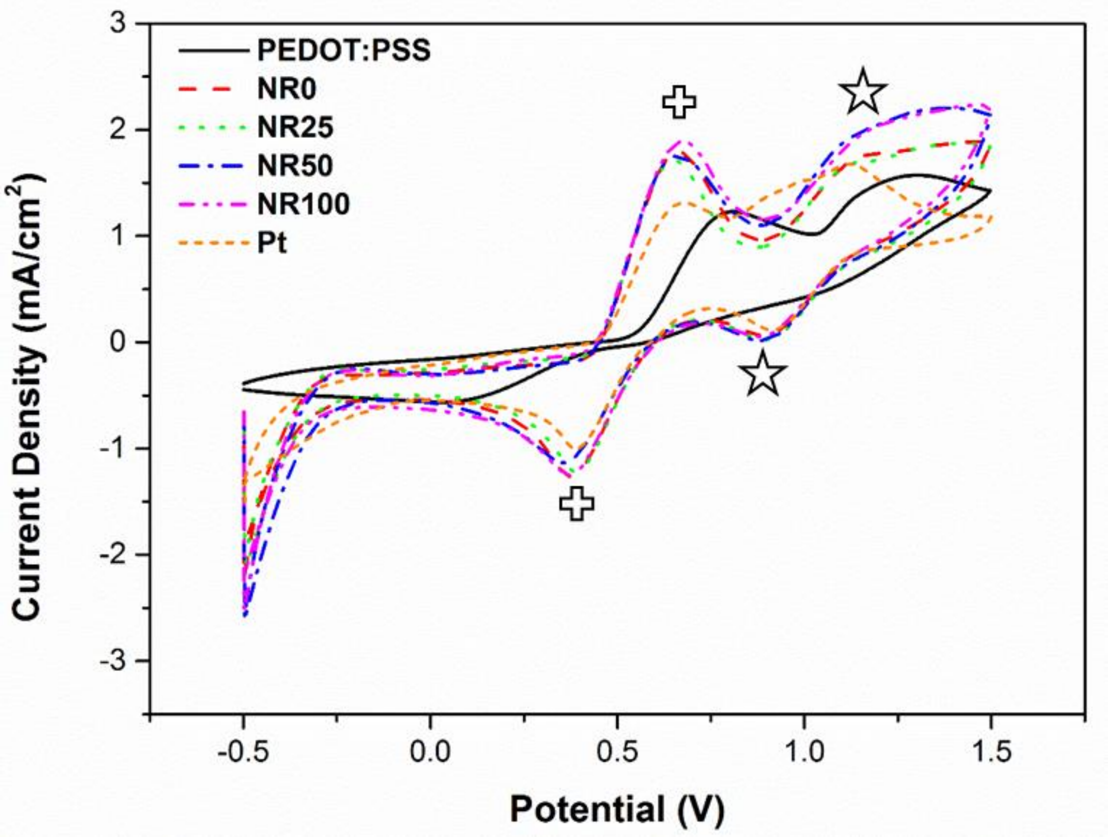

Figure 4.7 : CV curves of Pt, PEDOT:PSS and TiO_2-PEDOT:PSS composite electrodes according to I_3^-/I^- redox couple.

In order to understand the electrochemical characteristics of PEDOT:PSS and TiO_2-PEDOT:PSS composite electrodes, EIS measurements were carried out. For measurement, the symmetrical TiO_2-PEDOT:PSS/I_3^-/I^-/TiO_2-PEDOT:PSS were made by assembling two identical TiO_2-PEDOT:PSS (or PEDOT:PSS) on each side. Normally, these electrodes were separated by using hot melt spacer or Surlyn film but in this measurement distance between two symmetrical electrodes was kept constant (1 cm). These cell configuration can be used in order to eliminate the influence of the photoanode (Qiao, 2011; Shi, Deng, & Li, 2015). Figure 4.8 shows the nyquist plots of PEDOT:PSS (4.8-a) and TiO_2 based composite electrodes (4.8-b). Compare to the literature, similar plots were observed (Bu et al., 2013; Tsekouras, Mozer, & Wallace, 2008). In order to characterize Nyquist plots, they have been fitted with the equivalent circuit model at high frequency region (4.8-c) and the results with percentage erros were summarized in table 4.3.

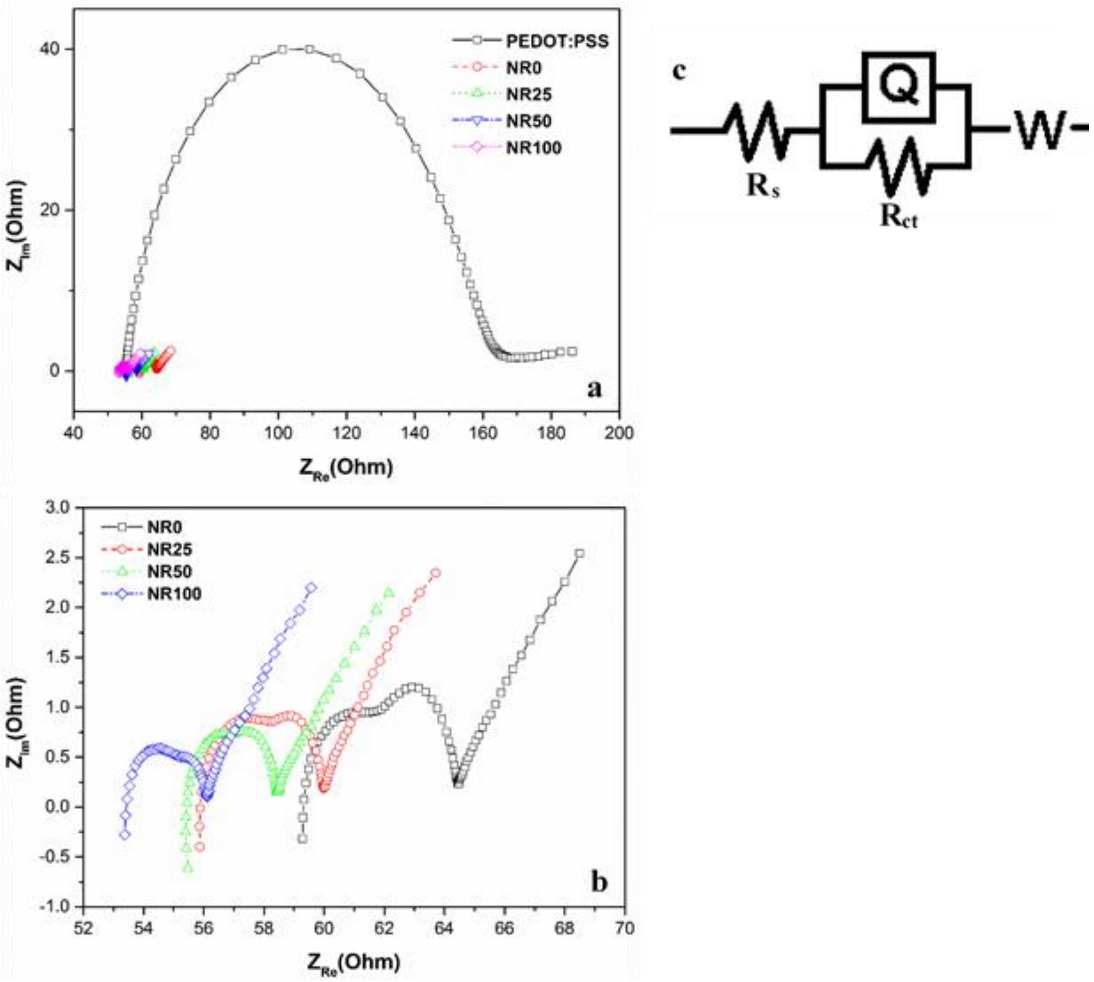

Figure 4.8 : Nyquist plots of the symmetrical cell of PEDOT:PSS (a) and composite electrodes (b). Equivalent circuit model which matches for the highest frequency region (c).

R_s is the high frequency intercept on the real axis shows series resistance and R_{ct} is the charge transfer resistance at the counter electrode/electrolyte interface for I_3^-/I^- reaction (Joshi et al., 2010). R_s and R_{ct} describe the resistance of the substrate and the catalytic activity of the electrodes for reducing I_3^- ions, respectively. The R_{ct} values of TiO_2-PEDOT:PSS composite electrodes (≈3-5 Ω) were lower than pristine PEDOT:PSS electrode (109 Ω) which indicates that the less over potential for an electron transferring from the TiO_2-PEDOT:PSS electrodes to electrolyte. Moreover, the R_{ct} values decreased with TiO_2 nanorod incorporation as seen in table 4.3 probably due to better electron transport properties of nanorods compare to nanoparticles. Besides the charge transfer resistance, the series resistance of the counter electrode (R_s) is another important parameter which affects fill factor of the DSSC. High series resistance causes low fill factor. Interestingly, we found that NR100 has the lowest sheet resistance and the other composite electrodes have similar values which indicated that TiO_2-PEDOT:PSS electrodes has prominent conductivity. The EIS analyses explained that why NR100 sample showed (not too much) higher current density for reducing of I_3^-.

Table 4.3 : The fitted EIS parameters of symmetrical cells.

	PEDOT:PSS	**NR0**	**NR25**	**NR50**	**NR100**
R_s (ohm)	54.76±0.61%	59.08±0.26%	55.71±0.19%	55.34±0.19%	53.09±0.38%
R_{ct} (ohm)	108.80±0.81%	5.67±3.5%	4.43±3.03%	3.27±4.12%	3.24±7.32%
Chi Squ. (10^{-5})	0.54	2	1.9	1.8	1.8

4.3 Conclusion

TiO_2-PEDOT:PSS nanocomposite electrodes with different morphologies were prepared on FTO glass, succesfully. We found that, the catalytic activity of PEDOT:PSS film was significantly improved after adding TiO_2 nanoparticles/nanorods. Although NR0 has the highest electroactive area, NR100 exhibited almost same (a little higher) catalytic activity for reduction of I_3^-. Moreover, we found that R_{ct} values strongly depends on TiO_2 nanorods content into the composites and it was decreased by increasing TiO_2 nanorods content. Hence, NR100 electrode exhibited lowest R_{ct} and R_s values. In addition, these results showed that both electro-active area and electron transport properties of a material have a great impact on design of the counter electrodes for DSSC application.

5. ELECTROCHEMICAL AND MORPHOLOGICAL ANALYSIS OF POLY(3,4-ALKYLENEDIOXYTHIOPHENE)-MODIFIED TiO_2 NANOROD ELECTRODES[4]

Dye-sensitized solar cells (DSSCs) are great candidates as next generation photovoltaic devices to substitute for Si-based solar cells since they have high theoretical energy conversion efficiency and low fabrication cost (Sakurai et al., 2009; Zhao et al., 2014). A typical DSSC consists of three main components: dye-sensitized photoanode, electrolyte containing redox active couples (I_3^-/I^-) and a counter electrode (CE) with a catalytic layer deposited on FTO substrate (Bu et al., 2013).

One of the most curicial components of DSSC, the counter electrode works as a catalyst for the reduction of I_3^- to I^-. Platinum (Pt) is commonly used as the counter electrode for reducing triiodide to iodide (Saad, Feteha, Ebrahim, Soliman, & Abdel-Fattah, 2014). However, Pt is an expensive substance and corrosion of the Pt occurs in the presence of I_3^-/I^- redox couple (Bu et al., 2013; Cha, Koo, Seo, & Lee, 2010). Therefore, the exploration of alternative counter electrodes to replace Pt in DSSCs is one of the most favorable topic for improving cell performance and stability at a low cost. Many reported materials have been used as the substitute for Pt based counter electrode like conductive polymer and carbon based electrodes (Imoto et al., 2003; Lee et al., 2009; Q. Li et al., 2008; Roy-Mayhew, Bozym, Punckt, & Aksay, 2010; Xia, Chen, & Yanagida, 2011). As a conductive polymer, PEDOT: PSS has attracted much attention amoung to Pt free counter electrodes because of good catalytic activity, better film performing property, low cost and easy coating. However, many researchers observed that pure PEDOT:PSS counter electrodes generate lower cell efficiency than Pt-based DSSC. In order to overcome this problem, other materials (carbonaceous and inorganic) are incorporated in PEDOT: PSS (H. Wang, Wei, &

---

[4] This chapter based on the paper “Balkan, T. and Sarac, A.S. (2016). Electrochemical and Morphological Analysis of Poly(3,4-Alkylenedioxythiophene)-Modified TiO_2 Nanorod Electrodes, *Journal of Nanoscience and Nanotechnology* (in press).’’

Hu, 2013; Xu et al., 2012; Yun, Ra, & Rhee, 2013). Because, the combination of metal oxide (inorganic element) with a conductive polymer (organic component) creates opportunities to construct high-quality organic/inorganic interface which may result in a synergistic effect, i.e. exhibit superior properties such as high surface area, high catalytic activity and chemical/electrochemical stability (Maiaugree et al., 2012; Siuzdak, Sawczak, & Lisowska-Oleksiak, 2015; Sudhagar et al., 2011). To our knowledge, some publications focused on the preparation and characterization of poly(3,4- propylenedioxythiophene) (PProdot) and its derivatives as counter electrodes for DSSC application (Ahmad et al., 2012; Lee et al., 2009) but as far as we know this is the first time that modified TiO_2 nanorods-PProdot hybrid electrode was fabricated.

In the present work, we report the electrocatalytic activity on triiodide reduction of poly(3,4-alkylenedioxythiophene) and poly(3,4-propylenedioxythiophene)/modified TiO_2 nanorod (NR) (PProdot/TiO_2 NR) films prepared by electrochemical polymerization. It was found that surface modification of TiO_2 with APTES provides better electrocatalytic activity compare to unmodified TiO_2. In addition, a linear relation between surface roughness and electrocatalytic activity on triiodide reduction was found. Compared to all prepared electrodes, poly(3,4-propylenedioxythiophene)/modified TiO_2/FTO represented best electrocatalytic activity because of synergistic catalytic effect by combination of TiO_2 nanorods and poly(3,4-propylenedioxythiophene). Also, it was noted that all electrodes showed comparable electrocatalytic performance with conventional Pt electrode for the reduction of triiodide.

5.1 Experimental Part

5.1.1 Materials

Conductive glasses (fluoride doped tin oxide glass, FTO, with sheet resistance of 7 ohm/sq, Solaronix, Aubonne, Switzerland) were used as a substrate. Anhydrous lithium iodide (LiI), lithium perclorate ($LiClO_4$), iodine (I_2), tetrabutylammonium hexafluorophosphate (Bu_4NPF_6), 4-tertiary butyl pyridine (TBP) were purchased from Sigma-Aldrich (Missouri, USA). 3,4-propylenedioxythiophene (Prodot), 3,4-(2,2-dimethylpropylenedioxy)thiophene (Prodot-Me_2), 3,4-(2,2-

diethylpropylenedioxy)thiophene (Prodot-Et$_2$), 3-aminopropyltriethoxysilane (APTES), Titanium (IV) oxide (anatase, < 25nm) also were purchased from Sigma-Aldrich (Missouri, USA). All chemicals were used without further purification. Ethyl alcohol, isopropyl alcohol (IPA) and acetonitrile (ACN) were supplied from Merck (Darmstat, Germany).

5.1.2 Preparation and functionalization of TiO$_2$/FTO electrode

TiO$_2$ NR/FTO electrode was produced as follows: first, TiO$_2$ nanofibers were fabricated according to our previous work (Solcova et al., 2014). Then, produced electrospun TiO$_2$ nanofibers were broken mechanically with using ball milling method in order to obtain TiO$_2$ nanorods (Fujihara et al., 2007). TiO$_2$ nanorods can be seen in figure 5.3. Afterwards, 0.05 g of TiO$_2$ nanorods was ultrasonically dispersed in 250 µl acetic acid (Merck) until obtaining homogeneous dispersed solution. Ethylene glycol and ethyl cellulose were then added into the solution to get a paste. The TiO$_2$ nanorods paste were coated on the FTO glass with using glass rod followed by drying 85^{o}C. Finally, the film was annealed at for 450^{o}C for 1h (rate of heating is 2.5^{o}C/min).

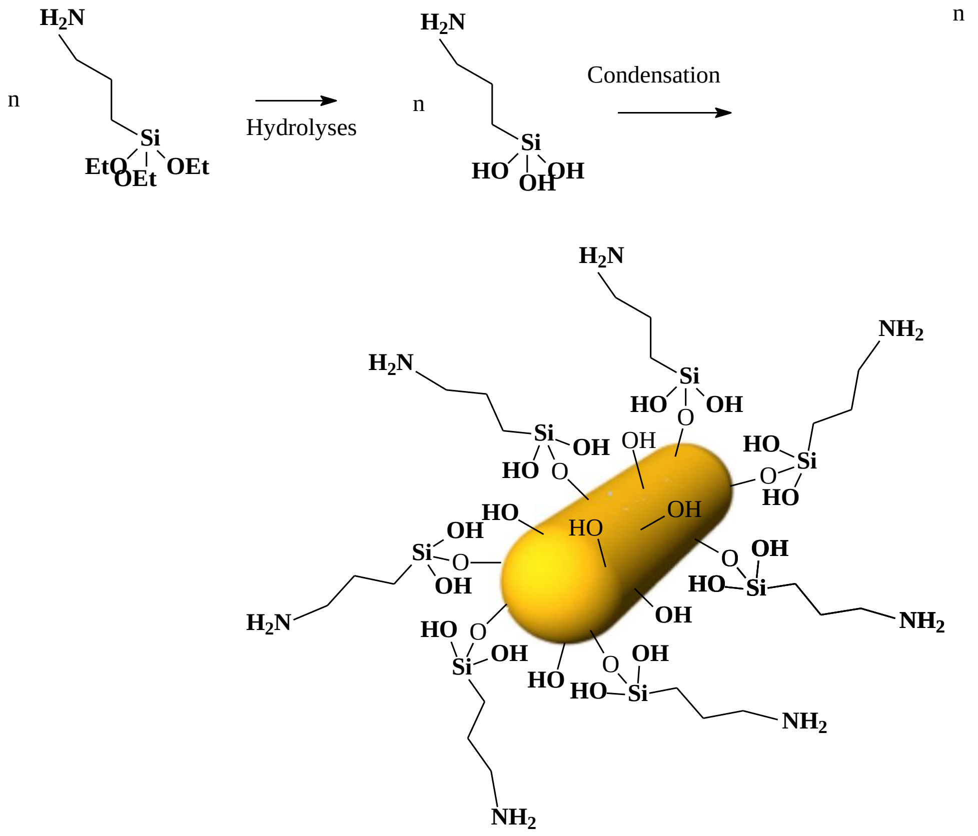

Figure 5.1 : Schematic view of TiO$_2$ nanorods surface modification.

For surface modification of TiO_2 nanorods, the produced TiO_2 NR/FTO electrode was immersed inside a solution containing 15 mL of IPA, 150 µl APTES and 6 drops pure water. The solution was placed in a water bath at 70°C for 30 min. The electrode was removed and rinsed with IPA and dried under N_2 stream (Luitel & Zamborini, 2013). This is labelled as modified (APTiO_2 NR/FTO) electrode. We thought that functionalization provides chemical connection between the TiO_2 NR surface and conductive polymer as described in figure 5.1 and figure 5.2.

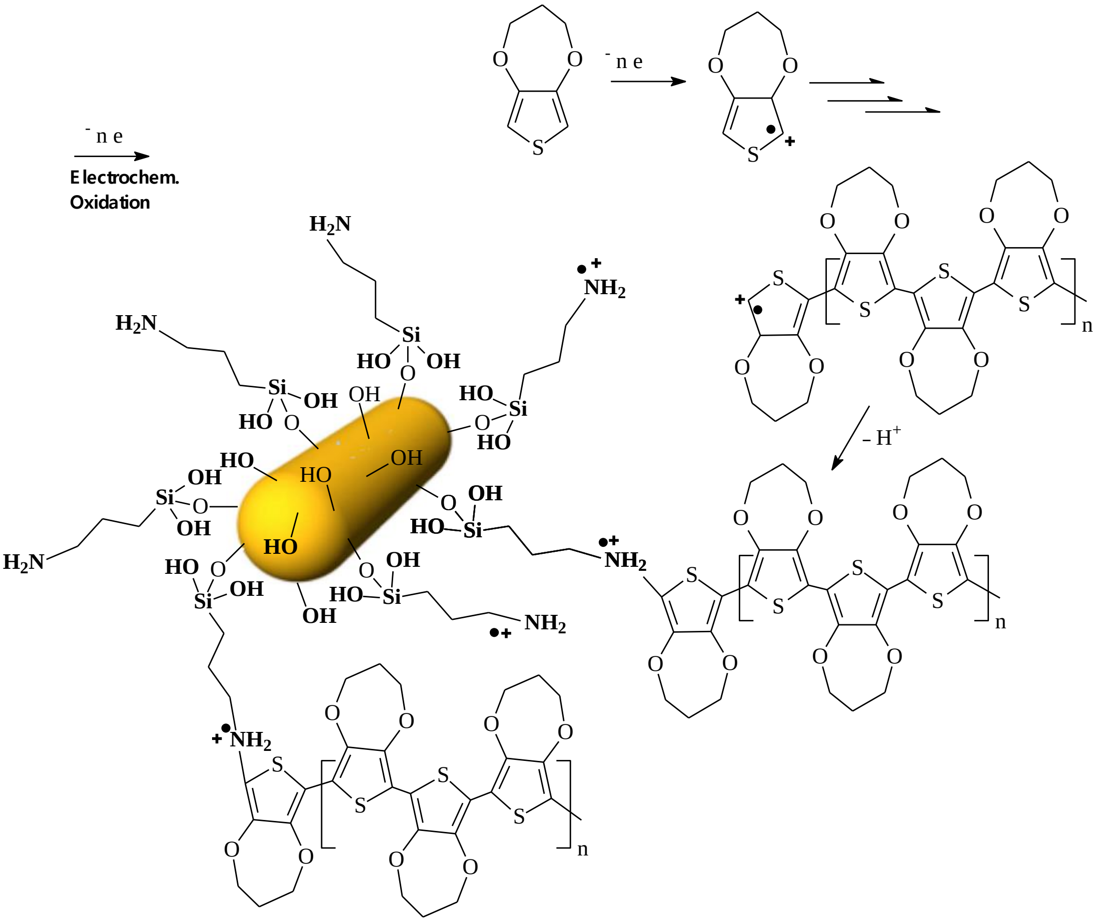

Figure 5.2 : Schematic illustration of the PProdot-APTiO_2 NR electrode fabrication.

5.1.3 Preparation of PProdot and PProdot/TiO_2 NR electrodes

Electrochemical polymerization of 3,4-propyleneenedioxythiophene was performed in ACN containing 0.1 M Bu_4NPF_6 and 0.01 M monomer. A three electrode cell configuration was employed consist of FTO and TiO_2 NR and NP/FTO as working electrode, Pt wire as counter electrode and Ag wire as a reference electrode. The conducting polymer films were electrodeposited onto FTO and TiO_2 NR/FTO glasses (it was waited 5 min in solution before polymerization in order to increase penetration of monomer inside of TiO_2 layer) by applying a constant potential of 2 V for 60 s (Parstat 2263, Tennessee, USA). In addition, for a comprasion, platinum electrode was fabricated by spray coating from 0.01 M H_2PtCl_6 (Sigma-Aldrich) solution in isopropanol (Merck) and sintering at 450^{o}C for 30 min.

5.1.4 Characterization

The morphological properties of electrodeposited films were investigated with using scanning electron microscopy (SEM, Hitachi TM-1000, Tokio, Japan) and atomic force microscopy (AFM, Nanosurf Easy Scan-2, Liestal, Switzerland). The catalytic activitiy of electrodes for I_3^- reduction was measured by cyclic voltammetry (CV) in a three compartment cell at a scan rate of 20 mV/s in 10 mM LiI, 1mM I_2 and 0.1 M $LiClO_4$ in an ACN solution (Gamry REF 600, USA). The active polymer area was investigated by CV in 5 mM $K_3Fe(CN)_6$ and 0.1 M KCl solution at a scan rate of 25, 50, 100, 150, 200 and 250 mV/s. The electrochemical impedance data~~s~~ (Gamry REF 600, USA) were measured by using the symmetric sandwich-type configuration to understand charge transfer process at the interface between the electrolyte and the counter electrode frequency varied from 0.01 Hz to 100 kHz with an AC amplitude 10 mV. For EIS measurement, a solution which contains 0.5 M LiI, 0.05 M I_2 and 0.5 M TBP in ACN was prepared.

5.2 Results and Discussion

5.2.1 Morphological characterization of electrodes

The reaction routes decribed in figure 5.1 includes APTES hydrolysis and surface attachment by the formation of Ti−O−Si bonds, leading to monolayer and/or multilayer formation as it was studied in detail in the case of iron oxide nanoparticles (Y. Liu, Li, Li, & He, 2013). We expected that the APTES precursor film is supposed to improve the contact between the TiO_2 nanorods and PProdot film, hence electrocatalytic activity of electrodes for triiodide reduction can be increased (Yuan et al., 2013). This is probably due to the favorable specific interactions of the Lewis acid-base type between the basic amino group (n donor) and positively charged Poly(3,4-propylenedioxythiophene) backbone (n acceptor) (figure 5.2) (Kızılcan, Öz, Ustamehmetoğlu, & Akar, 2006; X. Wang, Wang, Yang, Li, & Liu, 2013). The effect of modification on morphological properties of electrodes were investigated with SEM. For this purpose, Prodot was polymerized on the unmodified TiO_2 NR/FTO and APTES modified TiO_2 NR/FTO (labelled as $APTiO_2$ NR) electrodes under constant current 3 mA (≈2 V) for 30 s. Figure 5.3 exhibits SEM images of PProdot/TiO_2 NR and PProdot/$APTiO_2$ NR electrodes. According to figure 5.3, almost same surface morphologies were obtained for both electrodes. Obviously, PProdot was polymerized succesfully on TiO_2 nanorods. Also it was noted that for the unmodified electrode surface was covered slightly with PProdot compare to modified electrode surface may be due to the modification.

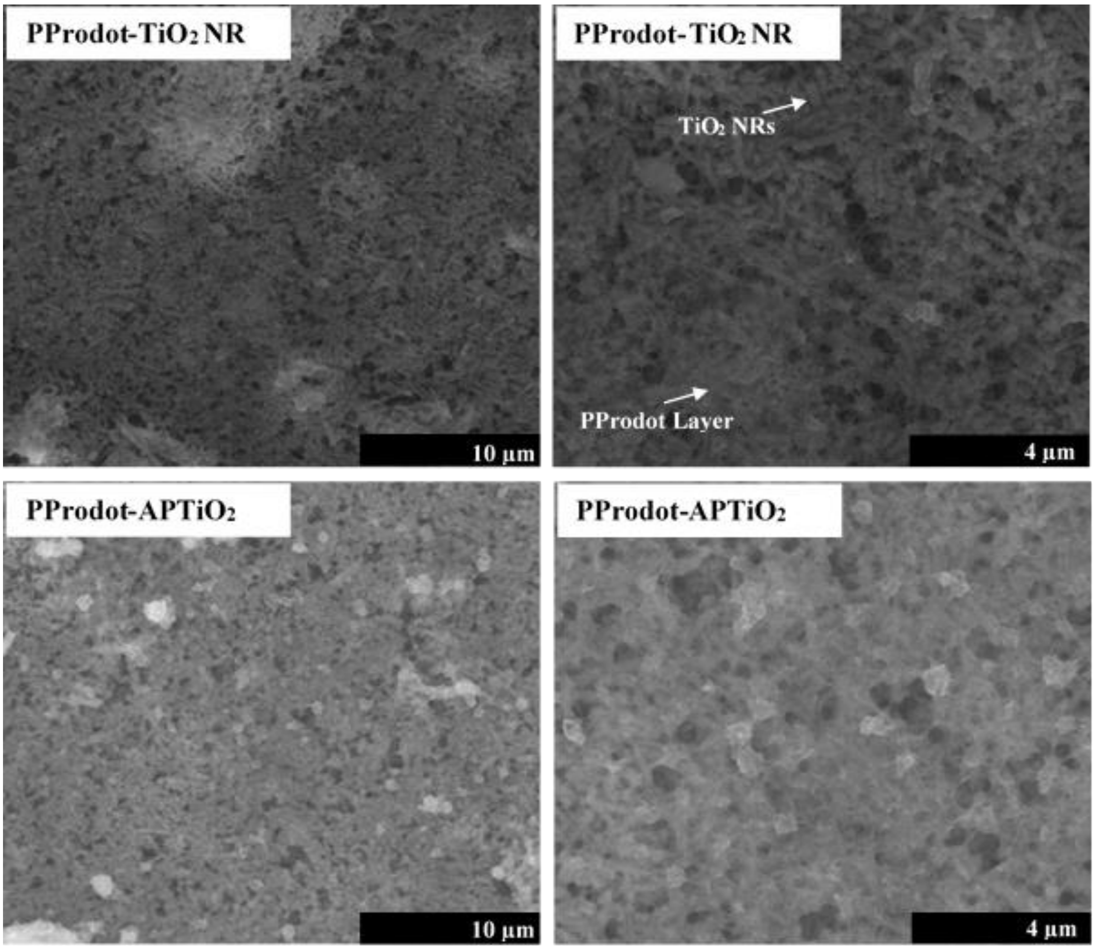

Figure 5.3 : SEM images of PProdot-TiO_2 NR (unmodified) (top) and PProdot-$APTiO_2$ NR (modified) (down) electrodes.

In order to support advantage of modification effect on electrode properties, one more experiment as carried out. For this purpose, unmodified and modified TiO_2 nano particles/FTO (nanoparticles were used instead of nanorods, another steps were same as explained in experimental section) electrodes were fabricated and then electrocatalytic ability of electrodes for triiodide reduction were analyzed. Figure 5.4 shows cyclic voltamograms of unmodified and modified electrodes. After silanization, higher current density value was obtained compare to unmodified TiO_2/PProdot electrodes (detailed analysis of CV graph can be found in section 3.2) which explains benefit of the modification. Therefore, the PProdot/APTiO_2 electrode was preferred to use for further experiments in this study.

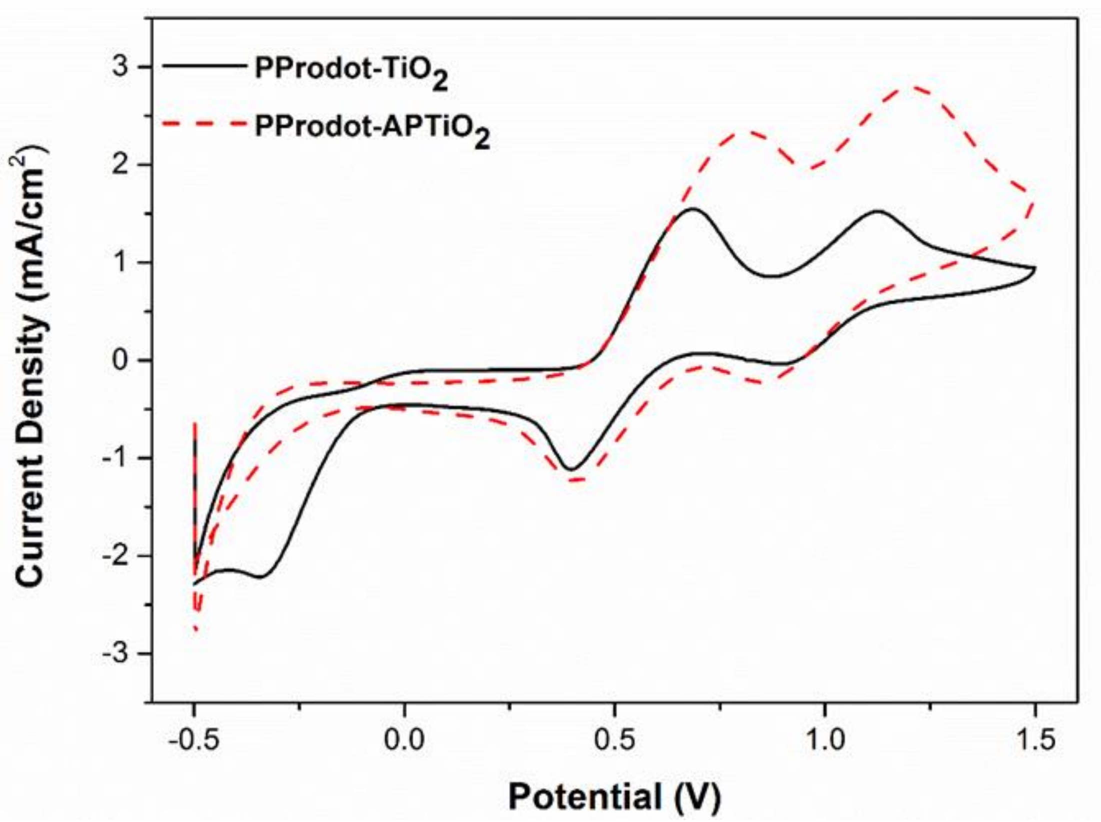

Figure 5.4 : Cyclic Voltamograms of PProdot-TiO_2 and PProdot-APTiO_2 electrodes in I_3^-/I^- redox couple solution.

Figure 5.5 shows the low magnification SEM images and AFM images of PProdot, PProdot-Me_2, PProdot-Et_2 and PProdot-TiO_2 NR electrodes, respectively. It can be seen that from SEM images, pure poly(3,4-alkylenedioxythiophene) surfaces were very smooth but after combined with APTES modified TiO_2 nanorods (PProdot-APTiO_2 NR) the film surface became porous and rough. These results were supported with AFM images. The surface root mean square roughness (RMS) values that obtained from AFM images of PProdot, PProdot-Me_2, PProdot-Et_2 and PProdot/TiO_2 NR were found 28, 24, 16 and 83 nm, respectively. The PProdot/TiO_2 NR film showed highest RMS value indicating that the film possessed the largest surface area amoung the other electrodes. In addition, we obtained that surface character of PProdot, PProdot-Me_2, PProdot-Et_2 electrodes haven't changed very much with changing functional groups of PProdot main structure.

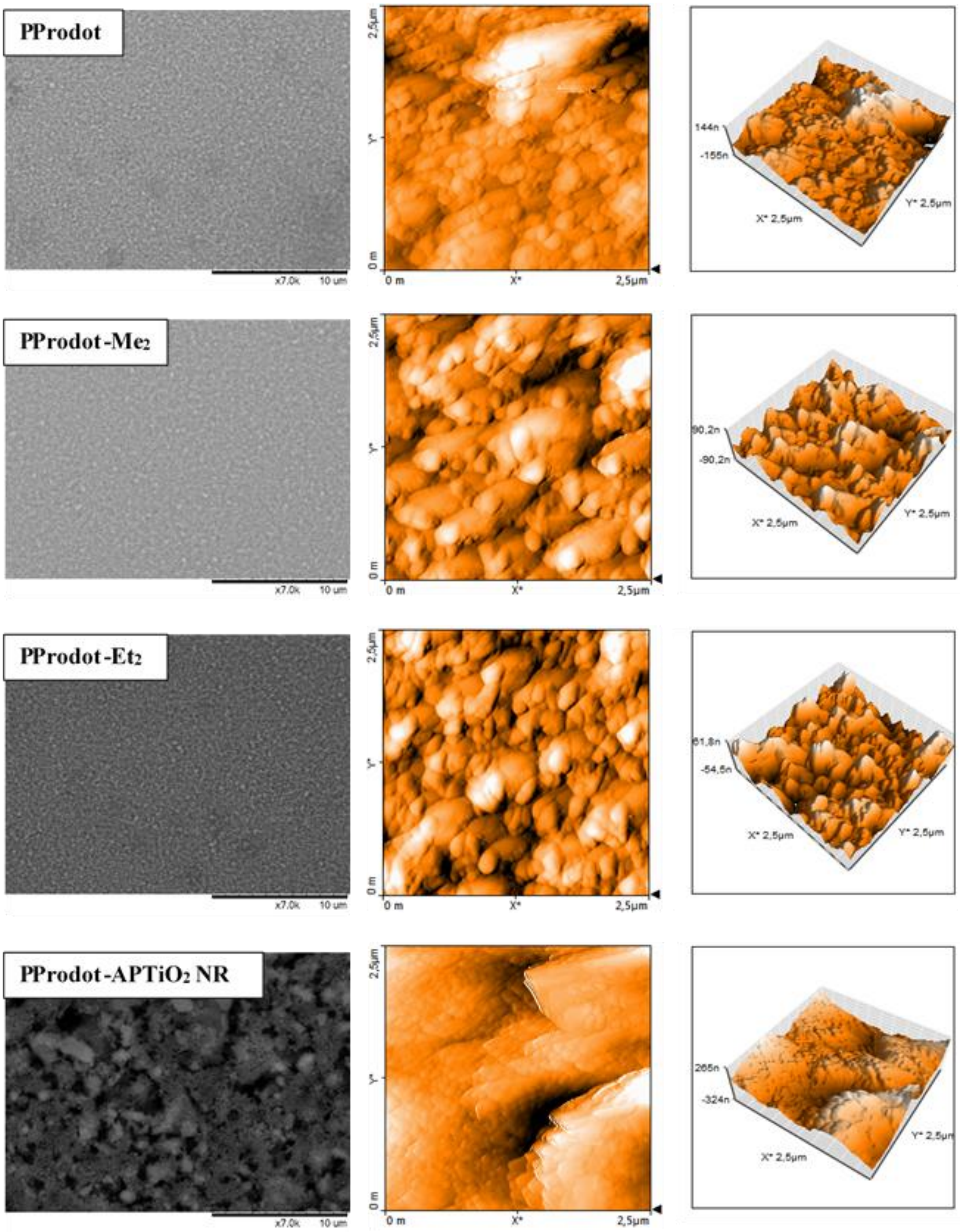

Figure 5.5 : SEM and AFM images of fabricated electrodes.

5.2.2 Cyclic Voltammetry Analysis

In order to estimate electro-active area of electrodes, cyclic voltammetry technique was used at different scanning rates in $K_3[Fe(CN)_6]$ solution. Figure 5.6 (a-d) represents cyclic voltamograms of the PProdot, PProdot-Me_2, PProdot-Et_2 and PProdot-$APTiO_2$ NR electrodes, respectively. It was obtained that current density increases with increasing scanning rate. The reduction current density of $Fe(CN)_6^{-3/-4}$

versus the square root of the scanning rate curves of the pure poly(3,4-alkylenedioxythiophene) and PProdot/APTiO$_2$ NR electrodes were shown in Figure 5.6-e. Ip–$\upsilon^{1/2}$ curves are obeyed to the Randles–Sevcik equation (Maiaugree et al., 2012; Sarac, Gilsing, Gencturk, & Schulz, 2007).

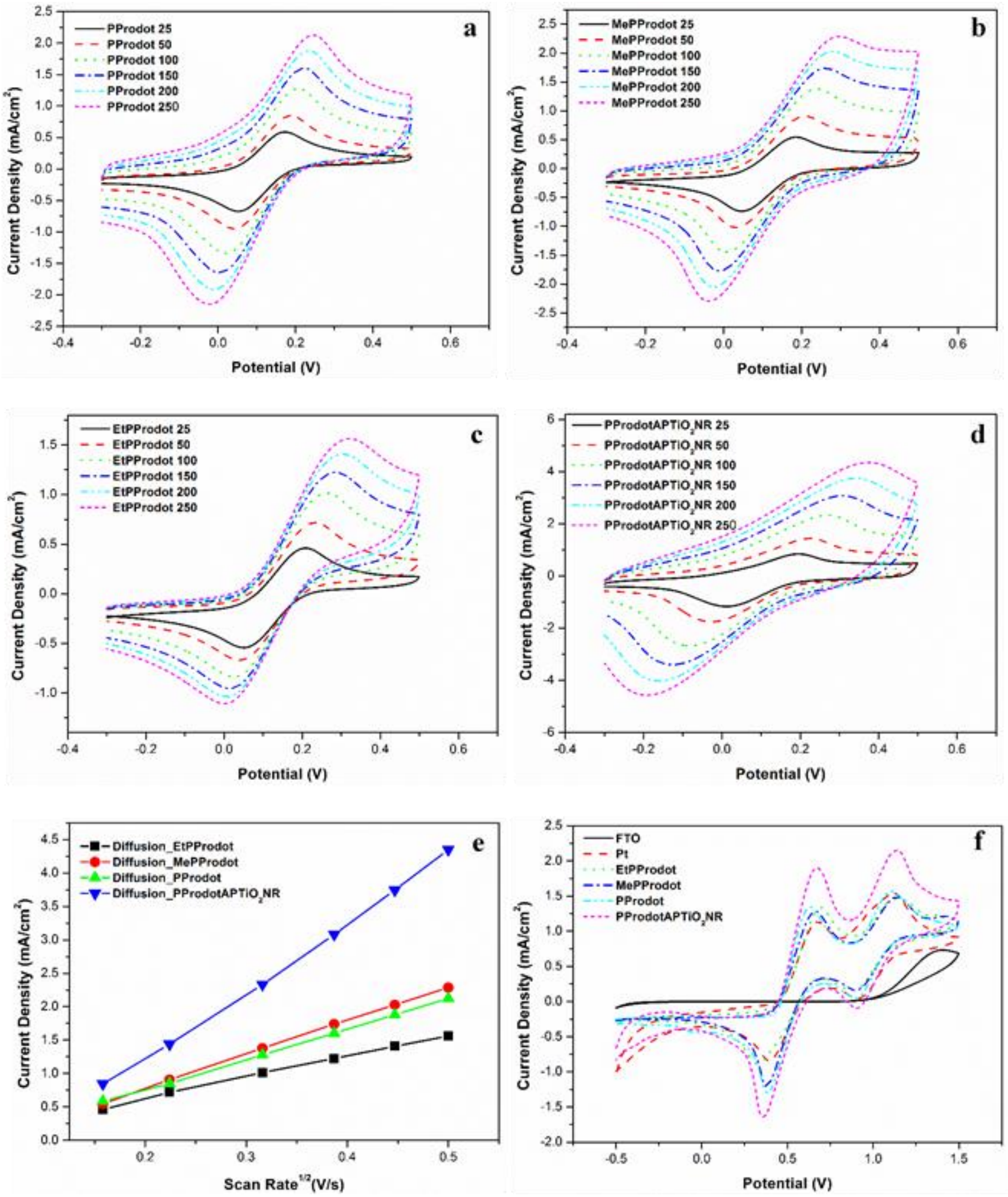

Figure 5.6 : CV curves of PProdot, PProdot-Me$_2$, PProdot-Et$_2$ and PProdot-APTiO$_2$ NR electrodes at different scan rates in K$_3$[(FeCN$_6$)] solution (a-d). Curves of Ip–$\upsilon^{1/2}$ and their values (e). CV curves of I$_3^-$/I$^-$ redox couple for all electrodes (f).

The magnitude of the reduction slopes of the PProdot/APTiO$_2$ NR electrode was higher than that of the pure poly(3,4-alkylenedioxythiophene) electrodes. n, D and C values in the equation should be the same for PProdot and PProdot/APTiO$_2$ NR since the same polymer and solution were used in each case. This assumes that the TiO_2 NRs do not show oxidation and reduction with $Fe(CN)_6^{-3/-4}$. Thus, the slope of Ip–$\upsilon^{1/2}$ curves varies only with the film active area. The increase in slopes of PProdot/APTiO$_2$ NR electrodes confirms the enlargment of their active areas (Maiaugree et al., 2012). These results were compatible with surface roughness values. According to AFM measurement, highest surface roughness was found for PProdot/APTiO$_2$ electrode. CV of the I_3^-/I^- redox couple in the pure poly(3,4-alkylenedioxythiophene), PProdot/APTiO$_2$ NR electrodes and the Pt electrode were presented in Figure 5.6-f. The Pt electrodes exhibited two main peaks: the negative peak is associated with the reduction of triiodide ($I_3^- + 2e \longrightarrow 3I^-$), and the positive peak is associated with the oxidation reaction ($3I_2 + 2e \longrightarrow 2I_3^-$) (Y.-F. Lin, Li, & Ho, 2016). The redox current density of I_3^-/I^- in the pure poly(3,4-alkylenedioxythiophene) electrodes are nearly same that in the Pt electrode. Also, it was obtained that the current density of reduction peak for composite electrode significantly increased from 1.13 mA to 1.90 mA when modified TiO_2 nanorods were combined with PProdot. The reduction peak position of all electrodes were about the same compared to the Pt electrode. This result suggested that TiO_2 nanorods improved catalytic activity of pure PProdot as expected. One possible reason for improved catalytic activity may be nanorods acted as filler when they combined with PProdot and providing better contact between the PProdot and I_3^-. Therefore, PProdot/APTiO$_2$ NR matrix render a synergistic catalytic effect compared to pure PProdot and other electrodes (Sudhagar et al., 2011). Another reason can be explained by increasing surface area after combination with modified TiO_2 nanorods. Figure 5.7 represents relation between surface roughness, slope values (figure 5.6-e) and current density of I_3^-/I^- (figure 5.6-f). It was obvious that current density can be manipulated by changing electro-active surface area which was related with RMS values. Because, since same polymer was used for fabrication of PProdot and PProdot/APTiO$_2$ electrodes, either surface roughness (from 28 nm to 83 nm) or slope of I_p- $\upsilon^{1/2}$ curve rised after adding TiO_2 nanorods. Hence, electrocatalytic ability of the electrodes strongly depends on specially electro-active surface area. Moreover, it was noted that there was no strong influence of functional groups on surface roughness so may be this is the reason why current density of PProdot, PProdot-Me$_2$ and PProdot-Et$_2$ for triiodide reduction were almost same.

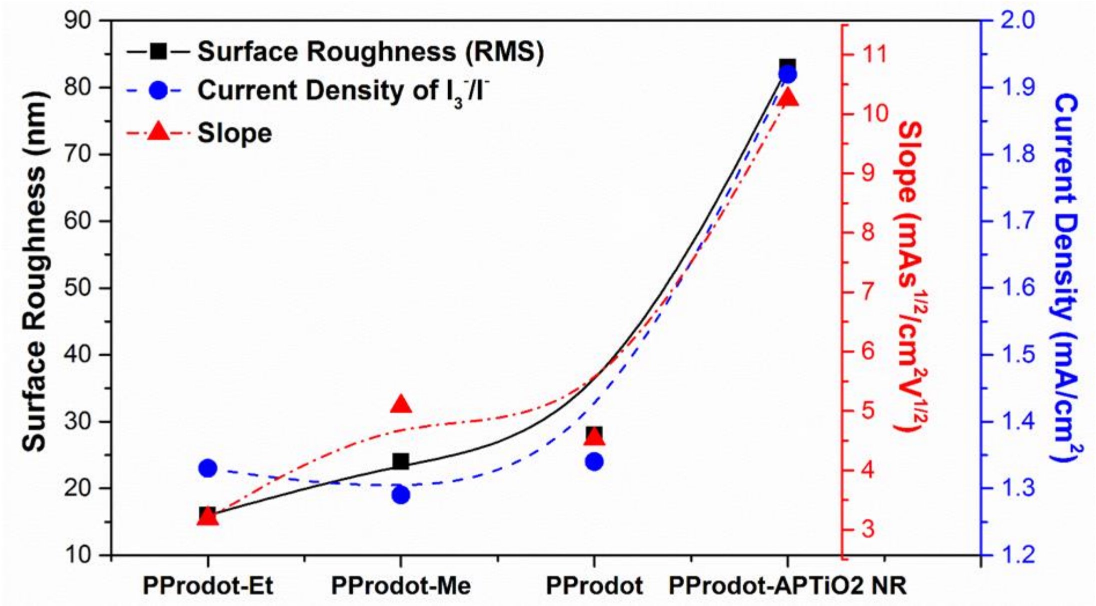

Figure 5.7 : Relation between surface roughness (RMS), slopes (figure 5.6-e) and current density of I_3^-/I^- redox couple (figure 5.6-f) for all electrodes.

5.2.3 Electrochemical impedance analysis of electrodes

Electrochemical impedance spectroscopy (EIS) was counducted in order to understand the electrochemical characteristics of fabricated electrodes. The symmetrical for example PProdot/PProdot and PProdot-APTiO$_2$/PProdot-APTiO$_2$ electrochemical cells were prepared by assembling two identical PProdot (or PProdot-APTiO$_2$) electrodes on each side separated with an electrolyte solution of I_3^-/I^- redox couple (Bu et al., 2013). Normally, these electrodes were separated by using hot melt spacer or Surlyn film but in this measurement distance between two symmetrical electrodes was kept constant (nearly 1 cm). These two symmetrical cells provides to eliminate the influence of photoanode. The low and high magnification of Nyquist plots for all electrodes were seen in figure 5.8 (a-b). For each curves except PProdot/redox couple/PProdot, showed two semicircles. The explanation of such EIS spectrum has been well-established. Typically, the intersection of high frequency semicircle at real axis expresses ohmic series resistance of device (R_s). The diameter of high frequency semicircle represents the charge transfer resistance (R_{ct}) at electrode and electrolyte interface, while the arc at lower frequency range can be assigned to the Nernst diffusion impedance within the electrolyte (Shi et al., 2015; Sudhagar et al., 2011). Amoung all the electrodes, the PProdot/APTiO$_2$ electrode has the smallest semicircle in the nyquist plot at high frequency region, suggesting that there is a small R_{ct} which is in accordance with the high performance for reduction of I_3^- ions in the CV measurement (figure 5.6-f) (Shi et al., 2015; Tsekouras et al., 2008). The diameter of semicircle increased for PProdot, PProdot-Me_2 and PProdot-Et_2 electrodes respectively which were almost matched with CV results. Besides the charge transfer impedance, the serial (or sheet) resistance (R_s) of the electrode related to the intrinsic resistance of assembled cells is another important parameter affecting the performance of counter electrode and it can also be obtained from EIS (Koo et al., 2006). As known from the literature, high R_s value causes lower fill factor, hence lower cell efficiency for DSSC (Bu et al., 2013). The value of R_s can be obtained from intercept point with zero imaginary part. We found that PProdot/APTiO_2 NR has the smallest sheet resistance. PProdot, PProdot-Me_2 have similar values and PProdot-Et_2 has the biggest sheet resistance. Actually, TiO_2 is a known metal oxide which has low conductivity and when they were combined with PProdot, it can be expected to obtain high sheet resistance compare to pure PProdot electrodes. But, results demontrated that PProdot/APTiO_2 has a prominent conductivity. Similar trend was obtained by Hu et. all as our work (H. Wang et al., 2013).

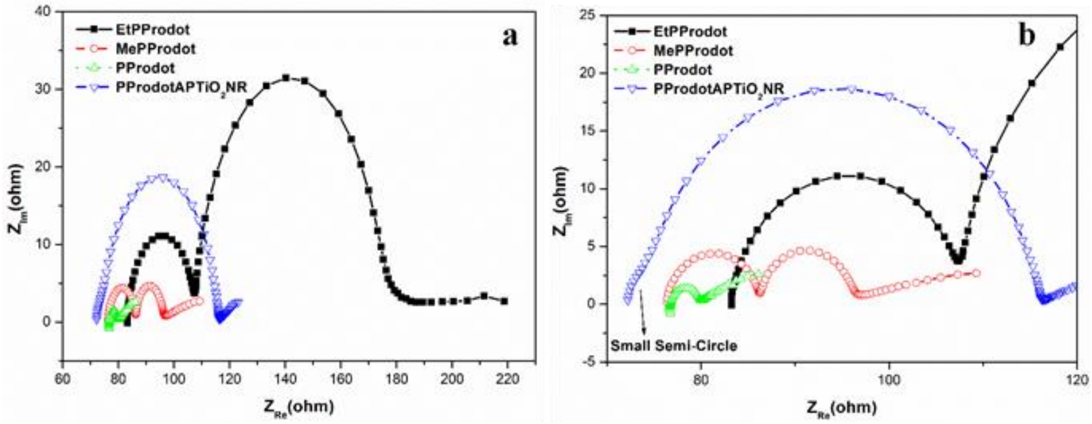

Figure 5.8 : Low magnification (a) and high magnification (b) nyquist plots of the electrodes.

5.3 Conclusion

We have succesfully electropolymerized Prodot on TiO_2 nanorods in order to produce PProdot/TiO_2 NR hybrid electrode which has a potential as counter electrodes for DSSC application. We found that modification of TiO_2 surfaces with APTES provides higher electrocatalytic ability and better interaction between TiO_2 and PProdot. According to EIS and CV results, PProdot/APTiO_2 hybrid electrode showed great electrocatalytic activity for I_3^- reduction. More importantly, a relation between surface roughness, electroactive surface area and electrocatalytic ability was obtained. An obvious enhancement of the hybrid PProdot/APTiO_2 surface area was observed after combination of TiO_2 nanorods and poly(3,4-propylenedioxythiophene) compare to the pure PProdot electrode, hence electrochemical activity increased. This phenomena was supported by both AFM and electrochemical measurements. Also, it was noted that there was no significant changing depends on functional groups on PProdot for such as surface roughness and current density for redox couple reduction.

6. CONCLUSIONS AND RECOMMENDATIONS

The design and fabrication of electrodes (such as counter electrode and photoanode) are essential task for a dye-sensitized solar cell (DSSC). Here the main purpose to fabricate TiO_2 based electrodes (composite with and without conductive polymer) onto transparent conductive oxides (TCO) and characterize them. In order to facilitate understanding of the thesis, the thesis was consisted of four main chapter except introduction part.

Chapter 2 describes the production procedure of TiO_2 nanofibers. Pure TiO_2 nanofibers were prepared via electrospinning technique and the precursor used is titanium tetra isopropoxide (Ti(Iso)). PVP was peferred as carrier polymer matrix for Ti(Iso) during electrospinning. Produced nanofibers were analyzed by XRD, FTIR-ATR spectroscopy, Raman spectroscopy, SEM and TGA. In addition, textural properties (S_{BET}, S_{meso}, V_{micro}, pore-size distribution) of nanofibers were evaluated from nitrogen physical adsorption-desorption isotherms. It was found that the average diameter of TiO_2 nanofibers can be manipulated depending on the PVP/Ti(Iso) ratio at the beginning of electrospinning. The calcination temperature at 450°C, which guarantees no organic residual and really good texture properties (surface area about 100 m^2/g), was chosen as the optimal calcination temperature for the preparation of TiO_2 nanofibers. According to XRD and Raman analysis, all prepared samples at 450°C possess TiO_2 in the anatase form. The photoelectrochemical efficiency of the nanofiber TiO_2 layers was determined by the amperometry measurements. It was proved that TiO_2 nanofiber layers/ITO electrodes prepared by electrospinning (TiO_2 thin nanofiber layers on ITO glass used as photoanode) showed really good photoinduced properties. It was noted that a very thin film of TiO_2 nanofiber layer was deposited onto ITO-glass since we also observed partial cracks on nanofiber layer after calcination due to the shrinking effect and the poor adhesion. Therefore, this integration problem was examined in chapter 3.

Chapter 3 deals with fabrication of stable TiO_2/FTO photoanodes prepared by three different deposition techniques. Dip-coating/FTO, Dip-coating-Nanofiber/FTO and

Nanorod/FTO electrodes were produced by calcination of PVP/Ti(Iso) layer following to dip-coating of the sol-gel solution, electrospinning on the dip-coating solution and electrospraying of calcinated and breaked TiO_2 nanofibers, respectively. Furthermore, a comprasion of effects of various deposition techniques on the structural, photoelectrochemical and electrochemical impedance properties of these electrodes were performed. Crystal structure of the electrodes were deterimened by both XRD and Raman measurements, cyrstal size of electrode TiO_2 layer was calculated with using Scherrer equation from XRD datas. It was found that crystal size of TiO_2, integration of TiO_2 onto the FTO significantly affected electrochemical impedance and photo-electrochemical properties of samples. Dip-coating/FTO electrodes have the biggest crystal size, lowest charge transfer resistance and highest photocurrent among the other electrodes prepared in this study. With using information that came from chapter 2 and chapter 3, design of TiO_2/conductive polymer (CP) composite counter electrodes were described in next chapter.

Chapter 4 investigates how catalytic activity of counter electrodes changes by using TiO_2 nanorods instead of TiO_2 nanoparticles. Thus, TiO_2 nanorods were obtained by ball milling method from produced TiO_2 nanofibers as described in chapter 2. Afterwards, TiO_2-PEDOT:PSS composite counter electrodes which have different morpholgy were fabricated by mixing obtained TiO_2 nanorods, TiO_2 nanoparticles and PEDOT:PSS physically. Morphology of the electrodes were examined by SEM. XRD measurements proved incorporation of TiO_2 into the PEDOT:PSS. According to CV measurements, the catalytic activity of PEDOT:PSS film was significantly improved after adding TiO_2 nanoparticles/nanorods. Electrochemical impedance spectroscopy showed that charge transfer resistance (R_{ct}) values strongly depends on (morphology) TiO_2 nanorods content into the composites and it was decreased by increasing TiO_2 nanorods content.

In chapter 5, derivatives of PEDOT was used as conductive polymers and (3,4-alkylenedioxyhiophene) was deposited onto TiO_2 nanorods surface electrochemically. For comprasion, pure (3,4-alkylenedioxyhiophene) and its derivatives were polymerized onto FTO electrochemically as well. Moreover, modification of TiO_2 nanorods surface was carried out with using silane coupling agent (APTES). We found that modification enhanced conductive polymer-TiO_2 interaction, thus catalytic activity of counter electrodes increased after modification.

According to EIS and CV results, PProdot/APTiO$_2$ hybrid electrode showed better electrocatalytic activity for I_3^- reduction. More importantly, a relation between surface roughness, electroactive surface area and electrocatalytic ability was obtained. AFM measurements showed that an obvious enhancement of the hybrid PProdot-APTiO$_2$ surface area was observed after combination of TiO$_2$ nanorods and poly(3,4-propylenedioxythiophene) compare to the pure PProdot electrode, hence electrochemical activity increased. Also, it was noted that there was no significant changing depends on functional groups on PProdot for such as surface roughness and current density for redox couple reduction.

We also make recommendation that further research remain to be carried out to explore different efficient and cheap counter electrodes using various conductive polymer and metal oxide to yield novel metal oxide/conductive polymer composites improving pure polymer properties.

REFERENCES

Acevedo-Peña, P., Vázquez, G., Laverde, D., Pedraza-Rosas, J. E., Manríquez, J., & González, I. (2009). Electrochemical Characterization of TiO2 Films Formed by Cathodic EPD in Aqueous Media. *Journal of the Electrochemical Society, 156*(11), C377-C386.

Ahmad, S., Bessho, T., Kessler, F., Baranoff, E., Frey, J., Yi, C., Nazeeruddin, M. K. (2012). A new generation of platinum and iodine free efficient dye-sensitized solar cells. *Physical Chemistry Chemical Physics, 14*(30), 10631-10639.

Archana, P., Jose, R., Yusoff, M., & Ramakrishna, S. (2011). Near band-edge electron diffusion in electrospun Nb-doped anatase TiO2 nanofibers probed by electrochemical impedance spectroscopy. *Applied physics letters, 98*(15), 152106.

Balkan, T., Guler, Z., Morozova, M., Dytrych, P., Solcova, O., & Sarac, A. S. (2016). The effect of deposition on electrochemical impedance properties of TiO2/FTO photoanodes. *Journal of Electroceramics*, 1-10.

Barakat, N. A., Hamza, A., Al-Deyab, S. S., Qurashi, A., & Kim, H. Y. (2012). Titanium-based polymeric electrospun nanofiber mats as a novel organic semiconductor. *Materials Science and Engineering: B, 177*(1), 34-42.

Berger, H., Tang, H., & Levy, F. (1993). Growth and Raman spectroscopic characterization of TiO 2 anatase single crystals. *Journal of crystal growth, 130*(1), 108-112.

Berger, T., Lana-Villarreal, T., Monllor-Satoca, D., & Gómez, R. (2006). Charge transfer reductive doping of nanostructured TiO 2 thin films as a way to improve their photoelectrocatalytic performance. *Electrochemistry Communications, 8*(11), 1713-1718.

Bu, C., Tai, Q., Liu, Y., Guo, S., & Zhao, X. (2013). A transparent and stable polypyrrole counter electrode for dye-sensitized solar cell. *Journal of Power Sources, 221*, 78-83.

Cha, S. I., Koo, B., Seo, S., & Lee, D. Y. (2010). Pt-free transparent counter electrodes for dye-sensitized solar cells prepared from carbon nanotube micro-balls. *J. Mater. Chem., 20*(4), 659-662.

Chen, J., Li, K., Luo, Y., Guo, X., Li, D., Deng, M., . . . Meng, Q. (2009). A flexible carbon counter electrode for dye-sensitized solar cells. *Carbon, 47*(11), 2704-2708.

Chen, J., Zhang, J., Xian, Y., Ying, X., Liu, M., & Jin, L. (2005). Preparation and application of TiO 2 photocatalytic sensor for chemical oxygen demand determination in water research. *Water research, 39*(7), 1340-1346.

Chun, H.-H., & Jo, W.-K. (2014). Polymer material-supported titania nanofibers with different polyvinylpyrrolidone to TiO 2 ratios for degradation of vaporous trichloroethylene. *Journal of Industrial and Engineering Chemistry, 20*(3), 1010-1015.

Dagli, U., Guler, Z., & Sarac, A. S. (2015). Covalent immobilization of Tyrosinase on electrospun Polyacrylonitrile/Polyurethane/Poly (m-anthranilic acid) nanofibers: an electrochemical impedance study. *Polymer-Plastics Technology and Engineering, 54*(14), 1494-1504.

De Crombrugghe, A., Yunus, S., & Bertrand, P. (2008). Grafting and characterization of protein on polyaniline surface for biosensor applications. *Surface and Interface Analysis, 40*(3-4), 404-407.

Du, P., Song, L., Xiong, J., & Cui, C. (2013). Optimization of electrospun TiO2 nanofibers photoanode film for dye-sensitized solar cells through interfacial pre-treatment, controllable calcination, and surface post-treatment. *Surface and Interface Analysis, 45*(13), 1878-1883.

Eberspächer, P., Wismeth, E., Buchner, R., & Barthel, J. (2006). Ion association of alkaline and alkaline-earth metal perchlorates in acetonitrile. *Journal of molecular liquids, 129*(1), 3-12.

Enriquez, R., & Pichat, P. (2006). Different net effect of TiO2 sintering temperature on the photocatalytic removal rates of 4-chlorophenol, 4-chlorobenzoic acid and dichloroacetic acid in water. *Journal of Environmental Science and Health Part A, 41*(6), 955-966.

Formo, E., Lee, E., Campbell, D., & Xia, Y. (2008). Functionalization of electrospun TiO2 nanofibers with Pt nanoparticles and nanowires for catalytic applications. *Nano Letters, 8*(2), 668-672.

Fujihara, K., Kumar, A., Jose, R., Ramakrishna, S., & Uchida, S. (2007). Spray deposition of electrospun TiO2 nanorods for dye-sensitized solar cell. *Nanotechnology, 18*(36), 365709.

Fujishima, A., Rao, T. N., & Tryk, D. A. (2000). TiO 2 photocatalysts and diamond electrodes. *Electrochimica Acta, 45*(28), 4683-4690.

Gao, F., Wang, Y., Shi, D., Zhang, J., Wang, M., Jing, X., . . . Grätzel, M. (2008). Enhance the optical absorptivity of nanocrystalline TiO2 film with high molar extinction coefficient ruthenium sensitizers for high performance dye-sensitized solar cells. *Journal of the American Chemical Society, 130*(32), 10720-10728.

Giray, D., Balkan, T., Dietzel, B., & Sarac, A. S. (2013). Electrochemical impedance study on nanofibers of poly (m-anthranilic acid)/polyacrylonitrile blends. *European polymer journal, 49*(9), 2645-2653.

Gracia, F., Holgado, J. P., & González-Elipe, A. R. (2004). Photoefficiency and optical, microstructural, and structural properties of TiO2 thin films used as photoanodes. *Langmuir, 20*(5), 1688-1697.

Grätzel, M. (2001). Photoelectrochemical cells. *nature, 414*(6861), 338-344.

Gu, H., Su, X. d., & Loh, K. P. (2005). Electrochemical impedance sensing of DNA hybridization on conducting polymer film-modified diamond. *The Journal of Physical Chemistry B, 109*(28), 13611-13618.

Guler, Z., & Sarac, A. (2016). Electrochemical impedance and spectroscopy study of the EDC/NHS activation of the carboxyl groups on poly (ε-caprolactone)/poly (m-anthranilic acid) nanofibers. *Express Polymer Letters, 10*(2).

Hashimoto, K., Irie, H., & Fujishima, A. (2005). TiO2 photocatalysis: a historical overview and future prospects. *Japanese journal of applied physics, 44*(12R), 8269.

Hou, Y., Wang, D., Yang, X. H., Fang, W. Q., Zhang, B., Wang, H. F., . . . Yang, H. G. (2013). Rational screening low-cost counter electrodes for dye-sensitized solar cells. *Nature communications, 4*, 1583.

Imoto, K., Takahashi, K., Yamaguchi, T., Komura, T., Nakamura, J.-i., & Murata, K. (2003). High-performance carbon counter electrode for dye-sensitized solar cells. *Solar Energy Materials and Solar Cells, 79*(4), 459-469.

Jang, J. S., Ham, D. J., Ramasamy, E., Lee, J., & Lee, J. S. (2010). Platinum-free tungsten carbides as an efficient counter electrode for dye sensitized solar cells. *Chemical Communications, 46*(45), 8600-8602.

Jhang, W. H., Lin Y. J., Ruan, C. H., & Liu, D. S. (2013). Doping mechanism in poly (3, 4-ethylenedioxythiophene) doped with poly (4-styrenesulfonate): TiO_2 nanoparticles composite films. *Thin Solid Films*, 539, 323-329.

Jiang, Q., Li, G., & Gao, X. (2009). Highly ordered TiN nanotube arrays as counter electrodes for dye-sensitized solar cells. *Chemical Communications*(44), 6720-6722.

Joshi, P., Zhang, L., Chen, Q., Galipeau, D., Fong, H., & Qiao, Q. (2010). Electrospun carbon nanofibers as low-cost counter electrode for dye-sensitized solar cells. *ACS applied materials & interfaces, 2*(12), 3572-3577.

Juengsuwattananon, K., Rujitanaroj, P. O., Supaphol, P., Pimpha, N., & Matsuzawa, S. (2008). *Preparation of ultrafine TiO2 nanofibers and their application in removal of NOx in air.* Paper presented at the Materials Science Forum.

Jung, Y. H., Park, K.-H., Oh, J. S., Kim, D.-H., & Hong, C. K. (2013). Effect of TiO2 rutile nanorods on the photoelectrodes of dye-sensitized solar cells. *Nanoscale research letters, 8*(1), 1-6.

Kang, S. H., Choi, S. H., Kang, M. S., Kim, J. Y., Kim, H. S., Hyeon, T., & Sung, Y. E. (2008). Nanorod-based dye-sensitized solar cells with improved charge collection efficiency. *Advanced materials, 20*(1), 54-58.

Kerkez, O., & Boz, İ. (2014). Photo (electro) catalytic Activity of Cu 2+-modified TiO 2 nanorod array thin films under visible light irradiation. *Journal of Physics and Chemistry of Solids, 75*(5), 611-618.

Kityakarn, S., Pooarporn, Y., Songsiriritthigul, P., Worayingyong, A., Robl, S., Braun, A. M., & Wörner, M. (2012). (Photo) Electrochemical characterization of nanoporous TiO 2 and Ce-doped TiO 2 sol–gel film electrodes. *Electrochimica Acta, 83*, 113-124.

Kızılcan, N., Öz, N. K., Ustamehmetoğlu, B., & Akar, A. (2006). High conductive copolymers of polypyrrole-α, ω-diamine polydimethylsiloxane. *European polymer journal, 42*(10), 2361-2368.

Kokubo, H., Ding, B., Naka, T., Tsuchihira, H., & Shiratori, S. (2007). Multi-core cable-like TiO2 nanofibrous membranes for dye-sensitized solar cells. *Nanotechnology, 18*(16), 165604.

Koo, B.-K., Lee, D.-Y., Kim, H.-J., Lee, W.-J., Song, J.-S., & Kim, H.-J. (2006). Seasoning effect of dye-sensitized solar cells with different counter electrodes. *Journal of Electroceramics, 17*(1), 79-82.

Krysova, H., Trckova-Barakova, J., Prochazka, J., Zukal, A., Maixner, J., & Kavan, L. (2014). Titania nanofiber photoanodes for dye-sensitized solar cells. *Catalysis Today, 230,* 234-239.

Kwon, C. H., Shin, H., Kim, J. H., Choi, W. S., & Yoon, K. H. (2004). Degradation of methylene blue via photocatalysis of titanium dioxide. *Materials Chemistry and Physics, 86*(1), 78-82.

Lagarec, K., & Desgreniers, S. (1995). Raman study of single crystal anatase TiO 2 up to 70 GPa. *Solid state communications, 94*(7), 519-524.

Lazar, M. A., Varghese, S., & Nair, S. S. (2012). Photocatalytic water treatment by titanium dioxide: recent updates. *Catalysts, 2*(4), 572-601.

Lee, K.-M., Chen, P.-Y., Hsu, C.-Y., Huang, J.-H., Ho, W.-H., Chen, H.-C., & Ho, K.-C. (2009). A high-performance counter electrode based on poly (3, 4-alkylenedioxythiophene) for dye-sensitized solar cells. *Journal of Power Sources, 188*(1), 313-318.

Li C. T., Lee C. P., Li Y. Y., Yeh M. H., & Ho K. C. (2013). A composite film of TiS_2/PEDOT: PSS as the electrocatalyst for the counter electrode in dye-sensitized solar cells. *Journal of Materials Chemistry A, 1,* 14888-14896.

Li, D., & Xia, Y. (2003). Fabrication of titania nanofibers by electrospinning. *Nano Letters, 3*(4), 555-560.

Li, G. R., Wang, F., Jiang, Q. w., Gao, X. p., & Shen, P. w. (2010). Carbon Nanotubes with Titanium Nitride as a Low-Cost Counter-Electrode Material for Dye-Sensitized Solar Cells. *Angewandte Chemie International Edition, 49*(21), 3653-3656.

Li, H., Wang, J., Chu, Q., Wang, Z., Zhang, F., & Wang, S. (2009). Theoretical and experimental specific capacitance of polyaniline in sulfuric acid. *Journal of Power Sources, 190*(2), 578-586.

Li, Q., Wu, J., Tang, Q., Lan, Z., Li, P., Lin, J., & Fan, L. (2008). Application of microporous polyaniline counter electrode for dye-sensitized solar cells. *Electrochemistry Communications, 10*(9), 1299-1302.

Li, R., Liu, D., Zhou, D., Shi, Y., Wang, Y., & Wang, P. (2010). Influence of the electrolyte cation in organic dye-sensitized solar cells: lithium versus dimethylimidazolium. *Energy & Environmental Science, 3*(11), 1765-1772.

Lin, C.-H., Chao, J.-H., Liu, C.-H., Chang, J.-C., & Wang, F.-C. (2008). Effect of calcination temperature on the structure of a Pt/TiO2 (B) nanofiber and its photocatalytic activity in generating H2. *Langmuir, 24*(17), 9907-9915.

Lin, Y.-F., Li, C.-T., & Ho, K.-C. (2016). A template-free synthesis of the hierarchical hydroxymethyl PEDOT tube-coral array and its application in dye-sensitized solar cells. *Journal of Materials Chemistry A, 4*(2), 384-394.

Liu, B., & Aydil, E. S. (2009). Growth of oriented single-crystalline rutile TiO2 nanorods on transparent conducting substrates for dye-sensitized solar cells. *Journal of the American Chemical Society, 131*(11), 3985-3990.

Liu, Y., Li, Y., Li, X.-M., & He, T. (2013). Kinetics of (3-aminopropyl) triethoxylsilane (APTES) silanization of superparamagnetic iron oxide nanoparticles. *Langmuir, 29*(49), 15275-15282.

Liu, Y., Sun, D., Askari, S., Patel, J., Macias-Montero, M., Mitra, S., Zhang, R., Lin, W. F., Mariotti, D., & Maguire, P. (2015). Enhanced dispersion of TiO2 nanoparticles in a TiO2/PEDOT: PSS hybrid nanocomposite via plasma-liquid interactions. *Scientific Reports*, *5,* 15765-15776.

Luitel, T., & Zamborini, F. P. (2013). Covalent modification of photoanodes for stable dye-sensitized solar cells. *Langmuir, 29*(44), 13582-13594.

Lv, X., Zhang, H., & Chang, H. (2012). Improved photocatalytic activity of highly ordered TiO 2 nanowire arrays for methylene blue degradation. *Materials Chemistry and Physics, 136*(2), 789-795.

Maiaugree, W., Pimanpang, S., Towannang, M., Saekow, S., Jarernboon, W., & Amornkitbamrung, V. (2012). Optimization of TiO 2 nanoparticle mixed PEDOT–PSS counter electrodes for high efficiency dye sensitized solar cell. *Journal of Non-Crystalline Solids, 358*(17), 2489-2495.

Mane, R. S., Lee, W. J., Pathan, H. M., & Han, S.-H. (2005). Nanocrystalline TiO2/ZnO thin films: fabrication and application to dye-sensitized solar cells. *The Journal of Physical Chemistry B, 109*(51), 24254-24259.

Matějová, L., Matěj, Z., & Šolcová, O. (2012). A facile synthesis of well-defined titania nanocrystallites: Study on their growth, morphology and surface properties. *Microporous and mesoporous materials, 154*, 187-195.

Miettunen, K., Halme, J., Vahermaa, P., Saukkonen, T., Toivola, M., & Lund, P. (2009). Dye solar cells on ITO-PET substrate with TiO2 recombination blocking layers. *Journal of the Electrochemical Society, 156*(8), B876-B883.

Morand, R., Lopez, C., Koudelka-Hep, M., Kedzierzawski, P., & Augustynski, J. (2002). Photoelectrochemical behavior in low-conductivity media of nanostructured TiO2 films deposited on interdigitated microelectrode arrays. *The Journal of Physical Chemistry B, 106*(29), 7218-7224.

Morozova, M., Kluson, P., Krysa, J., Gwenin, C., & Solcova, O. (2011). Oxalic acid sensors based on sol–gel nanostructured TiO2 films. *Journal of sol-gel science and technology, 58*(1), 175-181.

Mukherjee, K., Teng, T.-H., Jose, R., & Ramakrishna, S. (2009). Electron transport in electrospun TiO2 nanofiber dye-sensitized solar cells. *Applied physics letters, 95*(1), 012101.

Mulmudi, H. K., Batabyal, S. K., Rao, M., Prabhakar, R. R., Mathews, N., Lam, Y. M., & Mhaisalkar, S. G. (2011). Solution processed transition metal sulfides: application as counter electrodes in dye sensitized solar cells (DSCs). *Physical Chemistry Chemical Physics, 13*(43), 19307-19309.

Nazeeruddin, M. K., Baranoff, E., & Grätzel, M. (2011). Dye-sensitized solar cells: a brief overview. *Solar Energy, 85*(6), 1172-1178.

O'regan, B., & Grfitzeli, M. (1991). A low-cost, high-efficiency solar cell based on dye-sensitized. *Nature, 353*(6346), 737-740.

Okuzaki H., Hosaka K., Suzuki H., & Ito T (2010). Electrically driven PEDOT/PSS actuators. Conference electrically driven PEDOT/PSS actuators. *International Society for Optics and Photonics, 7642*, 76422U.

Onozuka, K., Ding, B., Tsuge, Y., Naka, T., Yamazaki, M., Sugi, S., . . . Shiratori, S. (2006). Electrospinning processed nanofibrous TiO2 membranes for photovoltaic applications. *Nanotechnology, 17*(4), 1026.

Park, J.-Y., & Park, S.-M. (2009). DNA hybridization sensors based on electrochemical impedance spectroscopy as a detection tool. *Sensors, 9*(12), 9513-9532.

Park, J. Y., & Kim, S. S. (2009). Effects of processing parameters on the synthesis of TiO2 nanofibers by electrospinning. *Metals and Materials International, 15*(1), 95-99.

Porter, S., DeArmitt, C., Robinson, R., Kirby, J., & Bott, D. (1989). The Surface Characterization of Polyacrylonitrile-based Carbon Fibres by Electrochemical Techniques. *High Performance Polymers, 1*(1), 85-94.

Qiao, Q. (2011). *Carbon Nanostructures as Low Cost Counter Electrode for Dye-Sensitized Solar Cells*: INTECH Open Access Publisher.

Radecka, M., Wierzbicka, M., & Rekas, M. (2004). Photoelectrochemical cell studied by impedance spectroscopy. *Physica B: Condensed Matter, 351*(1), 121-128.

Rammelt, U., Hebestreit, N., Fikus, A., & Plieth, W. (2001). Investigation of polybithiophene/n-TiO 2 bilayers by electrochemical impedance spectroscopy and photoelectrochemistry. *Electrochimica Acta, 46*(15), 2363-2371.

Rao, K. N. (2002). Influence of deposition parameters on optical properties of TiO2 films. *Optical Engineering, 41*(9), 2357-2364.

Rodríguez-Sevilla, E., Ramírez-Silva, M.-T., Romero-Romo, M., Ibarra-Escutia, P., & Palomar-Pardavé, M. (2014). Electrochemical quantification of the antioxidant capacity of medicinal plants using biosensors. *Sensors, 14*(8), 14423-14439.

Roy-Mayhew, J. D., Bozym, D. J., Punckt, C., & Aksay, I. A. (2010). Functionalized graphene as a catalytic counter electrode in dye-sensitized solar cells. *Acs Nano, 4*(10), 6203-6211.

Saad, L., Feteha, M., Ebrahim, S., Soliman, M., & Abdel-Fattah, T. M. (2014). Dye Sensitized Solar Cell Based on Polyaniline-Carbon Nanotubes/Graphite Composite. *ECS Journal of Solid State Science and Technology, 3*(10), M55-M60.

Saito Y., Kubo W., Kitamura T., Wada Y., & Yanagida S. (2004). I^-/I_3^- redox reaction behavior on poly (3, 4-ethylenedioxythiophene) counter electrode in dye-sensitized solar cells. *Journal of Photochemistry and Photobiology A: Chemistry, 164*(1-3), 153-157.

Saji, V. S., & Pyo, M. (2010). Dye sensitized solar cell of TiO 2 nanoparticle/nanorod composites prepared via low-temperature synthesis in oleic acid. *Thin Solid Films, 518*(22), 6542-6546.

Sakurai, S., Jiang, H.-q., Takahashi, M., & Kobayashi, K. (2009). Enhanced performance of a dye-sensitized solar cell with a modified poly (3, 4-ethylenedioxythiophene)/TiO 2/FTO counter electrode. *Electrochimica Acta, 54*(23), 5463-5469.

Sarac, A. S., Gencturk, A., Schulz, B., Gilsing, H.-D., & Serantoni, M. (2007). Nanoscale Surface Morphology and Monomer Concentration Dependence on Impedance of Electrocoated 2, 2-Dimethyl-3, 4-Propylene-dioxythiophene on Carbon Fiber Microelectrode. *Journal of nanoscience and nanotechnology, 7*(10), 3543-3552.

Sarac, A. S., Gilsing, H.-D., Gencturk, A., & Schulz, B. (2007). Electrochemically polymerized 2, 2-dimethyl-3, 4-propylenedioxythiophene on carbon fiber for microsupercapacitor. *Progress in organic coatings, 60*(4), 281-286.

Saranya, K., Rameez, M., & Subramania, A. (2015). Developments in conducting polymer based counter electrodes for dye-sensitized solar cells–An overview. *European polymer journal, 66*, 207-227.

Schattauer, S., Reinhold, B., Albrecht, S., Fahrenson, C., Schubert, M., Janietz, S., & Neher, D. (2012). Influence of sintering on the structural and electronic properties of TiO2 nanoporous layers prepared via a non-sol–gel approach. *Colloid and Polymer Science, 290*(18), 1843-1854.

Schneider, P. (1995). Adsorption isotherms of microporous-mesoporous solids revisited. *Applied Catalysis A: General, 129*(2), 157-165.

Schneider, P., Hudec, P., & Solcova, O. (2008). Pore-volume and surface area in microporous–mesoporous solids. *Microporous and mesoporous materials, 115*(3), 491-496.

Seo, H., Son, M.-K., Itagaki, N., Koga, K., & Shiratani, M. (2016). Polymer counter electrode of poly (3, 4-ethylenedioxythiophene): Poly (4-styrenesulfonate) containing TiO_2 nano-particles for dye-sensitized solar cells. *Journal of Power Sources, 307*, 25-30.

Shi, Z., Deng, K., & Li, L. (2015). Pt-free and efficient counter electrode with nanostructured CoNi2S4 for dye-sensitized solar cells. *Scientific reports, 5*.

Siuzdak, K., Sawczak, M., & Lisowska-Oleksiak, A. (2015). Fabrication and properties of electrode material composed of ordered titania nanotubes and pEDOT: PSS. *Solid State Ionics, 271*, 56-62.

Solcova, O., Balkan, T., Guler, Z., Morozova, M., Dytrych, P., & Sarac, A. S. (2014). New Preparation Route of TiO2 Nanofibers by Electrospinning: Spectroscopic and Thermal Characterizations. *Science of Advanced Materials, 6*(12), 2618-2624.

Šolcová, O., Matějová, L., Krejčíková, S., Matěj, Z., Kužel, R., Strýhal, Z., & Benada, O. (2008). Structural Study of Tailored Titania Thin Layers. *Collection of Czechoslovak Chemical Communications, 73*(8), 1222-1230.

Song, M. Y., Kim, D. K., Ihn, K. J., Jo, S. M., & Kim, D. Y. (2004). Electrospun TiO2 electrodes for dye-sensitized solar cells. *Nanotechnology, 15*(12), 1861.

Sudhagar, P., Nagarajan, S., Lee, Y.-G., Song, D., Son, T., Cho, W., . . . Kang, Y. S. (2011). Synergistic catalytic effect of a composite (CoS/PEDOT: PSS) counter electrode on triiodide reduction in dye-sensitized solar cells. *ACS applied materials & interfaces, 3*(6), 1838-1843.

Tammawat, P., & Meethong, N. (2013). Synthesis and characterization of stable and binder-free electrodes of TiO 2 nanofibers for li-ion batteries. *Journal of Nanomaterials, 2013*, 1.

Tang, Y., Tao, J., Zhang, Y., Wu, T., Tao, H., & Bao, Z. (2008). Preparation and Characterization of TiO 2 Nanotube Arrays via Anodization of Titanium Films Deposited on FTO Conducting Glass at Room Temperature. *Acta Physico-Chimica Sinica, 24*(12), 2191-2197.

Thamaphat, K., Limsuwan, P., & Ngotawornchai, B. (2008). Phase characterization of TiO2 powder by XRD and TEM. *Kasetsart J.(Nat. Sci.), 42*(5), 357-361.

Theerthagiri, J., Senthil, A. R., Madhavan, J., & Maiyalagan, T. (2015). Recent Progress in Non-Platinum Counter Electrode Materials for Dye-Sensitized Solar Cells. *ChemElectroChem, 2*(7), 928-945.

Thompson, P. A., & Simon, J. D. (1993). Electrolyte effects on the energetics and dynamics of intermolecular electron transfer reactions. *Journal of the American Chemical Society, 115*(13), 5657-5664.

Toivola, M. (2010). Dye-sensitized solar cells on alternative substrates.

Tsekouras, G., Mozer, A. J., & Wallace, G. G. (2008). Enhanced performance of dye sensitized solar cells utilizing platinum electrodeposit counter electrodes. *Journal of the Electrochemical Society, 155*(7), K124-K128.

Vasudevan, P., Thomas, S., Biju, P., Sudarsanakumar, C., & Unnikrishnan, N. (2012). Synthesis and structural characterization of sol–gel derived titania/poly (vinyl pyrrolidone) nanocomposites. *Journal of sol-gel science and technology, 62*(1), 41-46.

Veerappan, G., Bojan, K., & Rhee, S.-W. (2012). Amorphous carbon as a flexible counter electrode for low cost and efficient dye sensitized solar cell. *Renewable Energy, 41*, 383-388.

Viswanathamurthi, P., Bhattarai, N., Kim, C., Kim, H., & Lee, D. (2004). Ruthenium doped TiO 2 fibers by electrospinning. *Inorganic Chemistry Communications, 7*(5), 679-682.

Wang, H., Wei, W., & Hu, Y. H. (2013). Efficient ZnO-based counter electrodes for dye-sensitized solar cells. *Journal of Materials Chemistry A, 1*(22), 6622-6628.

Wang, M., Anghel, A. M., Marsan, B. t., Cevey Ha, N.-L., Pootrakulchote, N., Zakeeruddin, S. M., & Grätzel, M. (2009). CoS supersedes Pt as efficient electrocatalyst for triiodide reduction in dye-sensitized solar cells. *Journal of the American Chemical Society, 131*(44), 15976-15977.

Wang, X., Wang, T., Yang, C., Li, H., & Liu, P. (2013). Well-defined flake-like polypyrrole grafted graphene nanosheets composites as electrode materials for supercapacitors with enhanced cycling stability. *Applied Surface Science, 287*, 242-251.

Watthanaarun, J., Pavarajarn, V., & Supaphol, P. (2005). Titanium (IV) oxide nanofibers by combined sol–gel and electrospinning techniques: preliminary report on effects of preparation conditions and secondary metal dopant. *Science and Technology of Advanced Materials, 6*(3), 240-245.

Wu, M., Lin, X., Wang, T., Qiu, J., & Ma, T. (2011). Low-cost dye-sensitized solar cell based on nine kinds of carbon counter electrodes. *Energy & Environmental Science, 4*(6), 2308-2315.

Wu, M., & Ma, T. (2014). Recent progress of counter electrode catalysts in dye-sensitized solar cells. *The Journal of Physical Chemistry C, 118*(30), 16727-16742.

Xia, J., Chen, L., & Yanagida, S. (2011). Application of polypyrrole as a counter electrode for a dye-sensitized solar cell. *Journal of Materials Chemistry, 21*(12), 4644-4649.

Xie, Y., & Fu, D. (2010). Photochemical performance and electrochemical capacitance of titania nanocomplexes. *Materials Research Bulletin, 45*(5), 628-635.

Xin, X., He, M., Han, W., Jung, J., & Lin, Z. (2011). Low-Cost Copper Zinc Tin Sulfide Counter Electrodes for High-Efficiency Dye-Sensitized Solar Cells. *Angewandte Chemie International Edition, 50*(49), 11739-11742.

Xu, H., Zhang, X., Zhang, C., Liu, Z., Zhou, X., Pang, S., . . . Zhang, L. (2012). Nanostructured titanium nitride/PEDOT: PSS composite films as counter electrodes of dye-sensitized solar cells. *ACS applied materials & interfaces, 4*(2), 1087-1092.

Ye, M., Wen, X., Wang, M., Iocozzia, J., Zhang, N., Lin, C., & Lin, Z. (2015). Recent advances in dye-sensitized solar cells: from photoanodes, sensitizers and electrolytes to counter electrodes. *Materials Today, 18*(3), 155-162.

Yella, A., Lee, H.-W., Tsao, H. N., Yi, C., Chandiran, A. K., Nazeeruddin, M. K., . . . Grätzel, M. (2011). Porphyrin-sensitized solar cells with cobalt (II/III)–based redox electrolyte exceed 12 percent efficiency. *Science, 334*(6056), 629-634.

Yu, J., Yu, H., Cheng, B., & Trapalis, C. (2006). Effects of calcination temperature on the microstructures and photocatalytic activity of titanate nanotubes. *Journal of Molecular Catalysis A: Chemical, 249*(1), 135-142.

Yuan, C., Guo, S., Wang, S., Liu, L., Chen, W., & Wang, E. (2013). Electropolymerization polyoxometalate (POM)-doped PEDOT film electrodes with mastoid microstructure and its application in dye-sensitized solar cells (DSSCs). *Industrial & Engineering Chemistry Research, 52*(20), 6694-6703.

Yue, G., Wu, J., Xiao, Y., Lin, J., Huang, M., Lan, Z., & Fan, L. (2013). Functionalized graphene/poly (3, 4-ethylenedioxythiophene):

polystyrenesulfonate as counter electrode catalyst for dye-sensitized solar cells. *Energy, 54*, 315-321.

Yun, D.-J., Ra, H., & Rhee, S.-W. (2013). Concentration effect of multiwalled carbon nanotube and poly (3, 4-ethylenedioxythiophene) polymerized with poly (4-styrenesulfonate) conjugated film on the catalytic activity for counter electrode in dye sensitized solar cells. *Renewable Energy*, *50*, 692-700.

Zhang, L., Li, Y., Zhang, Q., & Wang, H. (2013). Formation of the modified ultrafine anatase TiO 2 nanoparticles using the nanofiber as a microsized reactor. *CrystEngComm, 15*(8), 1607-1612.

Zhang, Y., Weidenkaff, A., & Reller, A. (2002). Mesoporous structure and phase transition of nanocrystalline TiO 2. *Materials Letters, 54*(5), 375-381.

Zhang, Z., Zhang, X., Xu, H., Liu, Z., Pang, S., Zhou, X., & Cui, G. (2012). CuInS2 nanocrystals/PEDOT: PSS composite counter electrode for dye-sensitized solar cells. *ACS applied materials & interfaces, 4*(11), 6242-6246.

Zhao, X., Li, M., Song, D., Cui, P., Zhang, Z., Zhao, Y., & Zhang, Z. (2014). A novel hierarchical Pt-and FTO-free counter electrode for dye-sensitized solar cell. *Nanoscale research letters, 9*(1), 1-5.

Zhou Q., Chen S., Zhang M., Wang L., Li Y., & Shi G. (2016). Solution-processed graphene composite films as free standing platinum-free counter electrodes for bendable dye sensitized solar cells. *Chinese Journal of Chemistry*, *34*(1), 59-66.

Zhou Q., & Shi G. (2016). Conducting polymer-based catalysts. *Journal of the American Chemical Society*, *138*(9), 2868-2876.

Zhu, R., Jiang, C.-Y., Liu, X.-Z., Liu, B., Kumar, A., & Ramakrishna, S. (2008). Improved adhesion of interconnected TiO2 nanofiber network on conductive substrate and its application in polymer photovoltaic devices. *Applied physics letters, 93*(1), 013102.

APPENDICES

APPENDIX A: SEM images and diameter distribution of PVP nanofibers.

APPENDIX A

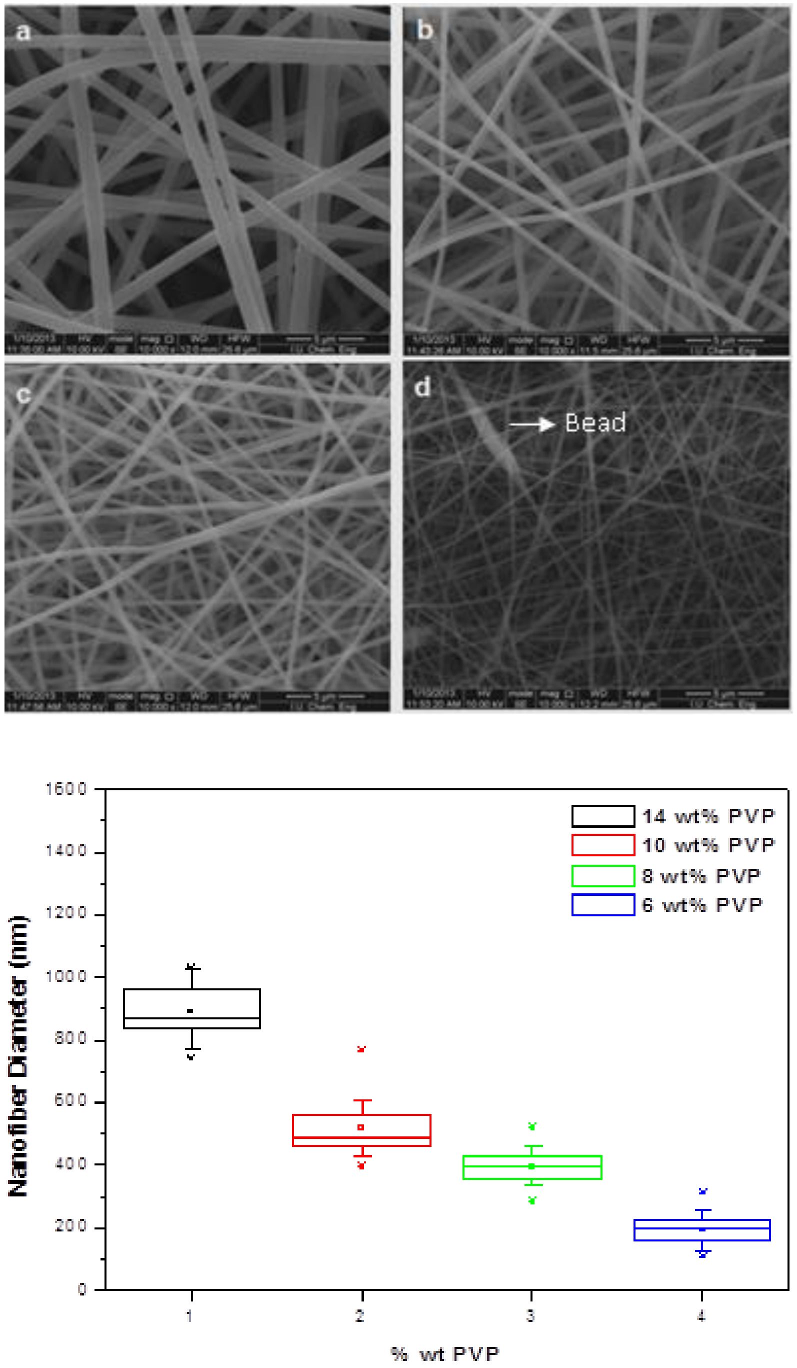

Figure A.1 : SEM images of PVP nanofibers a-) 14wt%, b-) 10wt%, c-) 8wt%, d-) 6 wt% and PVP nanofibers diameter distribution.

CURRICULUM VITAE

Name Surname : Timuçin BALKAN

Place and Date of Birth : İstanbul, 17/07/1986

E-Mail : timucinbalkan@hotmail.com

EDUCATION :

- **B.Sc.** : 2008, Uludag University, Faculty of Science and Letters, Chemistry
- **M.Sc.** : 2010, İstanbul Technical University, Faculty of Science and Letters, Polymer Science and Technology
- **Ph.D.** : 2016, İstanbul Technical University, Faculty of Science and Letters, Polymer Science and Technology

PROFESSIONAL EXPERIENCE AND REWARDS:

- 2009-2016 Research Assistant, Chemistry, İstanbul Technical University

PUBLICATIONS, PRESENTATIONS AND PATENTS ON THE THESIS:

- **Balkan, T.**, Sarac, A. S., 2015: Production of TiO_2 nanofibers by Electrospinning. 5th International Istanbul Textile Congress, September 11-12, 2015 İstanbul, Turkey.
- Solcova, O., **Balkan, T.**, Guler, Z., Morozova, M., Dytrych, P., Sarac, A. S., 2010. New Preparation Route of TiO_2 Nanofibers by Electrospinning: Spectroscopic and Thermal Characterization, *Science of Advanced Materials*, 6(12), 2618-2624.
- **Balkan, T.**, Guler, Z., Morozova, M., Dytrych, P., Solcova, O., Sarac, A. S., 2016. The Effect of Deposition on Electrochemical Impedance Properties of TiO_2/FTO Photoanodes, *Journal of Electroceramics*, 36(1), 102-111.

- **Balkan, T.**, Sarac, A. S., 2016. Electrochemical and Morphological Analysis of Poly (3,4-Alkylenedioxythiophene)-Modified TiO_2 Nanorod Electrodes, *Journal of Nanoscience and Nanotechnology* (accepted-in press).
- **Balkan, T.**, Sarac, A. S., 2016. Morphological Effect of Composite TiO_2 Nanorod-TiO_2 Nanoparticle/PEDOT:PSS Electrodes on Triiodide Reduction, *Express Polymer Letters* (accepted-in press).
- **Balkan, T.**, Gencturk, A., Sarac, A. S., 2016. TiO_2 Nano Çubuk İçeren Kompozit Yardımcı Elektrotların Üretim Yöntemleri. Dosya numarası: 2016/08800 (Başvuru Yapıldı)

OTHER PUBLICATIONS, PRESENTATIONS AND PATENTS:

- Lommens, P., Lambert, K., Loncke, F., De Muynck, D., Balkan, T., Vanhaecke, F. and Hens, Z., 2008. The growth of Co: ZnO/ZnO core/shell colloidal quantum dots: changes in nanocrystal size, concentration and dopant coordination. *ChemPhysChem*, 9(3), 484-491.
- Balkan, T., Sarac, A. S., 2011. Synthesis and characterization of electrically conductive composite films of polypyrrole/poly (acrylonitrile-co-styrene). *Fibers and Polymers*, 12(5), 565-571.
- Gungor, P. S., Balkan, T., Kose, G., Sarac, A. S., Kok, F. N., 2012. Polyblend nanofibers as tissue engineering matrices. *New Biotechnology*, 29, S112.
- Giray, D., Balkan, T., Dietzel, B., Sarac, A. S. 2013. Electrochemical impedance study on nanofibers of poly (m-anthranilic acid)/polyacrylonitrile blends. *European Polymer Journal*, 49(9), 2645-2653.
- Selcan Gungor-Ozkerim, P., Balkan, T., Kose, G. T., Sezai Sarac, A., Kok, F. N., 2014. Incorporation of growth factor loaded microspheres into polymeric electrospun nanofibers for tissue engineering applications. *Journal of Biomedical Materials Research Part A*, 102(6), 1897-1908.
- Polat, E., Güler, Z., Balkan, T., Sarac, A. S. 2016. Covalent streptavidin immobilization on electrospun poly (m-anthranilic acid)/polycaprolactone nanofibers and cytocompatibility. *Journal of Bioactive and Compatible Polymers: Biomedical Applications*, 31(3), 291-303.